CHARACTERIZATION OF *VRILLE* FUNCTION IN THE *DROSOPHILA* CIRCADIAN CLOCK

A Dissertation

by

KUSHAN LAKSHITHA GUNAWARDHANA

Submitted to the Office of Graduate and Professional Studies of
Texas A&M University
in partial fulfillment of the requirements for the degree of

DOCTOR OF PHILOSOPHY

Chair of Committee,	Paul E. Hardin
Committee Members,	James W. Erickson
	Jun-Yuan Ji
	Jerome S. Menet
	Mark J. Zoran
Head of Department,	Thomas D. Mcknight

May 2018

Major Subject: Biology

ABSTRACT

The *Drosophila* circadian clock is comprised of transcriptional feedback loops, which control rhythmic gene expression and are also responsible for daily rhythms in physiology, metabolism and behavior. The core feedback loop, which employs CLOCK-CYCLE (CLK-CYC) activators and PERIOD-TIMELESS (PER-TIM) repressors to drive rhythmic transcription peaking at dusk, is required for circadian timekeeping and overt behavioral rhythms. CLK-CYC also activates an interlocked feedback loop, which uses PAR DOMAIN PROTEIN 1ε (PDP1ε) activator and VRILLE (VRI) repressor to drive *Clk* and other rhythmic transcription peaking at dawn. In addition to its role in the clock, *vri* controls many developmental processes which are essential for early embryonic development, making *vri* null mutants embryonic lethal. This has hindered the ability to determine the role that *vri* plays within the circadian clock. The goal of my study is to determine if *vri* is necessary for circadian time keeping and/or output.

To achieve this goal, I first determined which transcripts were important for clock function. I generated an isoform specific *vri* mutant, which eliminated the expression of mRNAs that were thought to be essential for clock function. It turned out that these mutants are hypomorphic, as residual VRI expression was still observed in the clock cells of these mutants. Further analysis demonstrated that another *vri* mRNA isoform is expressed rhythmically under the control of the clock. Interestingly, the mutation impacted the abundance of short and long proteins, since the mutated mRNA can produce both VRI protein isoforms using an alternative translation initiation site.

Furthermore, the E-boxes that are used by CLK-CYC are important for development, since deletion of these E-boxes leads to embryonic lethality.

Then using a conditionally inactivatable transgene to rescue *vri* developmental lethality, I showed that clock function persists after *vri* inactivation, but activity rhythms were abolished. The inactivation of *vri* disrupts multiple output pathways thought to be important for activity rhythms, including Pigment-Dispersing Factor (PDF) accumulation and arborization rhythms in the small ventrolateral neuron (sLN_v) dorsal projection. These results demonstrate that *vri* acts as a key regulator of clock output, and suggests that the primary function of *vri* in *Drosophila* is to drive rhythmic transcription, which is required for overt rhythms.

DEDICATION

I dedicate this work to my parents and teachers, who taught me to think, understand and express, and to my wife whose constant confidence, support, care and love has earnestly helped to make this research a success.

ACKNOWLEDGEMENTS

I would like to thank my advisor, Prof. Paul E. Hardin. He is one of the best role models for a scientist, mentor and teacher. His continuous help and guidance was instrumental in completing my dissertation project. Dr. Hardin has been fully supportive and has given me the freedom to pursue various projects without any objections. He always provided insightful discussions about my research and encouraged me to try out novel techniques, which ultimately helped me in successfully completing this project. I also want to thank all my advisory committee members, Prof. James W. Erickson, Prof. Jun-Yuan Ji, Prof. Jerome S. Menet and Prof. Mark J. Zoran for sharing their intellectual and individual experiences to make me a better scientist. Their valuable discussions and suggestions throughout the course of this research helped me to become whom I am now. I wanted to express my gratitude to Prof. Bruce Riley, who helped me in many ways as a scientist and a mentor since the day I started my graduate life.

A good support system is important to surviving and staying sane in grad school. I was blessed with the best support system that I can ask for and eternally grateful for all the past and present members of the Hardin lab; Dr. Guruswamy Mahesh, Dr. Jerry Houl, Dr. Wangjie Yu, Dr. Parul Agrawal, Dr. Jian Zhou, Dr. Tianxin Liu, Courtney Caster, Paul Kim and Stephanie Durkacz. My lab family has always supported me in my up and downs and took care of me, when I was a thousand miles away from my family. I will treasure all the memories that I had in the Hardin lab. A special shout out goes to Courtney Caster for helping me to proofread my thesis and getting it into a presentable

format. Also, I am thankful for all members from the Center for Biological Clocks Research for their continuous support and feedback on my research, and also for sharing research materials and instruments with me. I am grateful to Prof. Rene Garcia for generously allowing me to use RT-PCR machine for my research.

I will forever be thankful to all my friends (too many to list here but you know who you are!) in College Station, who made my life a memorable one during the past seven years that I spent here.

I especially thank my mother, father, siblings and in-laws for providing me unconditional love and care, even when I am thousands of miles away from them. I would not have made it so far without them. I always had my family to count on when times were rough and hard, when my experiments were not working repeatedly. However, their continuous encouragement and instilling confidence kept me going and helped in successfully finishing my project.

Finally, I am thankful to the best outcome of my last seven years, my soul-mate, my wife! She was my ultimate support system for the last couple of years. She took care of me, fed me, did all house work on her own, listened to continuous problems I faced with my experiments yet loved me unconditionally without expecting anything in return so I can focus on my research. The last couple of years have not been an easy ride, both academically and personally, I am truly thankful to Nadisha, for sticking by my side and playing an instrumental role in my life as a wife.

CONTRIBUTORS AND FUNDING SOURCES

Contributors

The research that is described in this thesis document was supervised by my Dissertation Advisory Committee consisting of Prof. Paul E. Hardin (chair), Prof. Mark J. Zoran, Prof. James W. Erickson and Prof. Jerome S. Menet of the Department of Biology, and Prof. Jun-Yuan Ji, Department of Molecular and Cellular Medicine, Texas A&M University.

All the work described in the dissertation was accomplished by myself, under the supervision and guidance of my Dissertation Advisory Committee chair Prof. Paul E. Hardin.

Funding

There are no outside funding contributions to acknowledge related to the research and compilation of this document.

TABLE OF CONTENTS

Page

LIST OF FIGURES

Page

LIST OF TABLES

Page

CHAPTER I

INTRODUCTION

The circadian clock: an autonomous daily timekeeping mechanism

The Earth completes a full rotation around its own axis in 24 hours, and this time period is generally known as a 'day'. Over the course a day, the geophysical environment that we live in undergoes various changes with respect to many parameters including illumination, temperature, magnetism, salinity, humidity, nutrient availability, and predation. Furthermore, most of these changes are highly predictable, and organisms have the capacity to anticipate these environmental changes and make necessary preparations to cope with them. This ability to anticipate environmental changes provides an enormous evolutionary advantage and helps organisms adapt within their biological niche (Dodd, et al. 2005; Paranjpe and Sharma 2005). The biological phenomenon that enables organisms to anticipate daily environmental changes is called the circadian (*circa* = approximately; *dies* = a day) clock (Pittendrigh 1993).

The circadian clock is composed of three components: input pathways, output pathways and the oscillator (Bell-Pedersen, et al. 2005). The oscillator is responsible for keeping time. Changes in the environment are perceived by sensory proteins and relayed are to the oscillator via input pathways. These input signals are known as 'zeitgebers' (time givers), where light is the most common zeitgeber. In addition to light, temperature, magnetism, feeding behaviors, sociological behaviors can also act as zeitgebers to entrain the circadian system (Boothroyd and Young 2008; Ehlers 1992).

Upon receiving these zeitgebers, the oscillator is reset so it can be in synchrony with the environment (or to entrain the clock) by shifting forward (phase advance) or backward (phase delay) depending on when the zeitgeber is introduced (Aschoff 1999). The oscillator controls downstream biological processes such as physiology, metabolism, and behavior by controlling genes that control these biological processes via output pathways (Hardin and Panda 2013; Tataroglu and Emery 2014).

There are three cardinal properties of rhythms controlled by circadian clocks: they are entrained by environment zeitgebers, they are temperature compensated, and they have a period of ~24 hours in constant conditions (Hong, et al. 2007). In the absence of any zeitgebers, the oscillator continues to operate with a period of ~24 hours, hence circadian rhythms are endogenous. Almost all biochemical reactions increase their reaction rates when the temperature of the system is increased, thus increasing the speed of downstream biological processes. On the contrary, the period of circadian rhythm is kept constant within a physiological range of constant temperatures, which means that the oscillator is temperature compensated (Narasimamurthy and Virshup 2017).

An interlocked feedback loop mechanism forms the oscillator

The circadian clock keeps time via transcriptional feedback loops. In the core feedback loop, positive elements activate the transcription of the negative elements, which repress their own transcription by negatively impacting the activity of positive elements. With time, negative elements are eliminated, which de-represses the activity of positive elements, thus initiating the next cycle of gene transcription (Bell-Pedersen, et

al. 2005; Hardin and Panda 2013). Even though the mechanism is conceptually simple, in reality the process is very complex and each step is temporally regulated via post transcriptional and translational mechanisms to expand this process into a ~24 hour long feedback mechanism (Hardin 2011). The core feedback loop also drives additional positive and negative transcriptional regulators that form an interconnected feedback loop, which is essential for the propagation and strengthening of the rhythms generated by the oscillator (Benito, et al. 2007; Saithong, et al. 2010; Uriu and Tei 2017).

Genome-wide microarray analyses demonstrate that the expressions of many genes are rhythmic (30-64% of cyanobacteria genes, 10-40% of *Neurospora* genes, 31-41% of *Arabidopsis* genes, 19% of *Drosophila* genes and 46% of mice genes) and are under the control of the circadian oscillator (Doherty and Kay 2010; Li and Zhang 2015; Zhang, et al. 2014). However, the mRNA expressions of these output genes peak at different times of the day and are classified into two major groups. The first group of genes is directly controlled by the core feedback loop and their mRNAs peak near dusk. The second group of genes is expressed anti-phase to the first group and is likely controlled by the interlocked feedback loop. Nonetheless, the expressions of these output genes have a period of ~24 hours, and their rhythmic expression aids in the regulation of downstream biological processes that control rhythms in physiology, metabolism, and behavior.

In *Drosophila*, *Clk* and *cyc* encode positive elements of the core feedback loop (Figure 1). CLK and CYC proteins are basic Helix-Loop-Helix (bHLH) transcription factors that heterodimerize and bind E-box elements located on promoters of target

genes, known as clock controlled genes (ccgs), whose mRNAs peak around dusk. The negative elements of the *Drosophila* core feedback loop are *per* and *tim*, are ccgs activated by CLK-CYC. The mRNA levels of *per* and *tim* reach their maximum around Zeitgeber Time 14 (ZT14, where ZT0 is lights on and ZT12 is lights off). However, PER and TIM proteins do not oscillate in unison with their mRNAs and their peak of expressions are delayed by 6-8 hrs due to post translational modifications such as phosphorylation. DOUBLE TIME (DBT), CASEIN KINASE 2 (CK2) and SHAGGY (SGG) kinases phosphorylate PER and TIM (Tataroglu and Emery 2015). DBT mediated phosphorylation events destabilize PER and lead to SLIMB F-box protein induced PER degradation. CK2 phosphorylates PER at S149, S151 and S153 and SGG phosphorylates the S657 of PER and these phosphorylation events promote nuclear localization of the PER complex around ZT18. SGG also interacts with CRYPTOCHROME (CRY) and acts to stabilize CRY protein. This subsequently stabilizes TIM, as CRY is responsible for initiating TIM degradation. PER and TIM phosphorylation is counterbalanced by protein phosphatase 2a (PP2a) and protein phosphatase 1 (PP1)-mediated dephosphorylation, respectively, which stabilizes PER and TIM (Hardin 2011; Hardin and Panda 2013).

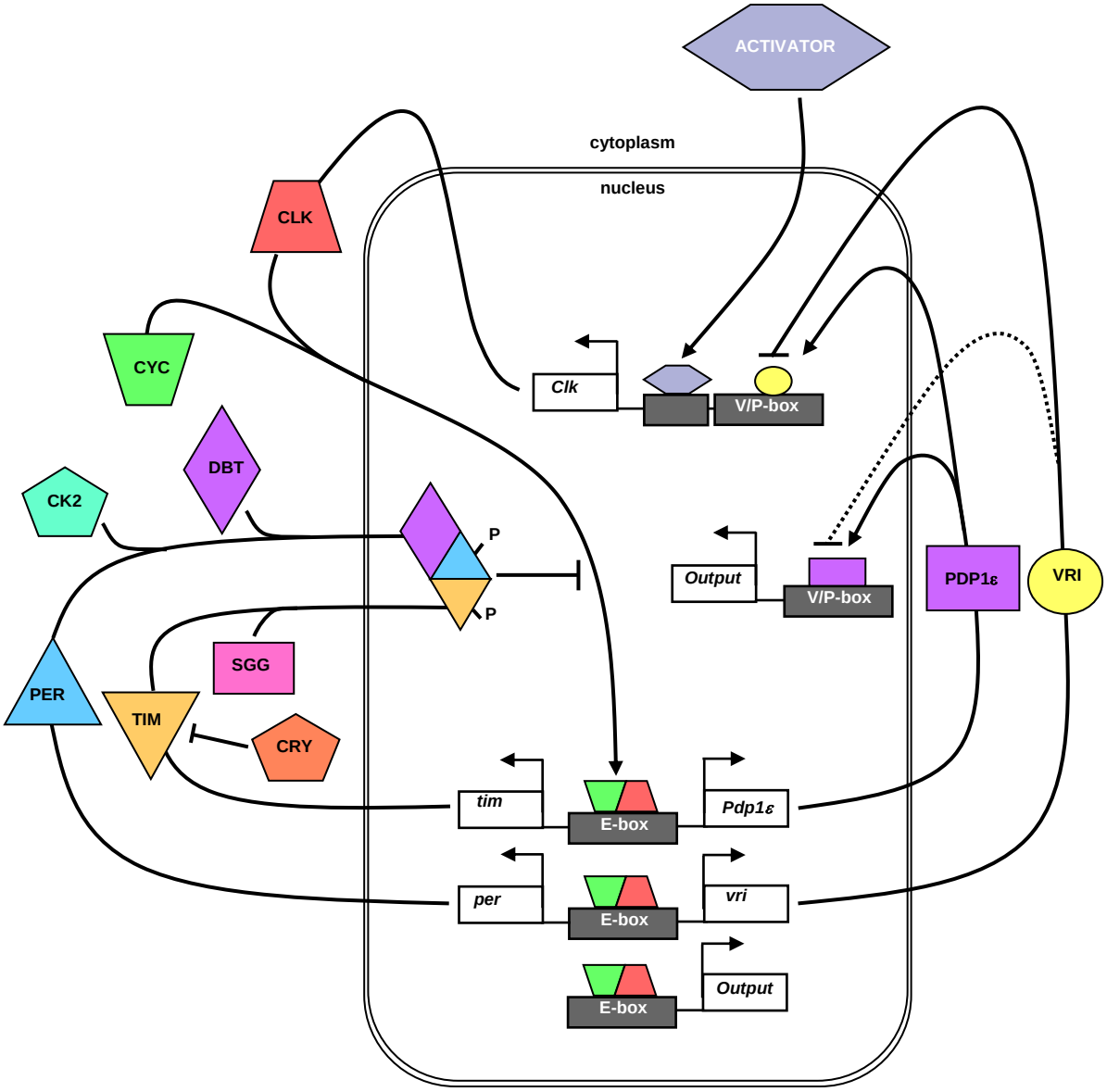

Figure 1. Model of the Interlocked transcriptional feedback loops that keep circadian rhythms in *Drosophila*.
All genes and regulatory elements are color coded and described in the text. Double solid lines represent the nuclear membrane; 'P' attached to a color shape denotes a phosphorylation of that protein; solid lines represent known activation and repression functions; broken lines represent probable activation and repression functions. Modified from (Benito, et al. 2007).

Once PER-TIM enters the nucleus, it interacts with and inhibits CLK-CYC transcription. Within the nucleus, PER is progressively phosphorylated and this ultimately triggers its degradation in the early morning via proteasome-mediated degradation pathways (Yu, et al. 2006). Degradation of PER leads to a decrease in PER binding to CLK-CYC, and allows CLK-CYC to bind E-boxes of ccgs activating their transcription and initiating the next cycle. CRY is a blue light photoreceptor found in flies and is orthologous to plant blue light photoreceptors. CRY is very important for light dependent phase resetting (Emery, et al. 1998). CRY gets activated by blue light, and triggers CRY binding to TIM, and leading to TIM degradation induced by JETLAG F-box protein (Koh, et al. 2006). Loss of TIM reduces PER stability, enabling DBT mediated phosphorylation and subsequent degradation of PER. Light activated CRY protein is also subjected to JETLAG induced degradation via the proteasome, but at a slower pace, since JETLAG has higher affinity for TIM (Peschel, et al. 2009).

As shown in the Figure 1, *vri* and *Pdp1ε* are also activated by CLK-CYC and form an interlocked feedback loop by controlling the transcription of *Clk* mRNA. Since *vri* and *Pdp1ε* are directly activated by CLK-CYC, their rhythmic mRNA expression parallels that of *per* and *tim*. Among these four genes, *vri* is unique because its protein cycles in phase with its mRNA, which peaks in early evening at ZT15 (Figure 2). This allows VRI to act as a repressor of *Clk* mRNA, as the levels of *Clk* mRNA is at its nadir at this time point (Cyran, et al. 2003; Glossop, et al. 2003). PDP1ε peaks in unison with PER and TIM but the protein peaks 6 hours after the mRNA peaks due to uncharacterized post-transcriptional regulatory events. This coincides with the rising

phase of *Clk* mRNA transcription which is expected since PDP1ε acts as the activator of *Clk* transcription (Figure 2, (Cyran, et al. 2003; Glossop, et al. 2003)).

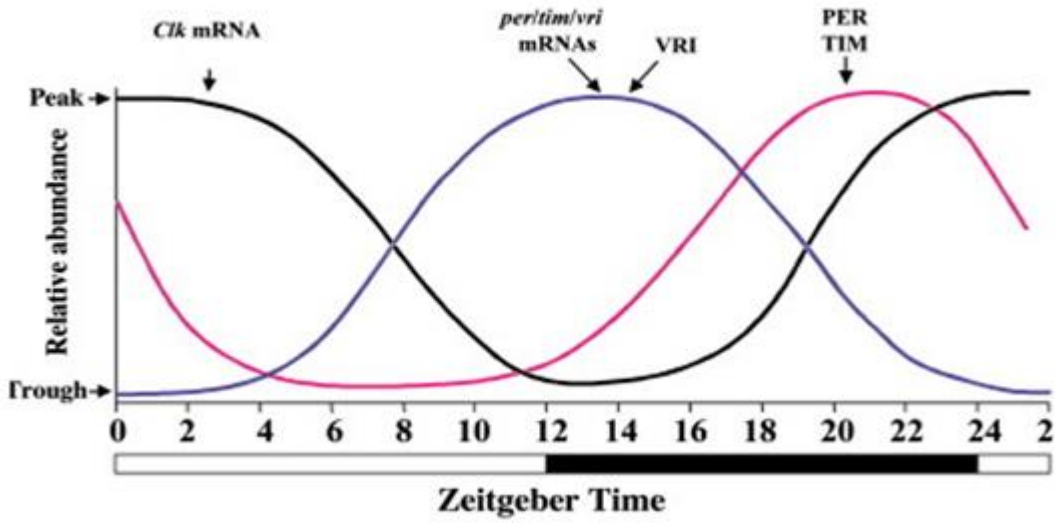

Figure 2. mRNA and protein rhythms of clock genes.
A representation of rhythmic mRNA or protein expression of *Clk*, *per*, *tim* and *vri* during an LD cycle. The white bar represents the light phase; the black bar represents the dark phase. Reprinted from (Glossop, et al. 2003).

VRI and PDP1ε bind to D-box elements on the promoter of *Clk* to exert their respective repressor and activator functions (Cyran, et al. 2003; Glossop, et al. 2003). It has been proposed that VRI and PDP1ε bind to these promoter elements by competing with one another, and the differential phase of expression of these two proteins facilitates this competitive binding model (Cyran, et al. 2003). Moreover, *cry* mRNA is also under the control of this interlocked feedback loop. There are D-box elements in the promoter of *cry*, and VRI and PDP1ε bind to these elements to regulate *cry* transcription (Glossop, et al. 2003). Both *Clk* and *cry* have a similar mRNA profile with both peaking near dawn, anti-phasic to the direct targets of CLK-CYC. Thus, it is predicted that the

interlocked feedback loop controls rhythmic expression of output genes for those mRNAs which peak near dawn (Hardin and Panda 2013).

Transcriptional regulation of *vri*

The *vri* gene is located on the left arm of *Drosophila* chromosome 2 (2L) and encodes a basic-zipper transcription factor having a typical basic DNA binding domain and a leucine zipper domain which mediates homo- and heterodimerization (George and Terracol 1997; Vinson, et al. 1989). Five different transcripts of *vri* have been characterized and they use three alternate first exons. The characterized *vri* transcripts can be classified into two classes based on their size, ~3.3 kB and ~3.8 kB, and are the predominant *vri* RNA bands observed on Northern blots using adult head RNA (Figure 3). Both these bands oscillate in a clock dependent manner (Blau and Young 1999). *vri*-A, *vri*-E and *vri*-F migrate together as a ~3.8 kB band, while *vri*-D migrates as a ~3.3 kB band. Evidence for the existence of *vri*-C comes from embryonic EST libraries, yet a ~3.0 kB band was not reported on Northern blots that have been run with embryonic RNA extracts or any other developmental stage. Interestingly, these Northern blots show other uncharacterized transcripts of *vri* of sizes 6.2 kB and 4.9 kB that are expressed in early embryonic stages and then cease expression (Figure 3). Also, another group of mRNAs of size 1.6 kB and 1.9 kB get transcribed from the larval stage onward (George and Terracol 1997). It is possible that these uncharacterized mRNA bands are a result of

non-specific probe binding to a mRNA of another gene, since none of these mRNAs are reported in genome-wide RNA-Seq experiments.

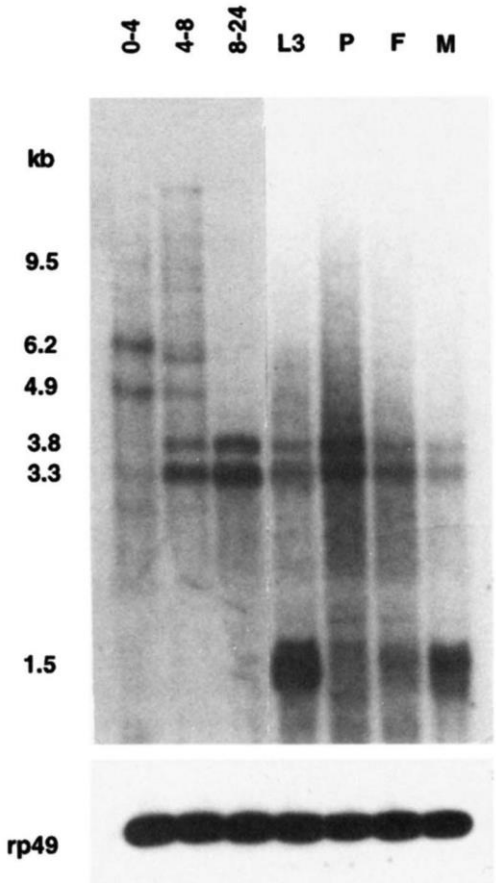

Transcript	Length of mRNA (nucleotides)	Length of peptide (amino acids)	Predicted molecular weight (kDa)
vri-RA	3841	729	78.3
vri-RC	3058	610	64.9
vri-RD	3455	729	78.3
vri-RE	3890	610	64.9
vri-RF	4068	729	78.3

Figure 3. *vri* RNA expression during development.
(Left Figure) 10µg of RNA used from indicated developmental stages. Embryonic stages are as follows 0-4, 0-8 and 8-24 h after egg laying; L3, 3rd instar larva stage (3-5 days after egg laying); P, Pupal stage (6-7 days after egg laying); F, adult female; M, adult male. Control loading performed with *rp*49. Reprinted from (George and Terracol 1997). (Right Table) Summary table of all characterized *vri* mRNA (source: Flybase.org). kDa, kiloDalton

The promoter for *vri*-A, *vri*-D and *vri*-F (*vri*-ADF) mRNAs contains five E-boxes (Blau and Young 1999). Luciferase mediated in-vitro promoter analysis experiments show that the CLK-CYC complex binds to these E-boxes to activate *vri*

expression in S2 cells. Furthermore, in *Clk*^{jrk} and *cyc*^{0} mutants *vri* mRNA is expressed at a low basal level in head RNA extracts, while in *tim*^{01} mutants *vri* mRNA is expressed at constitutively high levels, demonstrating that *vri* is under the direct control of the core feedback loop (Blau and Young 1999). In fact, with CLK Chip-chip experiments, the *vri* promoter shows the highest affinity for CLK-CYC binding compared to all other ccgs (Abruzzi, et al. 2011). Thus, *vri*-ADF mRNAs are rhythmically transcribed by CLK-CYC binding to these E-box elements.

In addition, ChIP-chip experiments have demonstrated that CLK-CYC binding to the promoter produces the *vri*-E transcript, but at a lower binding affinity (Abruzzi, et al. 2011). Sequence analysis showed two E-boxes on this region of the promoter. Furthermore, there are two more E-box clusters on the promoter and on the 1st intron of *vri*-E transcript. However, neither of them have reported to be bound by CLK-CYC. Moreover, *vri*-E transcript has not been analyzed to see if it is rhythmically expressed.

Dynamic expression of VRI protein

vri-ADF mRNA encodes for a 729 amino acid VRI protein (long VRI), and the *vri*-C and *vri*-E (*vri*-CE) transcripts code for a 610 amino acid VRI protein (short VRI) (Figure 3). On western blots, one major VRI band runs below the 89 kDa marker and another minor VRI band runs above 89 kDa marker. Both of these proteins are expressed rhythmically (Glossop, et al. 2003). Interestingly, neither of these protein bands correspond to the predicted molecular weights of long VRI and short VRI, plus there are other discrepancies observed with Western blot analysis. For instance, the long VRI

protein which is translated from *vri*-ADF mRNAs is significantly lower in abundance compared to short VRI protein, even though *vri*-ADF mRNAs are the most abundant mRNA species. Moreover, short VRI is the most abundant protein isoform even though its mRNAs are low in abundance. In addition to these discrepancies post-translational modifications of VRI are also poorly understood. VRI does undergo phosphorylation, but no studies to date have examined whether this post-translational modification has any impact on VRI function, stability or other properties (Glossop, et al. 2003). Given the discrepancies in *vri* mRNA and protein isoform expression and the uncharacterized phosphorylation of VRI, suggests an exhaustive analysis of both *vri* mRNA and protein is necessary before we can understand the mechanisms though which *vri* is regulated.

Based on in-situ hybridization experiments *vri* mRNA is detected as early as the syncytial blastoderm stage (Embryonic Stage 4, ES 4), before zygotic transcription has initiated (George and Terracol 1997). This maternal *vri* mRNA is responsible for embryonic developmental functions which will be discussed later. Also, zygotic VRI is crucial later in fly development (Szuplewski, et al. 2003). In clock cells, initial appearance of VRI is noted during ES16-ES17, soon after the initiation of CLK expression, which happens roughly around ES16 (Houl, et al. 2008; Houl 2009). During embryonic and larval stages the expression of VRI can be detected in non-clock cells, but in adult flies VRI expression is restricted to clock cells in all analyzed tissues (Glossop, et al. 2003; Houl 2009).

The central pacemaker neuronal network of *Drosophila*

In *Drosophila*, approximately 150 brain neurons form a pacemaker cell network that controls behavioral rhythms. Based on their anatomical location, size and the neuropeptides that they secrete, pacemaker neurons have been classified into seven subgroups including three groups of dorsal neurons, Dorsal Neuron 1, 2 and 3 (DN_1, DN_2 and DN_3), and four groups of lateral neurons, dorsal Lateral Neurons (LN_d), Lateral Posterior Neurons (LPN), small and large ventral Lateral Neurons (sLN_v and lLN_v) (Figure 4, (Helfrich-Forster 2005)). VRI is rhythmically expressed in all pacemaker neurons in adults and even in pacemaker neurons at ES16 (Houl 2009). Even though a complete network of neurons is essential for robust and coherent control of circadian behaviors, several lines of evidence indicate that LN_vs are sufficient to maintain behavioral rhythms in the absence of Zeitgebers (Ewer, et al. 1992; Helfrich-Forster 1998).

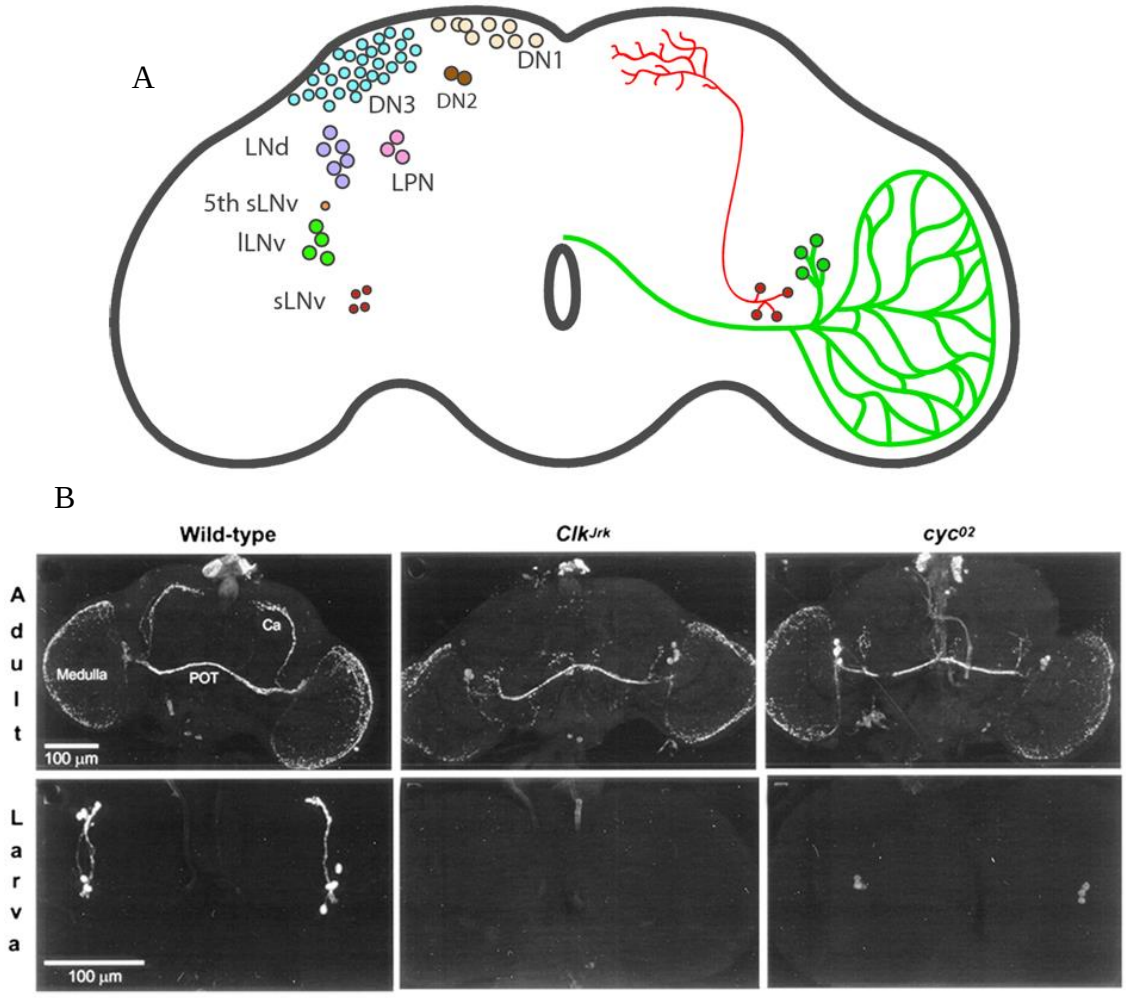

Figure 4. Neuroanatomy of pacemaker neurons and PDF expression
(A) Representation of anatomical locations of seven groups of brain pacemaker neurons and PDF positive neuronal projections of *D*rosophila. DN_1: Dorsal Neuron 1, DN_2: Dorsal Neuron 2, DN_3: Dorsal Neuron 3, LN_d: dorsal Lateral Neuron, LPN: Lateral Posterior Neurons, sLN_v: small ventral Lateral Neurons and lLN_v: large ventral Lateral Neurons (Nara I. Muraro 2014). (B) PDF positive projections of adult and larval brains of w^{1118}, Clk^{jrk} and cyc^{0} flies. Reprinted from (Park, et al. 2000).

Although the anatomical location of each group of pacemaker neuron is well understood, connectivity between these neuronal groups has not been characterized extensively. Some neurons like lLN_vs, LN_ds and DN_1s send contralateral projections

connecting the same group of pacemaker neurons to the other hemisphere, while neurons like sLN_vs make connections with DNs (Cavanaugh, et al. 2014; Helfrich-Forster, et al. 2007). The connection from sLN_vs to DNs, called the sLNv dorsal projection, has been thoroughly studied due to its importance in maintaining overt behaviors (Figure 4). The dorsal projection mainly uses PIGMENT DISPERSING FACTOR (PDF) neuropeptide to communicate with DNs (Abruzzi, et al. 2017). Mutations that affect the development of dorsal neurons or the expression of PDF or its receptor, PDFR, results in arrhythmic activity showing the importance of PDF mediated communication for behavioral rhythms (Agrawal and Hardin 2016; Mertens, et al. 2005; Park, et al. 2000; Renn, et al. 1999).

Moreover, axonal termini of sLN_v dorsal neurons undergo daily changes in arborization (Fernandez, et al. 2008; Frenkel and Ceriani 2011). In the early morning, sLN_v dorsal projection termini are extensively arborized making many synaptic connections with DNs, whereas during the evening sLN_v dorsal projection arbors regressed resulting in fewer synaptic connections. Interestingly, PDF expression in sLN_vs is severally reduced or absent in many clock gene mutants such as *Clk*, *cyc* and *Lar* null mutants (Figure 4, (Agrawal and Hardin 2016; Park, et al. 2000)). cyc^0 mutants have a defect in PDF transportation to these projections, while in *Lar* null mutants, the development of sLN_v dorsal projections is compromised. Thus, intricate regulation of PDF expression and temporal regulation of neuronal connectivity among sLN_v and DNs is crucial for behavioral rhythms.

VRI is important for fly development and circadian clocks

vri was initially identified and characterized as a dominant maternal enhancer of embryonic dorsoventral patterning defects in *easter* (*ea*) and *decapentaplegic* (*dpp*) mutants. Homozygous *vri* mutants are severely ventralized with a reduced and wrinkled dorsal epidermis, deformed head skeleton and defective germ band retraction, which leads to lethality in early embryonic development (George and Terracol 1997). Also, *vri* acts as an enhancer of *Mothers against dpp* (*Mad*). *Mad* mutants show wing phenotypes such as a shortened L5 vein, extra vein material along the L2 vein and a defect in tracheal growth (George and Terracol 1997). Post-embryonically, *vri* genetically interacts with many actin binding proteins, thus helping to control cell growth and proliferation via the regulation of the actin cytoskeleton (Szuplewski, et al. 2003).

The *vri* gene also contributes to biological clock function in *Drosophila*. Since *vri* mutants are embryonic lethal, characterization of *vri* function with respect to biological timekeeping was done using *vri* overexpression. Overexpressing VRI downregulates PER and TIM levels within the core feedback loop (Blau and Young 1999). Later experiments showed that reduced PER and TIM levels are due to lower levels of CLK because VRI acts to repress *Clk* transcription (Cyran, et al. 2003; Glossop, et al. 2003). Similarly, VRI acts as a repressor of *cry*, which is expressed in phase with *Clk* mRNA (Glossop, et al. 2003). Thus, VRI is predicted to regulate many rhythmic genes whose expression peaks near dawn (Hardin 2011).

PDF expression is also downregulated when VRI is overexpressed. However, *pdf* mRNA levels are unaffected by VRI overexpression, suggesting that VRI regulates PDF

expression post-transcriptionally (Blau and Young 1999). Flies that overexpress VRI in clock cells exhibit longer activity periods (~2 hours) and with stronger VRI overexpression lines, arrhythmic behavioral activity was observed (Blau and Young 1999). Since VRI overexpression causes cell growth defects including reduced cell size in wings and smaller eyes with reduced ommatidia (Szuplewski, et al. 2003), it is possible that such development defects may contribute to the behavioral arrhythmicity observed in *vri* overexpression flies. Thus, proper characterization of *vri* function using adult null mutants is crucial to understand how *vri* regulate clock functions independent of its development functions.

VRI and PDP1ε regulate rhythmic transcription within the interlocked feedback loop

VRI uses a conserved *cis* element, the D-box, in the *Clk* promoter to repress *Clk* mRNA transcription (Glossop, et al. 2003). D-box elements (ATTACATAAT) were initially characterized as targets of the D-box binding protein (DBP), which binds onto the D-site of the albumin promoter to activate its transcription (Iyer, et al. 1991). D-boxes are important *cis* elements used by many clock genes in flies and mice. In *Drosophila*, *Pdp1*ε also binds to D-box elements to regulate target genes. In fact, PDP1ε uses the same D-boxes that VRI uses on the *Clk* promoter (Cyran, et al. 2003). Even though *vri* and *Pdp1*ε have similar mRNA expression profiles, PDP1ε peaks several hours after the peak of VRI, thus allowing VRI to repress target gene transcription. The proposed model suggests that PDP1ε has an overall higher affinity for the D-boxes than

VRI, therefore it can remove VRI from the promoters of target genes and facilitates their transcription when PDP1ε reaches its peak of expression around ZT22 and VRI levels begin to decline (Cyran, et al. 2003; Taylor III 2007).

Similar to VRI, PDP1ε is essential for development. *Pdp1*ε null mutants show normal development as embryos, but as larvae their growth is delayed or arrested and they die before pupation (Reddy, et al. 2006). *Pdp1*ε also produces multiple transcripts using different 1st exons, where *Pdp1*ε transcripts (*Pdp1*-RD *and Pdp1*-RJ) are thought to be crucial for clock function since the promoter for these transcripts contains E-boxes bound by CLK-CYC (Abruzzi, et al. 2011; Cyran, et al. 2003; Reddy, et al. 2000). Recently, an isoform specific mutant of *Pdp1*ε was generated by mutating 2nd exon unique to *Pdp1*ε transcripts. The resulting mutant, *Pdp1*^{3153}, is behaviorally arrhythmic and exhibits reduced CLK and CRY levels, although rhythmic PER expression confirms that the oscillator is functioning in *Pdp1*^{3153} mutant flies (Zheng, et al. 2009). Interestingly, *Pdp1*^{3153} flies are arrhythmic even during LD cycles, unlike other clock gene mutants. The arrhythmic nature of *Pdp1*^{3153} mutants during LD and DD cycles suggests that PDP1ε is important for light dependent and independent output gene expressions that controls activity rhythms. Based on the molecular and behavioral phenotypes of *vri* overexpression and *Pdp1*ε mutants, VRI and PDP1ε form an interlocked feedback loop that controls the expression of rhythmic output genes that peak near dawn (Hardin 2011).

Mammals and flies share a conserved time keeping mechanism

As in *Drosophila*, the mammalian circadian oscillator is composed of interlocked transcriptional feedback loops (Figure 5). Many *Drosophila* oscillator components have mammalian orthologs or functional equivalents. In mammals BRAIN AND MUSCLE ARNT-LIKE PROTEIN-1 (BMAL1) is the mammalian ortholog of CYC, which dimerizes with mammalian CLOCK and binds to E-boxes to activate target genes. (Hardin and Panda 2013; Partch, et al. 2014).

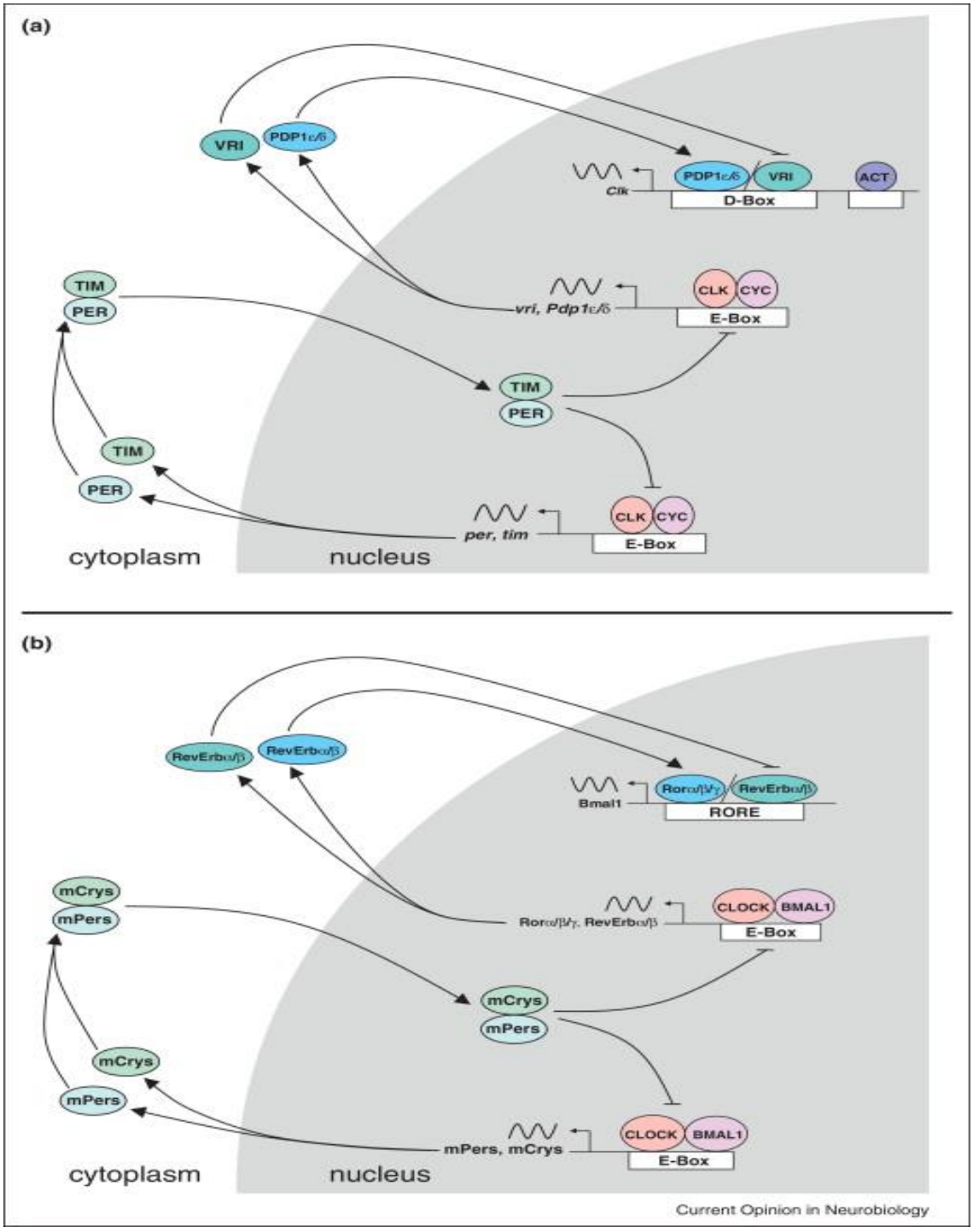

Figure 5. Comparison of *Drosophila* and Mammalian clockwork.
Genetic architecture of core and interlocked feedback loops of (a) *Drosophila* and (b) mammals. All genes and their interactions are described in the text. Reprinted from (Hardin and Panda 2013).

In mammals, PERs (mPER1, mPER2 and mPER3) and CRYs (mCRY1 and mCRY2) form the negative limb of the core transcriptional feedback loop. As in *Drosophila*, genes encoding these negative elements are activated by the BMAL1-CLOCK complex. Accumulating levels of mPERs and mCRYs interact to promote mPER-mCRY protein stabilization and nuclear translocation. Once, the mPER-mCRY heterodimer enters the nucleus, it interacts with and inhibits the positive elements, thereby repressing their own transcription (Yu and Hardin 2006). In mammals, CRY is the primary inhibitor, whereas in flies PER is the primary inhibitor (Hardin 2006; Reppert and Weaver 2002). Unlike CRY in *Drosophila*, mCRYs do not function as photoreceptors rather mammals perceive light inputs through the retina and then through retinal hypothalamic tract (RHT), master pacemaker neurons located in the suprachiasmatic nucleus (SCN) of the hypothalamus receive these light zeitgebers.

The interlocked feedback loop seen in *Drosophila* is conserved in mammals. Functional equivalents of VRI and PDP1ε, two REV-ERBs (REV-ERBα/β coded by *Nr1d1* and *Nr1d2* genes) and three RETINOID ACID RECEPTOR-RELATED ORPHAN RECEPTORs (RORα, RORβ and RORγ), repress and activate the expression of *Bmal1* transcription in mammals (Takahashi 2017). However, the REV-ERBs and RORs are nuclear receptors rather than bZIP transcription factors like VRI and PDP1ε. REV-ERBs and RORs bind ROR Elements (RORE) to regulate transcription instead of D-boxes (Guillaumond, et al. 2005; Preitner, et al. 2002). Like PDP1ε mutants, ROR mutants show reduced amplitude rhythms of *Bmal1* suggesting that the RORs are dispensable for *Bmal1* rhythms (Liu, et al. 2008). Mutants that eliminate the function of

two *Rev-Erb* genes on the other hand disrupt *Bmal1* rhythms, the core feedback loop function and behavioral rhythms in mammals (Cho, et al. 2012). Thus, REV-ERBs appear to play a more prominent role than RORs in the mammalian circadian clock.

In mammals, another interlocked feedback loop is present that is composed of PAR-bZIP factors DBP, TEF (Thyrotroph Embryonic Factor) and HLF (Hepatic Leukaemia Factor), which are mammalian orthologs of PDP1ε and E4 BINDING PROTEIN-4 (E4BP4, also known as Nuclear Factor, Interleukin-3, NFIL3), and which is a mammalian ortholog of VRI. As in *Drosophila*, PAR-bZIP factors and E4BP4 bind D-box elements to carry out their transcriptional activation or repression functions. Mice deficient of only one or two members of the PAR-bZIP factors display mild clock phenotypes, suggesting that the three paralogs execute partially redundant functions (Gachon, et al. 2011; Lopez-Molina, et al. 1997). However, mice deficient in all three PAR-bZIP factors have a reduced life span due to epileptic seizures (Gachon, et al. 2004). Also, knockdown of E4BP4 using shRNA, lengthens the *Per2* period by ~2 hours, suggesting that E4BP4 plays an important role in controlling the period of the oscillator (Yamajuku, et al. 2011), Just like in *Drosophila*, mammal ccg expression is controlled by interlocked feedback loops. However, mammalian ccgs contain E-box, RORE and/or D-box elements forming a combinatorial promoter to control their phase of expression, while *Drosophila* uses only E- and D-box elements (Takahashi 2017; Ueda, et al. 2005).

Project Aims

Since both *Pdp1ε* and *Ror* mutants exhibit low amplitude rhythms of *Clk* and *Bmal1* and the molecular clock continues to function in these mutants, it was thought that the interlocked feedback loops are accessory or supporting loops for the core feedback loop (Liu, et al. 2008; Zheng, et al. 2009). However, with the recent discovery that molecular clock function and behavioral rhythms are abolished in *Rev-Erb* double mutants (Cho, et al. 2012), interlocked feedback loops, and particularly repressor elements in these loops maybe more important than previously thought.

Since *vri* null mutants are embryonic lethal (George and Terracol 1997), experiments to test whether *vri* is required for clock function and/or output have not been carried out. The characterization of *vri* function within the clock is based on the phenotypes exhibited by VRI overexpression flies. However, VRI overexpression results in cell growth defects and apoptosis driven cell number and tissue reduction (Szuplewski, et al. 2003), thus it poses the question are the phenotypes that were observed in VRI overexpression lines due to a clock defect or a developmental defect, or a combination of both.

The strategy used to generate isoform specific mutants of *Pdp1ε* transcripts, i.e mutating the second exons that are clock regulated, is intriguing and opens up the possibility of generating a similar *vri*-ADF (circadian transcripts of *vri*) mutant. I generated a *vri*-ADF isoform specific mutant, which deleted the 1st exon unique to *vri*-ADF mRNAs. However, the *vri*-ADF isoform specific mutation did not eliminate *vri* expression in clock cells but I did uncover important aspects of *vri* regulation such as

vri-ADF and *vri*-E mRNAs are rhythmically expressed under the clock as well as *vri*-ADF mRNAs code for both long and short VRIs due to the use of alternative translation initiation sites as described in Chapter II.

To generate a *vri* null mutant, I used another strategy in which I rescue *vri* lethality while eliminating *vri* function in adults using an inactivatable *vri* transgene as described in Chapter III. Using this inactivatable *vri* transgene I discovered that *vri* null mutants are behaviorally arrhythmic, yet the circadian clock persists suggesting that *vri* is only necessary for clock output. Interestingly, inactivating *vri* in LN_vs decreases *pdf* mRNA and protein accumulation at the post-transcriptional level in sLN_vs resulted in PDF not being transported to the sLN_v dorsal projections. Indeed, *vri* is also required for daily rhythms in sLN_v dorsal projection arborization, which support activity rhythms. Overall, my results suggest that *vri* functions as a key regulator of clock output by driving rhythmic transcription of target genes that peak near dawn.

CHAPTER II

CIRCADIAN AND DEVELOPMENTAL REGULATION OF *VRILLE* TRANSCRIPTION IN *DROSOPHILA*

Background

The *vri* gene of *Drosophila* encodes a bZIP transcriptional repressor that was initially identified as an enhancer of *decapentaplegic* (*dpp*) dorsoventral patterning defects (George and Terracol 1997). *vri* null mutants show multiple embryo patterning defects that cause lethality before hatching as L1 larvae (George and Terracol 1997), and patches of *vri* mutant tissue in adults show patterning and proliferation defects (George and Terracol 1997; Szuplewski, et al. 2003). Subsequently, *vri* was recovered in a screen for circadian clock controlled transcripts present in adult heads (Blau and Young 1999). Since *vri* mutants are embryonic lethal, *vri* function in the clock was first characterized via overexpression studies. When *vri* is overexpressed, circadian activity rhythms are lengthened or abolished, indicating that *vri* functions within the circadian clock (Blau and Young 1999). Indeed, *vri* rhythmically represses transcription of *Clock* (*Clk*), a key activator within the *Drosophila* timekeeping mechanism (Hardin 2011), and other genes whose mRNAs cycle with a peak around dawn (Cyran, et al. 2003; Glossop, et al. 2003).

The *vri* gene produces two protein isoforms from five transcripts that use three different first exons (Gramates, et al. 2017; Szuplewski, et al. 2003). A 17 kB transgene that contains exons 1b, 1c and both common *vri* exons fails to rescue developmental lethality, suggesting that the *vri*-E transcript is necessary for development (George and

Terracol 1997). Although RNA-seq detects little if any *vri*-C mRNA, *vri*-E mRNA is detected in embryos, pupae and adults, and *vri*-ADF mRNA is present at all developmental stages (Gramates, et al. 2017). Rhythmic *vri* transcription is thought to be mediated by CLK-CYCLE (CLK-CYC) binding to E-box regulatory elements situated in the *vri* promotors (Abruzzi, et al. 2011; Blau and Young 1999; Cyran, et al. 2003). Nevertheless, how *vri* expression is regulated? what is the significance of each transcript or protein for development and clock function? needs to be further characterized to understand VRI functions.

Here I generated two mutants to eliminate CLK-CYC dependent transcription of *vri*-ADF. First is a mutant transgene that lack four E-boxes situated near the *vri*-ADF promoter and they showed that these E-boxes are required for viability, which suggests that E-boxes control *vri* mRNA transcription during development and rhythmic *vri*-ADF transcription in adults. The second is $vri^{\Delta 679}$ mutant, which removes a portion of 1st exon and intron 1 of *vri*-ADF and eliminates *vri*-ADF mRNA production. This mutant is homozygous viable, which shows that *vri*-ADF mRNA is dispensable and *vri*-E mRNA is sufficient for development. Both *vri*-ADF and *vri*-E mRNAs are rhythmically expressed, through rhythmic CLK-CYC binding to their promoters. Although *vri*-ADF mRNA and long VRI are absent in $vri^{\Delta 679}$ flies, low levels of short VRI protein derived from *vri*-E mRNA are sufficient for behavioral rhythms. Rhythmically expressed *vri*-ADF mRNA produces low levels of long VRI and high levels of short VRI. I find that the poor production of long VRI correlates with a weak Kozak sequence and high levels of short VRI correlates with a strong Kozak sequence. These results suggest that in

Drosophila, *vri*-ADF transcripts primarily support circadian function and *vri*-E transcripts support circadian and developmental functions.

Results

E-boxes located on the vri-ADF promoter are essential for development function

CLK-CYC binding to E-box regulatory elements having the canonical sequence CACGTG drives rhythmic transcription (Darlington, et al. 1998; Yu and Hardin 2006). Four canonical E-boxes are situated within 1kb to 2.2kb upstream of *vri*-ADF transcription start site (Blau and Young 1999). These E-boxes are centered on the strongest CLK-CYC binding site in the *Drosophila* genome (Abruzzi, et al. 2011), and likely account for the high levels of rhythmic *vri* transcription (Blau and Young 1999). Reversal of the central CG base pair of these E-boxes resulted in a reduction of transcriptional activation in S2 cells indicating that these E-boxes are necessary for CLK-CYC dependent rhythmic *vri*-ADF transcription (Blau and Young 1999).

To test importance of the E-boxes in the promoter of *vri*-ADF, I generated an E-box mutant transgene using a ~70 kB BAC clone (CH321-28E21) that contains all the necessary regulatory elements required to rescue the development lethality of *vri* null mutants and drive strong, rhythmic vri mRNA cycling (Refer Chapter III). Four characterized E-boxes in the promoter of *vri*-ADF were deleted using site directed mutagenesis to generate the *vri*70kb$^{\Delta E\text{-}Box}$ mutant (Figure 6), which was integrated into three independent docking sites (VK5, VK13 and VK20) on chromosome 3 using *PhiC32*-mediated recombination (Venken, et al. 2006). Surprisingly, none of the

*vri*70kb$^{\Delta E\text{-}Box}$ transgenic lines rescued the development lethality of the *vri*^{5} null mutant, which suggests that these E-boxes are essential for development. Yet, it is difficult to make a conclusion on how these E-boxes impact development functions.

Subsequent analysis on *vri* promoters showed that there is an intact E-box found in the in the promoter of *vri*-ADF (Figure 6). This E-box is found in the reverse orientation and has not been characterized before for CLK-CYC binding. Nonetheless, this won't impact my conclusion that E-boxes found in the promoter of *vri*-ADF is required for viability.

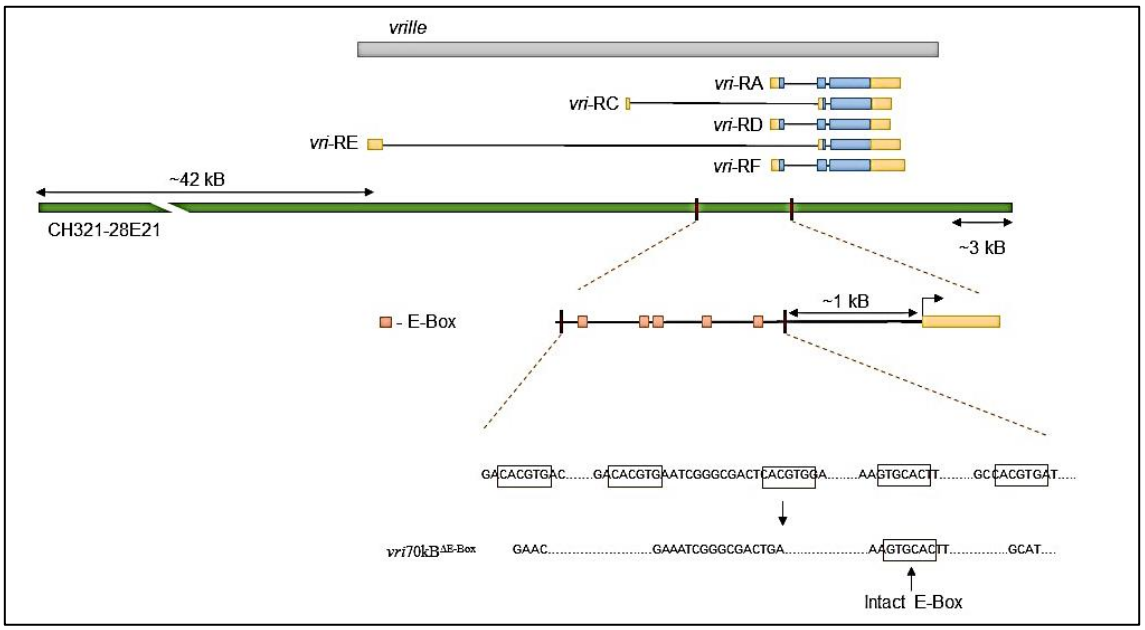

Figure 6. Schematic representation of *vri*70kb$^{\Delta E\text{-}Box}$ transgene generation
A ~70kB BAC clone was used to generate the *vri*70kb$^{\Delta E\text{-}Box}$ transgene. This BAC clone has ~42 kB upstream and ~3 kB downstream of the *vri* gene. There are 5 E-box located on the promoter of the *vri*-ADF. Using site directed mutagenesis I deleted the CACGTG sequences (indicated with squares) of 4 E-boxes in generating the *vri*70kb$^{\Delta E\text{-}Box}$ transgene. There is an intact E-box in the transgene as indicated.

vri-ADF transcription is dispensable for Drosophila development

Next, I sought to determine the functional significance of *vri*-ADF transcripts with respect to the clock by generating a mutant that eliminates these transcripts through deleting the 1st exon of *vri*-ADF (exon 1c) which is unique for *vri*-ADF. The vri^{d01873} P-element is inserted 4 bps upstream of the exon 1c transcription start site, is homozygous viable, and displays activity rhythms similar to those in w^{1118} wild-type controls (Table 1, Figure 7). Flies expressing P-element transposase were crossed with vri^{d01873} flies to excise the P-element, which contains the visible marker w^{+}. Although P-element transposase efficiently catalyzes precise P-element excision, imprecise excision occurs at a low rate (Figure 7, (Robertson, et al. 1988)).

Table 1. $vri^{\Delta 679}$ mutants show activity rhythms with a shorter period.

Genotype	N	% Rhythmic	Period ± SEM	Strength ± SEM
w^{1118}	25	92.9	23.43± 0.09	83.22± 10.46
$vri^{d01873,\ a}$	57	94.7	23.29± 0.04	104.97± 6.76
$vri^{\Delta 679,\ b}$	62	93.5	22.80± 0.04	96.62± 5.07
$vri^{\Delta 679}$;*vri* 24kB	21	100.0	23.19± 0.06	106.63± 9.81

[a] Complete genotype is w^{1118}; vri^{d01873};+, [b] Complete genotype is w^{1118}; $vri^{\Delta 679}$;+ The period of $vri^{\Delta 679}$ activity rhythms is significantly shorter than all other genotypes ($P<1.3x10^{-11}$). N, total number of flies tested.

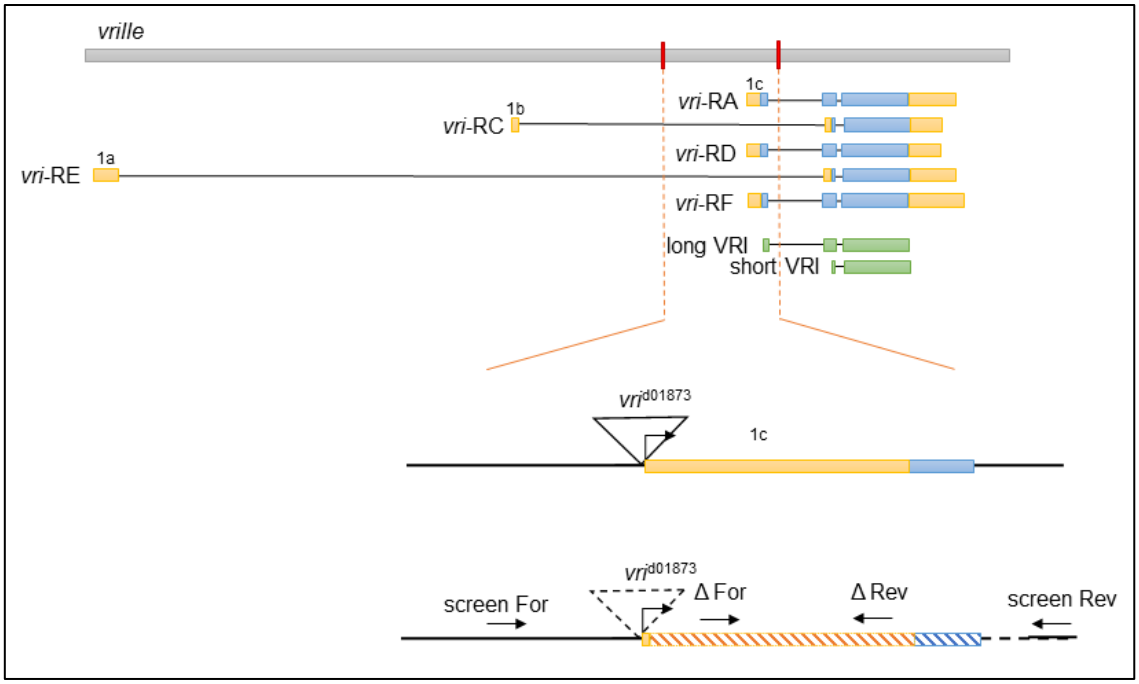

Figure 7. Generation of *vri*$^{\Delta 679}$ mutants
vri^{d01873} is inserted on the promoter of exon 1c that produce *vri*-ADF mRNA. *Δ2-3* P-element transposase was used to generate *vri*$^{\Delta 679}$ mutants, that lacks the region marked with diagonal or broken lines. Primers used for screening and characterization are indicated on the figure (Refer Table 2 for primer sequence information).

White-eyed progeny lacking the P-element were screened using 'screen' primers to identify flies carrying a deletion that disrupts exon 1c. The largest deletion mutant recovered, *vri* $^{\Delta 679}$, removes a 679bp region that includes all but the first 4 nucleotides of exon 1c and 167bp of intron 1 (Figure 7, Figure 8A). An 8bp sequence was inserted within the deleted region (data not shown), which may have resulted from a local hop of the P-element during the excision process (Tower, et al. 1993). Since the exon 1c transcription start is intact in *vri* $^{\Delta 679}$ flies, RT-qPCR was used to determine if exon 1c produces *vri* transcripts. The primers used to test for exon 1c containing transcripts produced amplification products in genomic DNA controls, but no amplification

products were generated via RT-PCR, suggesting that no transcripts are produced by exon 1c (Figure 8B). Despite the absence of *vri*-ADF mRNA expression, *vri* $^{\Delta 679}$ mutant flies are homozygous viable, confirming that intact exon 1c and *vri*-ADF mRNAs are not required for development.

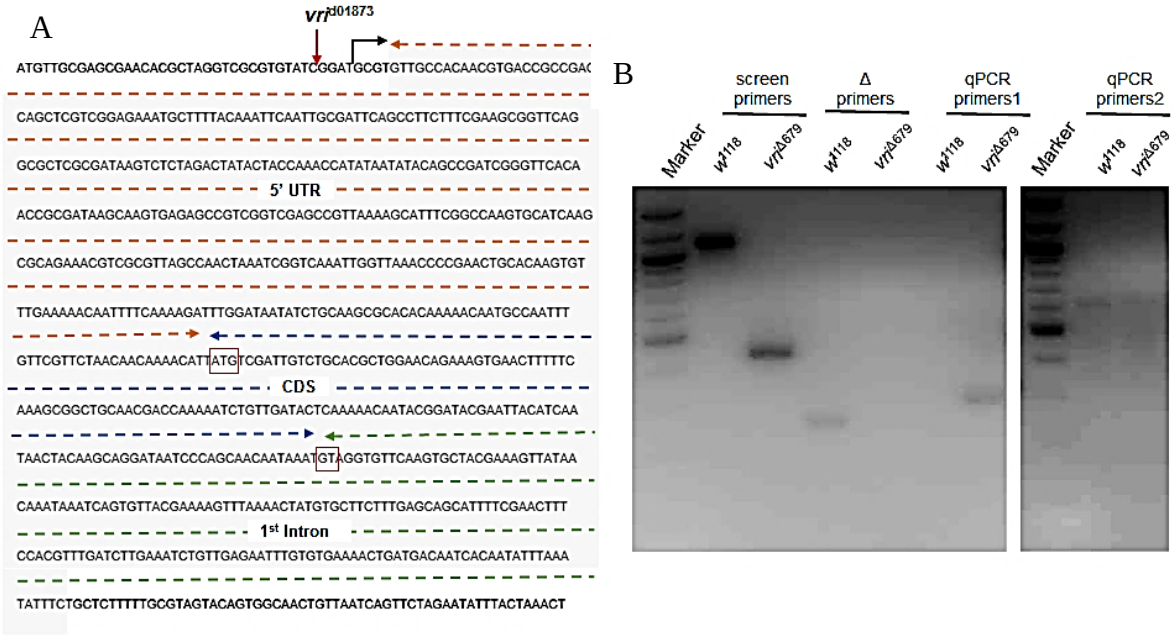

Figure 8. *vri*$^{\Delta 679}$ mutants lack *vri*-ADF transcript expression.
(A) *vri*$^{\Delta 679}$ mutants lacks the 5' UTR (except for the 1st four bps), the coding sequence (CDS) of 1st exon and a part of the 1st intron. This deletes out the start codon (ATG) and splice donor (GT) indicated with squares. (B) The gel is generated from genomic DNA (left) and cDNA (right) extracted from wild-type (*w*^{1118}) and *vri*$^{\Delta 679}$ mutants. The genomic DNA was amplified using screen primers, Δ primers and qPCR primers1. Control line produced a 1120 bp band with 'Screen' primers, whereas *vri*$^{\Delta 679}$ mutant produced a 441 bp band. Δ primer locations are indicated in Figure 7 and they give a 267 bp band only with wild-type. The qPCR forward primer contains the 4 remaining bases of the 5' UTR, the 8 bp coming from the P-element and the12 bps from the intact 1st intron (total 24 bps), while the reverse primer is Screen Rev is indicated in Figure 7. They gave a 275 bp band with *vri*$^{\Delta 679}$ mutants but not with wild-type controls. The gel to the left is generated using amplicons generated during qPCR using cDNA. qPCR was performed using a qPCR forward primer and a qPCR reverse primer. The qPCR reverse primer is located on 2nd exon. This primer pair did not give an amplicon during qPCR (Refer Table 2 for primer sequence information).

vri$^{\Delta 679}$ is a hypomorphic mutant

I expected *vri*$^{\Delta 679}$ mutants to be behaviorally arrhythmic because they lack the *vri*-ADF mRNAs thought to be required for clock output. Surprisingly, >93% of *vri*$^{\Delta 679}$ flies were rhythmic with a 0.5 h shorter period than w^{1118} controls (Table 1). Given the quasi-normal *vri*$^{\Delta 679}$ behavioral rhythms, I assessed VRI expression in *vri*$^{\Delta 679}$ brains. VRI levels in all *vri*$^{\Delta 679}$ brain pacemaker neurons were sharply reduced compared to w^{1118} control brains (Figure 9A). VRI expression in *vri*$^{\Delta 679}$ flies was then assessed in peripheral clock tissues. As in brain pacemaker neurons, retinal photoreceptor cells also exhibit a sharp reduction in VRI expression (Figure 9B). It was rather difficult to decide if photoreceptor cells also show low VRI expression due to the low signal to noise ratio. Likewise, VRI levels were low in Malpighian tubules (MTs) (Figure 9C), which mediate renal function in *Drosophila* (Dow 2009). The low VRI levels that remain in *vri*$^{\Delta 679}$ flies are rhythmically expressed in heads, photoreceptor cells and MTs + gut tissue (Figure 9D). Since *vri*$^{\Delta 679}$ flies lack *vri*-ADF transcripts, and the only other transcript produced in adults is *vri*-E, the low levels of VRI that remain in *vri*$^{\Delta 679}$ flies must be generated from *vri*-E mRNA.

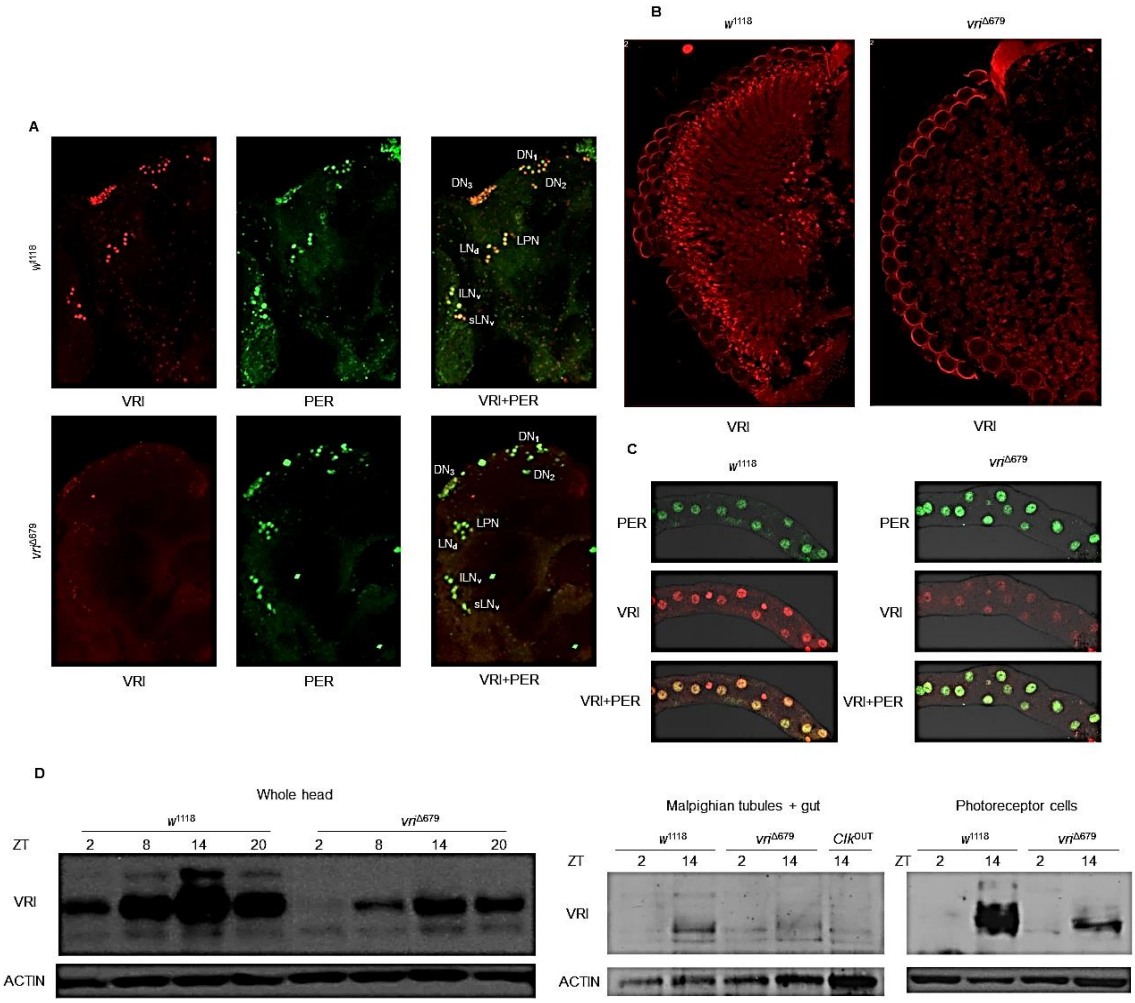

Figure 9. Low abundant rhythmic VRI expression is observed in *vri*$^{\Delta 679}$ mutants. (A) Brains from wild-type (w^{1118}) and *vri*$^{\Delta 679}$ mutant flies were collected at ZT20 and were immunostained with VRI (red) and PER (green) antisera. Merged VRI + PER images are shown in yellow. The following brain pacemaker neuron groups were detected: dorsal neuron 1 (DN_1), dorsal neuron 2 (DN_2), dorsal neuron 3 (DN_3), lateral posterior neuron (LPN), dorsal lateral neuron (LN_d), large ventrolateral neuron (lLN_v) and small ventrolateral neuron (sLN_v). (B) Cryo-sections of whole head going across eyes from w^{1118} and *vri*$^{\Delta 679}$ mutant flies collected at ZT20 were sectioned and immunostained with VRI (red) antiserum. (C) Malpighian tubules from w^{1118} and *vri*$^{\Delta 679}$ mutant flies were collected at ZT20 were immunostained with VRI (red) and PER (green) antisera. Merged VRI + PER images are shown as yellow. (D) Proteins from the indicated tissues of w^{1118}, *vri*$^{\Delta 679}$ and *Clk*^{OUT} mutant flies were collected during the LD cycle at specified times were used to generate western blots, which were probed with VRI antiserum to determine VRI abundance. ß-ACTIN (ACTIN) was used as a loading control.

To determine if *vri*-E mRNA is rhythmically expressed in adults with wild-type clocks, RT-qPCR was carried out on head RNA from control w^{1118} flies collected every 6h during a 12h light: 12h dark (LD) cycle. Forward primers situated in exon 1a or exon 1c were used in conjunction with a reverse primer in to amplify *vri*-E and *vri*-ADF transcripts, respectively. I find that both *vri*-ADF and *vri*-E are expressed rhythmically with a peak in expression at ZT15 and ZT9, respectively (Figure 10). However, the level of *vri*-E expression is drastically lower than that of *vri*-ADF. These results demonstrate that *vri*-ADF mRNAs constitute the vast majority of *vri* mRNA in fly heads.

Moreover, I found two clusters of E-Boxes found ~1.4kb and ~3.2kb upstream of exon 1a and another cluster of E-boxes on the 1st intron of *vri*-E (~2.5kb downstream from the transcription start site). The E-box cluster found ~3.2kb upstream of exon 1a corresponds to another strong CLK-CYC binding site (Abruzzi, et al. 2011). These results suggest reported CLK-CYC binding may account for the rhythmic expression of *vri*-E and the residual rhythmic VRI expression in $vri^{\Delta 679}$ mutants is due to *vri*-E mRNA.

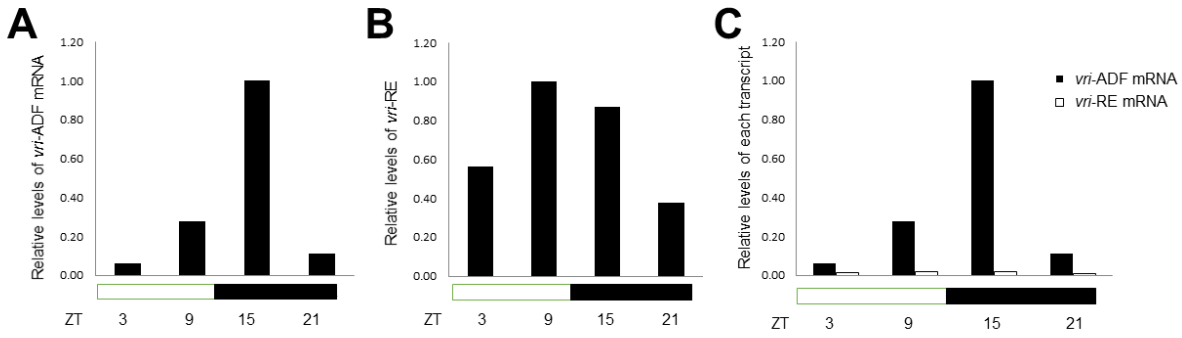

Figure 10. *vri*-ADF and *vri*-E mRNAs are expressed under the control of clock. (A) RT-qPCR quantification of *vri*-ADF mRNAs and (B) *vri*-E mRNA levels were from heads of w^{1118} flies collected during an LD cycle at the indicated times. (C) Comparison of *vri*-ADF and *vri*-E transcripts.

vri$^{\Delta 679}$ mutation affects the expression of long and short VRI proteins

Since the *vri*$^{\Delta 679}$ mutation eliminates *vri*-ADF mRNA expression, the low levels of VRI in these flies is thought to be produced by *vri*-E mRNA (Figure 9). However, abundance of both VRI protein isoforms are affected in *vri*$^{\Delta 679}$ flies (Figure 9D), which is surprising because *vri*$^{\Delta 679}$ mutation does not remove gene elements necessary for *vri*-E expression. Therefore, I speculated a gene mutation was introduced during the P-element mobilization, which affects the expression of *vri*-E (Tower, et al. 1993). If this is true, a gene complementation using *vri*-ADF specific transgene should not restore low abundant short VRI, however if it restores, then the conclusion is *vri*-ADF encodes both long and short VRI proteins. I used a 24kB BAC clone (CH322-102O15), which extends ~10 kB upstream and downstream of the *vri*-ADF transcription unit to complement the *vri*$^{\Delta 679}$ mutation (Figure 11A). This transgene, hereafter referred to as *vri*24kb, complemented the *vri*$^{\Delta 679}$ mutation by restoring the short period (~22.8h) activity rhythms of *vri*$^{\Delta 679}$ flies to ~23.2h, which is comparable to *vri*^{d01873} flies (Table 1), and also restored low VRI expression levels in *vri*$^{\Delta 679}$ brain pacemaker neurons and whole heads to wild-type intensities (Figure 11B-C). These results suggest that *vri*-ADF encodes both long and short VRI proteins, thus *vri*$^{\Delta 679}$ mutation affect the expression of both protein isoforms of VRI.

To identify the long VRI isoform produced by *vri*-ADF mRNA, I introduce a V5-3xHA epitope tag at the translation start of long VRI of *vri*24kb transgene (in future referred as V5-3xHA-*vri*24kb). To identify the large VRI isoform, western blots containing proteins from the heads of V5-3xHA-*vri*24kb and control *w*^{1118} flies were

collected at ZT14 and probed with VRI and HA antibodies. However, HA antibody was unable to detect a VRI band from the V5-3xHA-*vri*24kb strain (data not shown).

If the weak >90kDa VRI band in w^{1118} flies corresponds to long VRI, then the V5-3xHA tagged long VRI band may not be expressed at high enough levels to detect. Thus, I increased VRI levels by immunoprecipitating VRI from the heads of V5-3xHA-*vri*24kb flies collected at ZT14. These immunoprecipitates, along with head extracts from V5-3xHA-*vri*24kb and w^{1118} flies collected at ZT14, were used to prepare western blots that were probed with VRI and HA antibodies. VRI antibody detected three bands in V5-3xHA-*vri*24kb flies: a major band running at ~85kDa, a minor band running at >90kDa, and a minor band running at >95kDa (Figure 11D). Based on gel migration, the >95kDa band corresponds to V5-3xHA tagged long VRI that is also detected with HA antibody, the >90kDa band corresponds to the long VRI band in w^{1118} flies, and the ~85kDa band corresponds to the prominent VRI band in w^{1118} flies. These results demonstrate that long VRI is expressed at low levels compared to short VRI, and suggest that *vri*-ADF mRNA primarily produces short VRI rather than long VRI.

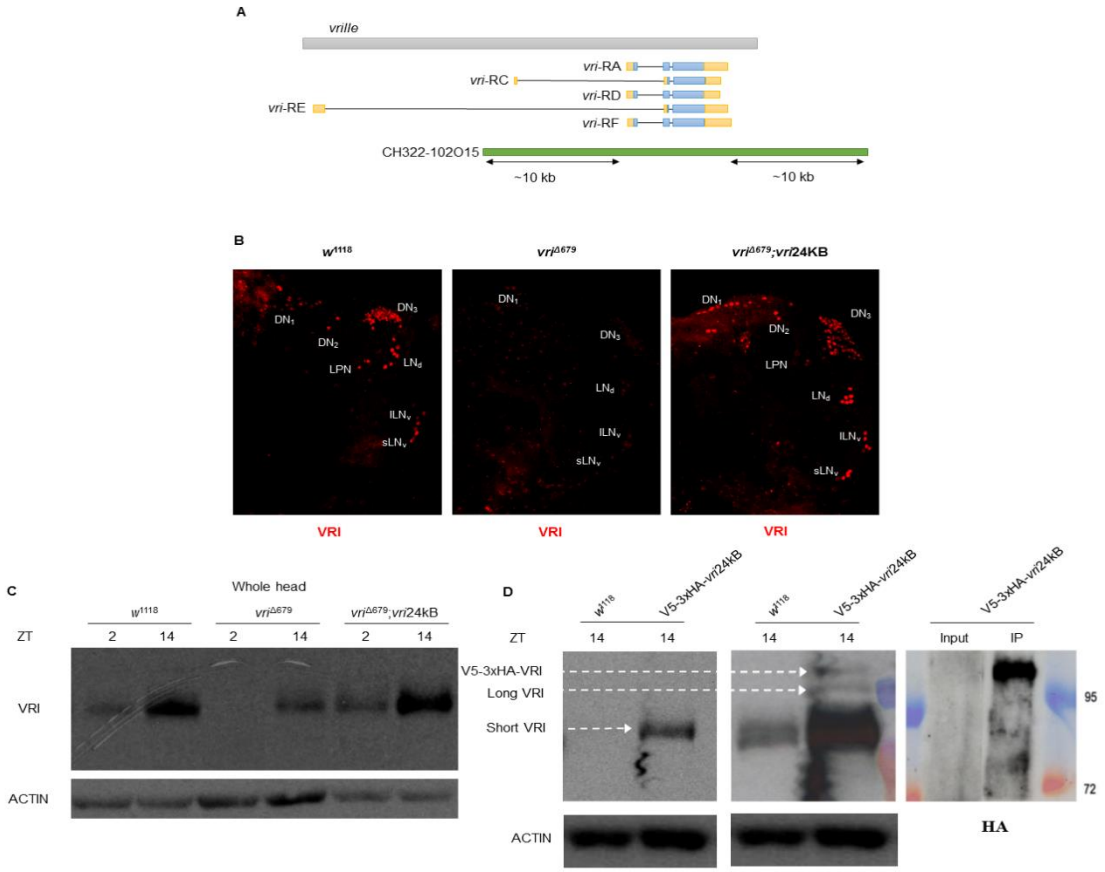

Figure 11. *vri*24kB transgene rescues *vri*$^{\Delta 679}$ mutant phenotypes.
(A) A ~24kB BAC clone was used to generate *vri*24kB and V5-3xHA-*vri*24kB transgenes. This BAC clone has ~10 kB upstream of the *vri*-ADF mRNA transcription start site and ~10 kB downstream of the *vri*-ADF mRNAs. (B) Brains from wild-type (w^{1118}), *vri*$^{\Delta 679}$ mutants and *vri*$^{\Delta 679}$; *vri*24kB flies were collected at ZT19 and were immunostained with VRI (red) antisera. The following brain pacemaker neuron groups were detected: dorsal neuron 1 (DN_1), dorsal neuron 2 (DN_2), dorsal neuron 3 (DN_3), lateral posterior neuron (LPN), dorsal lateral neuron (LN_d), large ventrolateral neuron (lLN_v) and small ventrolateral neuron (sLN_v). (C) Proteins from the heads of w^{1118}, *vri*$^{\Delta 679}$ mutants and *vri*$^{\Delta 679}$; *vri*24kB flies collected during LD at the specified times and were used to generate western blots, which were probed with VRI antiserum to determine VRI abundance. ß-ACTIN (ACTIN) was used as a loading control. (D) Proteins from the heads of w^{1118} and V5-3xHA-*vri*24kB flies collected at ZT14 and were used to generate western blots, which were probed with VRI antiserum to determine VRI abundance. Proteins extracted from the heads of V5-3xHA-*vri*24kB flies were IPed using HA conjugated beads and was used for western blotting. The membranes were probed with HA antiserum to label HA tagged proteins. Based on the migration speed, Long-VRI, Short-VRI and V5-3xHA-VRI were marked on the gel. ß-ACTIN (ACTIN) was used as a loading control.

A downstream short VRI AUG in vri-ADF mRNA having a strong Kozak sequence is preferred over the first AUG produces long and short VRI proteins

In adult flies, the prominent expression of short VRI is unexpected since *vri*-ADF mRNA represents the vast majority of all *vri* mRNA and encodes long VRI. To confirm that mRNA encoding long VRI produces short VRI, cDNA versions of long VRI coding sequences were overexpressed using either the Gal4/UAS system or the heatshock (hs) promoter, and also endogenous *vri*-ADF mRNA was overexpressed using the *vri*^{d01873} P-element, which is inserted 4bp upstream of exon 1c and drives Gal4 dependent expression via UAS sequences. In each case, both long and short VRI isoforms were produced, but heat induced hs-*vri* produced almost all long VRI, whereas *tim*(UAS)Gal4 driven UAS-*vri* and *tim*-Gal4 driven *vri*^{d01873} produced mostly short VRI (Figure 12A). This difference may stem from differences in the 5' UTRs that was used in these transgenic constructs.

The context sequence motif surrounding the AUG initiation codon influences mRNA translation efficiency and affects protein production. However, the optimal sequence differs among species. In many eukaryotes, strong initiation codons are accompanied by optimized Kozak sequence, which has an optimized sequence of GCCGCC[A|G]CC**AUG**G in *Drosophila* (Feng, et al. 1991). Using sequence analysis, I measured the strength of the Kozak sequence for the long VRI and short VRI start codons. Amazingly, the short VRI start codon had a stronger Kozak sequence with 8/13 identity while the long VRI start codon had a 5/13 identity (Figure 12B). In addition, previous work showed that having thymine on -3, -2, -1 and +4 locations with respect to

the translation initiation site make the initiation weaker (Feng, et al. 1991). The long VRI start codon had thymine at three out of four of these positions, whereas the short VRI start codon had no thymine in these positions (Figure 12B). These data suggest that the short VRI start codon possesses a strong Kozak sequence, which promotes translation with a higher probability.

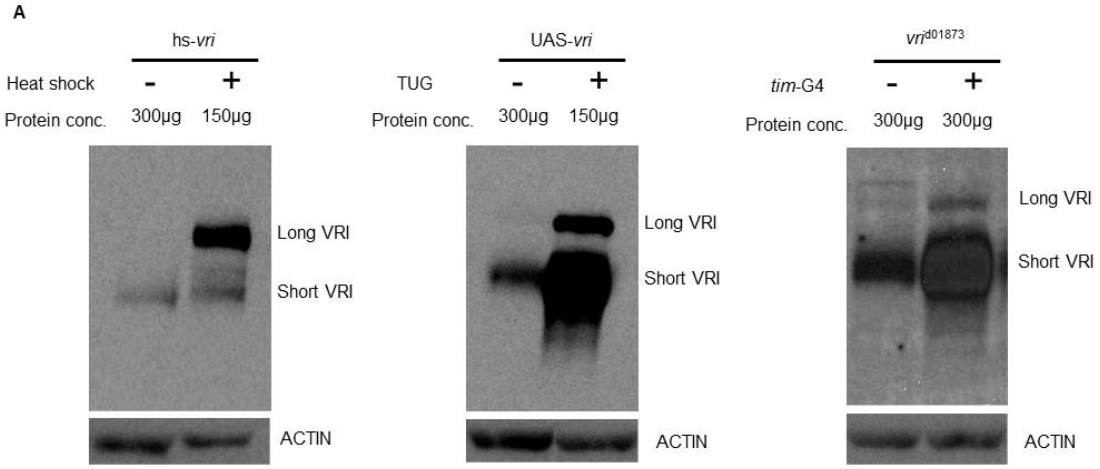

B

	-9	-8	-7	-6	-5	-4	-3	-2	-1	+1	+2	+3	+4	
Kozak sequence	**G**	**C**	**C**	**G**	**C**	**C**	**A/G**	**C**	**C**	**A**	**U**	**G**	**G**	
1st start codon	C	A	A	A	A	C	A	T	T	A	U	G	T	
	-	-	-	-	-	*	*	-	-	*	*	*	-	5/13
2nd start codon	T	C	C	A	C	A	G	C	A	A	U	G	C	
	-	*	*	-	*	-	*	*	-	*	*	*	-	8/13

Figure 12.vri-ADF mRNAs generate short protein using an alternative translation initiation site.
(A) Proteins from the heads of hs-*vri, +;* UAS-*vri*, *tim*-(UAS)-Gal4; UAS-*vri* (TUG; UAS-*vri*), *vri*^{d01873}; + and *vri*^{d01873}*;* tim-Gal4 (*vri*^{d01873}*;* tim-G4) flies collected after a heat shock (hs) if indicated and were used to generate western blots, which were probed with VRI antiserum to determine VRI abundance. Long VRI and short VRI proteins are indicated. ß-ACTIN (ACTIN) was used as a loading control. (C) Sequence similarities of Kozak sequence and two start codons are indicated. '*' indicates similarity and '-' indicates a difference. Numbers on the top specify the location of each base with respect to the 1st base of the start codon.

Conclusion

Previous work demonstrated that *vri* regulates developmental and clock-controlled processes in *Drosophila* (Blau and Young 1999; George and Terracol 1997). The *vri* gene produces multiple transcripts and two proteins during development and in adults (Blau and Young 1999; George and Terracol 1997; Glossop, et al. 2003), but it is unclear how important each transcript protein isoform is for development and clock functions. *vri* expression is activated upon CLK-CYC binding to E-boxes located on the promoter of *vri*. The strongest CLK-CYC binding site in the genome contains five E-boxes presents <2.2kb upstream of exon 1c (Abruzzi, et al. 2011), which presumably drives strong, rhythmic *vri*-ADF mRNA cycling. Mutations of these E-boxes in a transcriptional reporter construct, drastically reduced the reporter's transcription ability (Blau and Young 1999). When I tested whether the *vri*70kb$^{\Delta E\text{-box}}$ mutant, which removes multiple E-boxes upstream of exon 1c (Figure 7), eliminates *vri*-ADF mRNA cycling, I was surprised to find that these flies were not viable. This result suggests that E-boxes upstream of exon 1c are required for developmental expression of *vri*-E mRNA, which is sufficient to rescue developmental lethality. Several *Drosophila* bHLH transcription factors bind CACGTG E-boxes (Chang, et al. 2015; Jolley, et al. 2014). I speculate that during development one or more bHLH transcription factors bind E-boxes upstream of exon 1c and activate transcription from exon 1a.

The *vri*$^{\Delta 679}$ mutant specifically eliminates *vri*-ADF mRNA expression (Figure 8), which shortens the period of activity rhythms (Table 1). Since *vri*$^{\Delta 679}$ flies are homozygous viable, the only remaining *vri* mRNA expressed, *vri*-E, is sufficient to

rescue *vri* developmental and clock function. Although *vri*-E mRNA expression is dramatically lower than *vri*-ADF in adults, *vri*-E is rhythmically expressed (Figure 10). There is a CLK-CYC binding site containing two canonical E-boxes ~3.2kb upstream of exon 1a (Abruzzi, et al. 2011), which may account for *vri*-E mRNA cycling.

Long and short VRI isoforms are encoded by the *vri*-ADF and *vri*-E transcripts, respectively (Gramates, et al. 2017), but identifying short and long VRI bands on western blots has been a challenge since both VRI bands migrate much more slowly than the predicted short and long VRI molecular weights and the major VRI band in adults is the faster migrating band even though long VRI should be produced by abundant *vri*-ADF mRNA (Cyran, et al. 2003; Glossop, et al. 2003). The *vri*24kb transgene, rescued $vri^{\Delta 679}$ period shortening and restores high levels of rhythmic short VRI expression (Figure 11). This transgene was used generate another V5-3xHA-*vri*24kb transgene and used to identify the V5-HA tagged long VRI band. Based on gel migration, the HA tagged long VRI band corresponds to the slow migrating VRI band that runs at >90kDa, and I infer that the faster migrating band that runs at ~85kDa is short VRI.

Both long VRI and short VRI are produced by cDNAs or genomic DNA that encodes only long VRI (Figure 12). Since short VRI is produced using an in-frame AUG codon 119 amino acids downstream from the first AUG that initiates long VRI, I reasoned that the ribosome may not interact with the long VRI AUG as efficiently as the short VRI AUG. Indeed, the consensus Kozak sequence at the long VRI AUG is quite weak compared to that at the short VRI AUG.

Materials and Methods

Fly strains

The following fly strains were used in this study: w^{1118}, *st*[1] *Blm*[D2] *Sb*[1] P[*ry*[+t7.2]=*Δ2-3*]99B (P[*ry*+ *Δ2-3*], BDSC:8657), *tim*-Gal4 (Emery, et al. 1998), *tim*(UAS)Gal4 (Blau and Young 1999), $gl60^{j}$ (Moses, et al. 1989), vri^{d01873} (BDSC), UAS-*vri* (Blau and Young 1999) and hs-*vri* (Glossop, et al. 2003). Flies were reared on standard cornmeal/agar medium supplemented with yeast and kept in 12 h light/12 h dark (LD) cycles at 25°C

vri70kB$^{\Delta E\text{-}Box}$ transgene construction and transgenic fly generation

BAC clone CH321-28E21 (BacPac Resources) was used to generate the *vri*70kB$^{\Delta E\text{-}Box}$ transgene. Initially the E-boxes containing the region of the clone were sub-cloned into the TA vector (Invitrogen), using '*vri* E-box region' forward and reverse primers (Table 2). The resulting plasmid, $vri^{Ebox\text{-}TA}$, was used to mutate the E-boxes using the QuickChange II XL site directed mutagenesis kit (Stratagene, La Jolla, CA). For each E-Box, complementary forward and reverse primers were generated with the desired deletion (Table 2). All mutations were confirmed by sequencing. This plasmid is known as $vri^{\Delta Ebox\text{-}TA}$. The E-boxes containing region of the BAC clone was replaced by a *galK* selection gene with bacterial homologous recombination carried out using '*vri* E-box GalK homology' forward and reverse primers (Table 2). Then this *galK* gene was replaced with the E-box mutated PCR amplicon generated using '*vri* E-box region'

forward and reverse primers from *vri*$^{\Delta Ebox\text{-}TA}$ (Venken, et al. 2008). I used primers containing ~50 bp homology arms when carrying out the homologous recombination (see Table 2). After selection of recombinants and sequence verification, the resulting *vri*70kB$^{\Delta E\text{-}Box}$ transgene was inserted at VK5, VK13 and VK20 docking sites via *PhiC32*-mediated recombination (Venken, et al. 2006).

vri^{d01873} *P-element mobilization and vri*$^{\Delta 679}$ *mutant generation*

The *vri*^{d01873} insertional mutant line was initially backcrossed seven times to w^{1118} flies. Then *vri*^{d01873} flies were crossed to *P*[*ry*+ Δ2-3] flies containing the P-element transposase. Progeny of the cross that had white eyes were crossed to w^{1118}; *CyO*/*sco* flies. Once the chromosome that contained the P-element was homozygozous, the genomic DNA was extracted from 5-6 flies and screened for probable deletion with screen primers (Table 2, Figure 7).

Once *vri*$^{\Delta 679}$ mutant were determined using PCR and sequencing, the mutant line was backcrossed seven times to *vri*^{d01873} flies, to remove any anomalies that could have happened during the P-element mobilization event. This isogenized line was used for other experiments.

vri24kB and V5-3xHA-vri24kB transgenes construction and transgenic fly generation

BAC clone CH322-102O15 (BacPac Resources) was used to generate the *vri24*kb and V5-3xHA-*vri24*kb transgenes. The *vri24*kB transgene is a 24 kB BAC clone containing partial *vri* gene sequence (chr2L5295134 - chr2L5319513) without any

modifications. This transgene was inserted at the VK33 docking site via *PhiC32*-mediated recombination (Venken, et al. 2006).

The V5-3xHA-*vri24*kB transgene has an N-terminal V5 and 3xHA epitope introduced to the *vri24*kB transgene using homologous bacterial recombination (Venken, et al. 2008). The V5-3xHA epitopes were inserted immediately downstream of the start codon of *vri*-ADF mRNAs, using a V5-3xHA recombination cassette comprised of the V5-3xHA epitope sequence, a *Kanamycin* (*Kan*) gene flanked by loxP sites, and two homology arms generated via PCR using the 'V5-3xHA-vri Homology Forward' and 'V5-3xHA-vri Homology Reverse' primers (Table 2). After selection for recombinants and sequence verification, the *Kan* cassette was removed using CRE recombinase as described (Venken et. al 2008). After sequence verification, the resulting V5-3xHA-*vri24*kB transgene was inserted at the VK20 docking site via *PhiC32*-mediated recombination (Venken et. al., 2006).

Drosophila activity monitoring and behavior analysis

All fly strains used in behavior experiments were backcrossed seven times to w^{1118} flies to minimize effects due to differences in genetic background. Locomotor activity was monitored using the *Drosophila* Activity Monitor (DAM) system (Trikinetics). One to three days old male flies were placed in monitors, and activity was recorded for 3 days in 12:12 light-dark (LD) cycles and 7 days in contact darkness (DD) at 25ºC. Analyses of period, power and rhythm strength during constant darkness (DD)

was carried out using ClockLab (Actimetrics) software as previously described (Agrawal and Hardin 2016).

Immunostaining

Fly tissues were processed for immunostaining as previously described (Houl, et al. 2008), with minor modifications. Larval brains were dissected at the L3 stage and adult tissues were dissected 3-5 days after eclosion. Dissected tissues were fixed with 3.7% formaldehyde, washed and blocked in PAXD buffer (1X PBS, 5% BSA, 0.03% sodium deoxycholate, 0.03% tritonX100) with 5% donkey or goat serum for 1 hour, and incubated with primary and secondary antibodies diluted in PAXD buffer. The following primary antibodies were used: guinea pig anti-VRI GP3 1:25,000, rabbit anti-HA ab9110 (Abcam) 1:200, pre-absorbed rabbit anti-PER (a gift from Michael Rosbash Laboratory, Brandeis University). The following secondary antibodies were used at a 1:200 dilution: goat anti-rabbit Alexa 647 (Molecular Probes), goat anti-guinea pig Cy-3 (Jackson ImmunoResearch Laboratories, Inc.).

Cryosectioning

Wild type (w^{1118}) flies were sectioned into 10µM thickness sections and collected on slides. All sections were fixed with 3.7% formaldehyde for 15 minutes. The rest of the procedure was identical to the wholemount immunostaining procedure outlined under the immunostaining section.

Confocal microscopy and image analysis

Confocal imaging was carried out as described (Agrawal, et al. 2017), with minor modifications. Fly tissues were imaged using an Olympus FV1000 confocal microscope 20x /0.8 NA or 100x /1.4 NA oil immersion objective lenses. Serial optical scans were obtained at 3 μM intervals (with 20x objective lens) Original Olympus images were saved as 12-bit oib format. Preliminary image processing was carried out using either FV1000 confocal software or Adobe Photoshop.

Western blotting

Western blot analyses were conducted as described (Zhou, et al. 2016), with minor modifications. After protein extraction, equal amounts of RIPA S extract were run, transferred, and probed with guinea pig anti-VRI GP3, 1:5,000, rabbit anti-HA, 1:5,000 and mouse anti-beta-actin (Abcam), 1:20,000. Horseradish peroxidase-conjugated secondary antibodies (Sigma) against guinea pig, rabbit and mouse were diluted 1:5,000. Immunoblots were visualized using ECL plus (GE) reagent. For western experiments with hs-*vri* flies, the flies were subjected to a 37°C heat shock for 30 minutes and allowed to recover for 4 hours and then the protein was harvested.

RNA extraction, quantitative RT-PCR and data analysis

RNA extraction and quantitative RT-PCR was performed as described (Zhou, et al. 2016), with minor modifications. Flies were entrained in 12:12 light-dark (LD) for at least 3 days, collected at the indicated time points, and frozen. For RNA extracted from

embryos, larvae and pupae all sub-stages were pooled together to represent all sub-stages. Total RNA was isolated and cDNA was synthesized using Superscript II (Invitrogen). The reverse transcription (RT) product was amplified with SsoFast qPCR Supermix (Bio-Rad) in a Bio-Rad CFX96 Real-Time PCR System using pairs of gene-specific primers (Table 2). For each sample, mRNA quantity was determined. *rp49* mRNA levels were used as a normalization control when determining the relative levels of mRNA. Student two-tailed t-tests with unequal variances were performed to determine whether differences were statistically significant.

Oligo information

Table 2. Sequence information of oligo

Oligonucleotides	
Sequence name	**Sequence**
***vri*70kB$^{\Delta E\text{-}Box}$ generation**	
vri E-box region Forward	5' – GTTCCTTCTCTCGAAGGACCACT – 3'
vri E-box region Reverse	5' – GCTGGGGAGTTGGGAAAACTG – 3'
vri E-box 1 mutation Forward	5' – GCTGGTGCCTCCACGAACCGCTCCGC – 3'
vri E-box 1 mutation Reverse	5' – GGCTAGTGCAACGCTCCCCAACAGCC – 3'
vri E-box 2&3 mutation Forward	5' – AATCGGGCGACTGATATCGCGCAG – 3'
vri E-box 2&3 mutation Reverse	5' – TCCGGACCAATCGTAGTCGGATCCG – 3'
vri E-box 4 mutation Forward	5' – CCCATCTGTCGATTTGTTCGTCGTAC – 3'
vri E-box 4 mutation Reverse	5' – CGCTTTGAAACTTTGGATAGTTTAACAAGGGG – 3'
vri E-box GalK homology Forward	5' – TTGGCTTGCGTAGCCGACTCAAGTCGCCAACATGTGAGCCGTCGCAGGCCCCTGTTGACAATTAATCATCGGCA – 3'

Table 2. Continued.

Oligonucleotides	
Sequence name	**Sequence**
***vri*70kB$^{\Delta E\text{-}Box}$ generation** *vri* E-box GalK homology Reverse	5' – ATACGTACATATGTATATTTGAAGTTCCAATCAGTGA ATTTTTGGGTTTCTCAGCACTGTCCTGCTCCTT – 3'
***vri*$^{\Delta 679}$ generation** Screen Forward	5' – CGGCAATGTGATCGCTTGCAAC – 3'
Screen Reverse	5' – CATGCACGTACACTTAAGCGCTC – 3'
Δ Forward	5' – GATCGGGTTCACAACCGC – 3'
Δ Reverse	5' – GTTCACTTTCTGTTCCAGCGTG – 3'
Δ679 qPCR Forward	5' – GCGTCATGATGATGCTCTTTTGC – 3'
V5-3xHA-*vri*24kb generation V5-3xHA-*vri* Homology Forward	5' – AAGCGCACACAAAAACAATGCCAATTTGTTCGTTCTA ACAACAAAACATTGCAGCCCAATTCCGATCATATTC – 3'
V5-3xHA-*vri* Homology Reverse	5' – GTTCACTTTCTGTTCCAGCGTGCAGACAATCGAGGCG TAATCGGGCACATCGTAGGGGTAGCCGGCATAGTCCG GCACGTCATACGGATAGCCGGCGTAATCGGGCACATC GTAGGGGTAACCGGTACGCGTAGAATCGAGACCGAG GAGAGGGTTAGGGATAGGCTTACCCATTGGATCCCCT CGAGGGACCTAATAAC – 3'

Table 2. Continued.

Oligonucleotides	
Sequence name	**Sequence**
RT-qPCR primers	
vri-ADF qPCR Forward	5’ – ACGCTGGAACAGAAAGTGA – 3’
vri-E qPCR Forward	5’ – CATAACGACCAACGGCCG – 3’
vri-ACDEF qPCR Reverse	5’ – GCTAGTTTCTGCTGCAGTTG – 3’
vri qPCR Forward	5’ – ATGAACAACGTCCGGCTATC – 3’
vri qPCR Reverse	5’ – CTGCGGACTTATGGATCCTC – 3’
rp49 qPCR Forward	5’ – TACAGGCCCAAGATCGTGAA – 3’
rp49 qPCR Reverse	5’ – GCACTCTGTTGTCGATACCC – 3’

CHAPTER III

VRILLE CONTROLS PDF NEUROPEPTIDE ACCUMULATION AND ARBORIZATION RHYTHMS IN SMALL VENTROLATERAL NEURONS TO DRIVE RHYTHMIC BEHAVIOR IN *DROSOPHILA*

Background

As in other organisms, the core timekeeping loop in *Drosophila* functions in concert with interlocked feedback loops, which drive rhythmic transcription of activators within the core feedback loop (Hardin and Panda 2013; Partch, et al. 2014). The transcriptional repressor VRI is a core element of the *Drosophila* interlocked feedback loop, but the developmental lethality of *vri* mutants has precluded determining the role *vri* plays in circadian timekeeping and/or output. The impact of *vri* on clock function is based on *vri* overexpression, which reduces *tim* and *per* mRNAs due to repression of *Clk* transcription, and abolishes activity rhythms (Blau and Young 1999). In addition, *vri* overexpression in L3 larvae eliminates PDF accumulation despite normal levels of *pdf* mRNA in ventrolateral neurons (LN_vs) in the larval brain (Blau and Young 1999), suggesting that *vri* suppresses PDF accumulation at the post-transcriptional level. In adults, PDF expression in LN_vs is required for locomotor activity rhythms (Renn, et al. 1999), thus loss of *vri* would be predicted to abolish activity rhythms.

---

*This chapter is reprinted with permission from Gunawardhana KL, Hardin PE (2017). VRILLE controls PDF neuropeptide accumulation and arborization rhythms in small ventrolateral neurons to drive rhythmic behavior in *Drosophila*. Current Biology. Volume 27, Issue 22, Pages 3442-3453.e4.

VRI binds to D-boxes located on the promoter of Clk to repress transcription and it is hypothesized VRI also binds many other rhythmic output genes that peak near dawn, similar to Clk, to support metabolic, physiological and behavioral functions. Given the possibility that *vri* could affect the circadian transcription of many target genes, understanding the role that *vri* plays in the clock in of critical importance.

To determine whether *vri* is necessary for core feedback loop function and rhythmic behavior, I constructed a BAC transgene that rescues *vri* null mutant lethality, but can be conditionally inactivated to generate adult tissues that lack *vri* function. When *vri* function is eliminated in all clock cells or just LN_v pacemaker neurons, rhythms in locomotor activity are lost, but core feedback loop function persists, suggesting that *vri* is necessary for clock output. Inactivating *vri* in LN_vs decreases *pdf* mRNA and protein accumulation at the post-transcriptional level in small LN_vs (sLN_vs). The low levels of PDF in sLN_vs from cyc^{01} flies, which do not express *vri* (Blau and Young 1999), can be rescued by transient *vri* expression, demonstrating that VRI is sufficient for PDF accumulation. Restoring PDF in sLN_vs from *vri* inactivated flies does not rescue activity rhythms, suggesting that *vri* targets other processes required for rhythmic activity. Indeed, *vri* is also required for daily rhythms in sLN_v dorsal projection arborization, which support activity rhythms. My results suggest that *vri* functions as a key regulator of clock output by driving rhythmic transcription of target genes that peak near dawn.

Results

The vri70kb^{FRT} transgene rescues developmental lethality of vri null mutants and sustains wild-type circadian clock function

The *vri* gene uses three alternative first exons to generate five transcripts required for developmental and circadian functions (Gramates, et al. 2017). Since *vri* null mutants cause developmental lethality (George and Terracol 1997), I used a ~70kB BAC clone (CH321-28E21) to generate a *vri* transgene predicted to contain all regulatory elements necessary for developmental and circadian regulation (Figure 13A). To test whether *vri* is required for clock function in adults, two FRT sequences flanking the 3rd exon, which contains the bZIP domain, were introduced to effect conditional inactivation using FLP recombinase (see below). This transgene, which I refer to as *vri*70kb^{FRT}, rescued the developmental lethality of three *vri* null alleles: the *vri*^{k03801} and *vri*^{5} P-element inserts and the *vri*^{2} point mutant.

To determine whether the *vri*70kb^{FRT} transgene supports clock function, I assessed activity rhythms in *vri*70kb^{FRT} flies bearing endogenous wild-type or *vri*^{k03801}, *vri*^{5} or *vri*^{2} mutant alleles. In combination with the *vri*^{k03801}, *vri*^{5} or *vri*^{2} null alleles, the *vri*70kb^{FRT} transgene supported activity rhythms with a period similar to *w*^{1118} controls of ~23.5h (Table 3, Figure 13B). The percentage of rhythmic flies varied depending on the *vri* mutant allele, with *vri*^{k03801} and *vri*^{5} producing >85% rhythmic flies and *vri*^{2} only producing ~40% rhythmic flies (Table 3). This difference is likely due to isogenization: the *vri*^{k03801} and *vri*^{5} P-element inserts were isogenized to my *w*^{1118} control strain, but not

the *vri*^{2} point mutant. All subsequent experiments were carried out with flies bearing the *vri*^{5} allele and the *vri*70kb^{FRT} transgene. When *vri*70kb^{FRT} was tested with an endogenous wild-type *vri* allele, the period of activity rhythms was significantly ($p < 0.05$) lengthened to >23.8h (Table 3; Figure 13B), consistent with period lengthening in flies that overexpress *vri* (Blau and Young 1999).

Molecular rhythms in VRI expression were tested in whole heads, where most expression emanates from photoreceptor cells (Glossop, et al. 2003), and in brain pacemaker neurons. In heads, VRI produced by the *vri*70kb^{FRT} transgene cycled similarly to endogenous VRI in LD and DD, with highest levels between ZT11 and ZT19 during LD and between Circadian Time 11 (CT15, where CT0 is subjective lights on and CT12 is subjective lights off) and CT19 during the first day of DD (Figure 13C, D). In brains, VRI produced by the *vri*70kb^{FRT} transgene was detected in every group of circadian pacemaker neurons seen in *w*^{1118} controls (Figure 13E), and VRI levels cycled in LN_vs with high levels from CT11-CT19 and lower levels from CT23-CT7 (Figure 13F), consistent with VRI cycling in whole heads. These results demonstrate that the *vri*70kb^{FRT} transgene supports rhythms in *vri* expression indistinguishable from control flies.

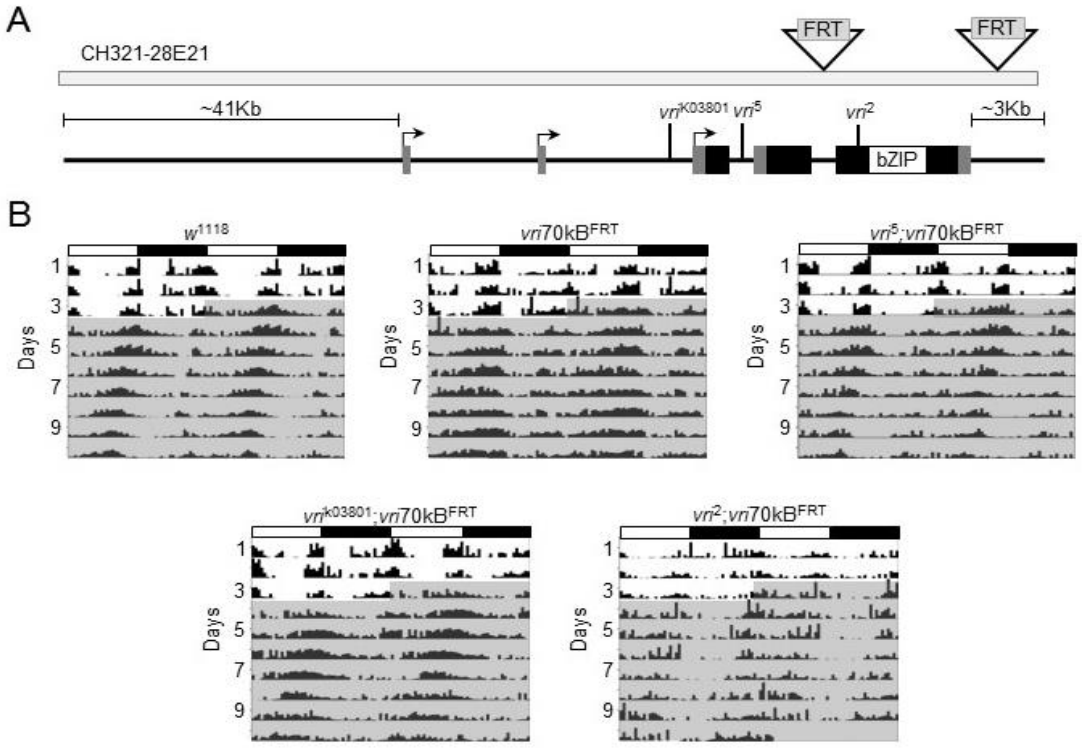

Figure 13. Behavioral and molecular analysis of *vri*70kb^{FRT} flies.
(A) A ~70kB BAC clone was used to rescue *vri* null mutants *vri*^{k03801}, *vri*^{5} and *vri*^{2}. The *vri*70kB^{FRT} transgene contains two FRT sequences flanking the 3rd exon, which contains the b-ZIP domain. (B) Representative actograms from flies of the indicated genotypes. Flies were entrained, monitored and analyzed as described (see Materials and Methods). White boxes, light phase of the LD cycle; black boxes, dark phase of the LD entrainment cycle; white background, LD portion of actogram; shaded background, DD portion of actogram. (C) Proteins from the heads of wild-type (*w*^{1118}) and *w*^{1118};*vri*^{5};*vri*70kB^{FRT} (*vri*70kB^{FRT}) flies collected during LD at the indicated times were used to generate western blots, which were probed with VRI antiserum to determine VRI abundance. (D) Quantification of VRI protein from heads of *vri*70kB^{FRT} flies collected at the indicated times during LD and DD was carried out as described from three independent sets of samples. ß-ACTIN (ACTIN) was used as a loading control. (E) Brains from *w*^{1118} and *vri*70kB^{FRT} flies collected on day 3 of DD were immunostained with VRI (red) and PER (green) antisera. Merged VRI + PER images are shown as yellow. The following brain pacemaker neuron groups were detected: dorsal neuron 1 (DN_1), dorsal neuron 2 (DN_2), dorsal neuron 3 (DN_3), lateral posterior neuron (LPN), dorsal lateral neuron (LN_d), large ventrolateral neuron (lLN_v) and small ventrolateral neuron (sLN_v). (F) Brains from *w*^{1118} and *vri*70kB^{FRT} flies collected at the indicated times on day 3 of DD were immunostained with VRI (red) antiserum. Immunostaining was imaged in LN_v pacemaker neurons as described (see Materials and Methods). See also Table 3.

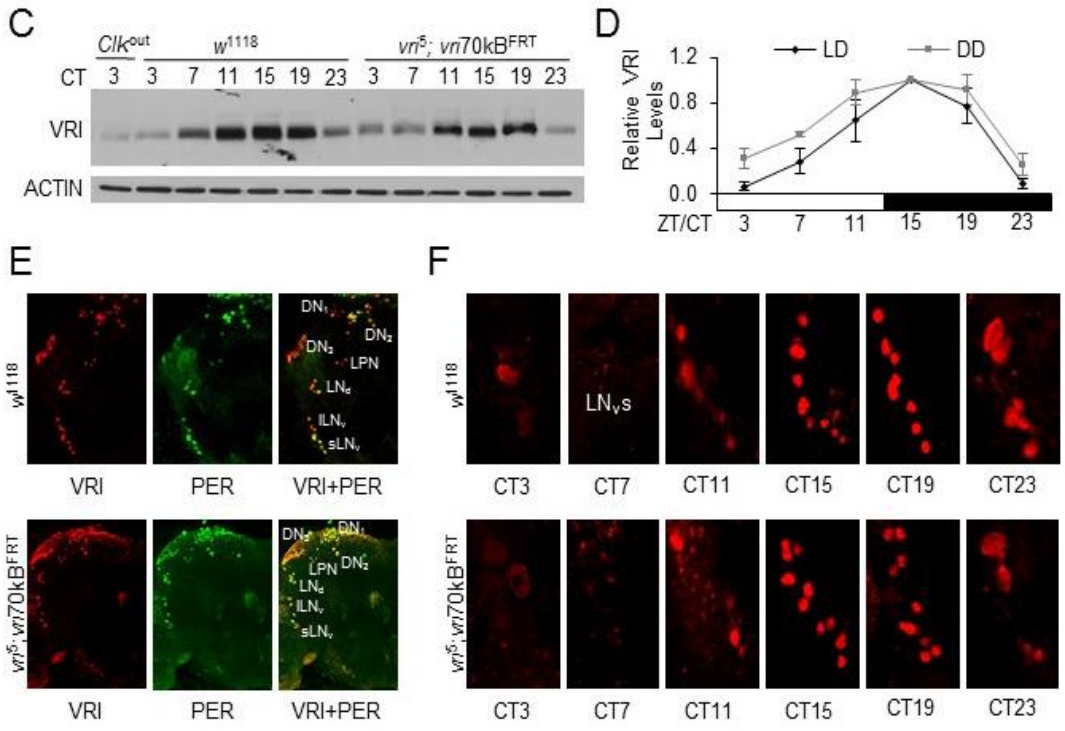

Figure 13. Continued.

Table 3. The *vri*70kb^{FRT} transgene supports activity rhythms in *vri* null mutants.

Genotype	N	% Rhythmic	Period ± SEM	Strength ± SEM
w^{1118}	58	96.5	23.52± 0.04	91.67± 5.60
*vri*70kB$^{FRT\ a}$	105	92.4	23.87± 0.15 [e]	72.59± 4.27
vri^{5};*vri*70kB$^{FRT\ b}$	107	86.0	23.43± 0.03	40.07± 2.08
vri^{k03801};*vri*70kB$^{FRT\ c}$	16	93.8	23.47± 0.11	49.03± 9.22
vri^{2};*vri*70kB$^{FRT\ d}$	26	42.3	23.27± 0.11	27.03± 5.51

[a] Complete genotype is w^{1118};+;*vri*70kB^{FRT}/+.[b] Complete genotype is w^{1118};vri^{5};*vri*70kB^{FRT}/+.[c] Complete genotype is w^{1118}; vri^{k03801};*vri*70kB^{FRT}/+.[d] w^{1118};vri^{2};*vri*70kB^{FRT}/+.[e] The period of *vri*70kB^{FRT} activity rhythms is significantly longer than all other genotypes (P<0.05). N, total number of flies tested.

The vri70kB^{FRT} transgene can be conditionally inactivated in space and time

My strategy for inactivating the *vri*70kb^{FRT} transgene was to catalyze recombination between the FRT elements flanking *vri* exon 3 by expressing FLP recombinase in different tissues and/or developmental stages using the UAS-GAL4 system (Figure 14A). Two clock cell specific Gal4 drivers were used to drive UAS-*flp*: *tim*-Gal4, which are expressed in all clock cells, and *pdf*-Gal4, which is expressed exclusively in large LN_vs (lLN_vs) and all sLN_vs except the 5th sLN_v (Emery, et al. 1998; Park, et al. 2000; Rieger, et al. 2006). The *vri*70kb^{FRT} transgene was verified in strains containing these drivers by the presence of a 392bp PCR product, while inactivation of the transgene by FRT mediated recombination was confirmed by the presence of a 649 bp PCR product (Figure 14B). Low levels of the 649 bp band were detected in the control *vri*70Kb^{FRT},UAS-*flp* genotype. When the *vri*70kb^{FRT} transgene was recombined with the *pdf*-Gal4 driver to generate *vri*70Kb^{FRT}, *pdf*-Gal4 flies the 649bp band was lost, suggesting that the low levels of inactive transgene in *vri*70Kb^{FRT},UAS-*flp* flies was due to leaky FLP expression.

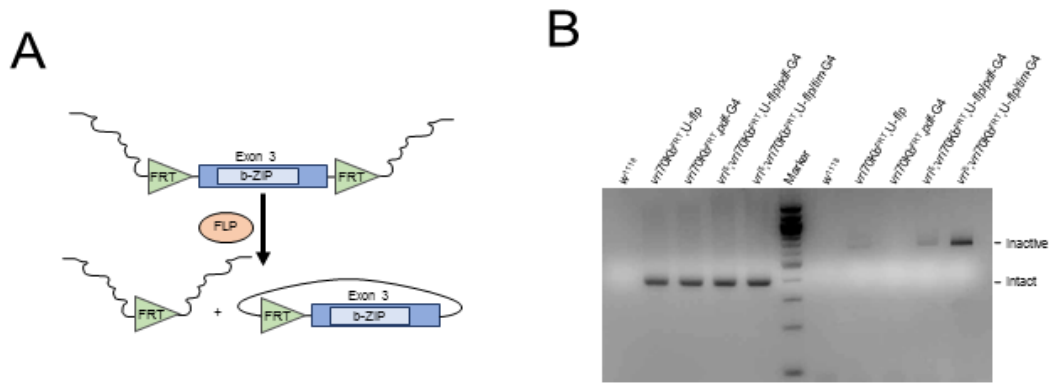

Figure 14. The *vri*70kB^{FRT} transgene can be effectively inactivated.
(A) Schematic outline of the strategy used to inactivate the *vri*70kB^{FRT} transgene. The intact *vri*70kB^{FRT} transgene is shown on top, and FLP catalyzed recombination products are shown on the bottom. Twisted black line, *vri* genomic DNA upstream and downstream of exon 3; FRT, flippase recognition target sequence; straight black line, sequence between FRT sites and exon 3; blue box, *vri* exon 3; white box, basic-zipper (b-ZIP) domain within *vri* exon 3; black arrow, recombination reaction; FLP, flippase recombinase generated via the UAS/GAL4 or UAS/GS systems. (B) PCR analysis of *vri*70kB^{FRT} transgene inactivation in w^{1118}, w^{1118};*vri*70kB^{FRT}, UAS-*flp* (*vri*70kB^{FRT}, U-flp), w^{1118};*vri*70kB^{FRT} , *pdf*-Gal4 (*vri*70kB^{FRT} , *pdf*-G4), w^{1118};*vri*^{5};*vri*70kB^{FRT}, UAS-flp/tim-Gal4 (*vri*^{5};*vri*70kB^{FRT}, U-*flp*/*pdf*-G4) and w^{1118}; *vri*^{5};*vri*70kB^{FRT}, UAS-*flp*/*tim*-Gal4 (*vri*^{5};*vri*70kB^{FRT}, U-*flp*/*tim*-G4) flies. Genomic DNA from each strain was isolated and amplified using primers that detect a 392bp intact or a 649bp inactivated *vri*70kB^{FRT} transgene band (Table 3; see Materials and Methods). A 100bp ladder was used as a molecular weight DNA marker.

Upon activation of UAS-*flp* with *tim*-Gal4 in *vri*^{5};*vri*70kb^{FRT} flies, VRI expression was eliminated in all brain pacemaker neurons, which are marked by PER (Figure 15A). Likewise, activation of UAS-*flp* by *pdf*-Gal4 in *vri*^{5};*vri*70kb^{FRT} flies eliminated VRI expression only in lLN_vs and sLN_vs, but persisted in other brain pacemaker neuron groups including the 5th sLNv (Figure 15A). These results demonstrate that tissue-specific activation of FLP efficiently inactivates *vri*.

To catalyze time-specific UAS-*flp*-mediated inactivation of *vri*, the Geneswitch system was employed (Osterwalder, et al. 2001; Roman, et al. 2001). In this system, Gal4 was modified so that it is only active in the presence of the progesterone analog mifepristone (RU486), which is administered to *Drosophila* in their food. An extant *pdf*-Geneswitch (*pdf*-GS) driver was used to activate UAS-*flp* expression in lLN_vs and sLN_vs once adults emerged from their pupal cases (Depetris-Chauvin, et al. 2011). Flies treated with RU486 lost VRI expression specifically in lLN_vs and sLN_vs (Figure 15A), while control flies treated with the vehicle used to dissolve RU486 (i.e ethanol) expressed VRI in all brain pacemaker neurons including lLN_vs and sLN_vs (Figure 15A). These experiments indicate that the *vri*70kB^{FRT} transgene can be efficiently inactivated in lLN_vs and sLN_vs at any developmental stage by the addition of RU486 to generate conditional *vri* mutants.

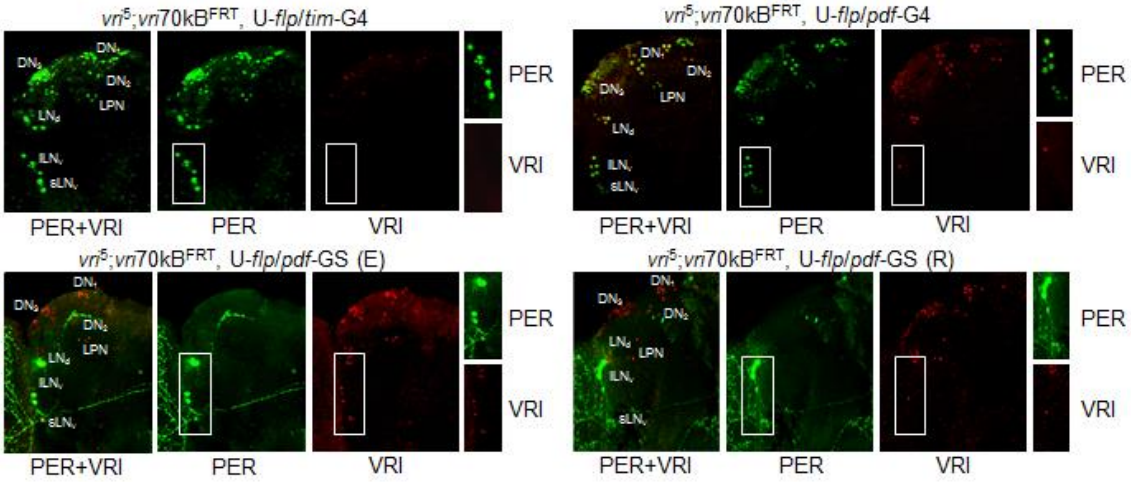

Figure 15. Tissue specific inactivation of the *vri*70kb^{FRT} transgene leads to arrhythmic activity in flies.

(A) Immunostaining of brains from *vri*^{5};*vri*70kB^{FRT}, U-*flp*/*tim*-G4, *vri*^{5};*vri*70kB^{FRT}, U-*flp*/*pdf*-G4 and *w*^{1118};*vri*^{5};*vri*70kB^{FRT}, UAS-*flp*/*pdf*-GeneSwitch (*vri*^{5};*vri*70kB^{FRT},U-*flp*/*pdf*-GS) flies collected at CT20 on DD day 3 with VRI (red) and PER (green) antisera. Merged VRI + PER images are shown as yellow. The *vri*^{5};*vri*70kB^{FRT},U-*flp*/*pdf*-GS flies were treated with ethanol (E) vehicle as a control or RU486 (R) dissolved in vehicle to induce GS activity. White boxes, LN_v region magnified on the right. Symbols denoting groups of pacemaker neurons are as described in Figure 13. (B) Representative actograms from flies of the indicated genotypes. Flies were entrained, monitored and analyzed as described (see Materials and Methods). White boxes, light phase of the LD entrainment cycle; black boxes, dark phase of the LD cycle; white background, LD portion of actogram; shaded background, DD portion of actogram. (C) Average activity histograms indicating relative levels of locomotion for the indicated genotypes during LD days 2-7 are shown. Zeitgeber Time (ZT), time in hours during an LD cycle where lights-on is ZT0 and lights-off is ZT12; white bars, daytime activity; black bars, night time activity; 16 flies were tested for each genotype.

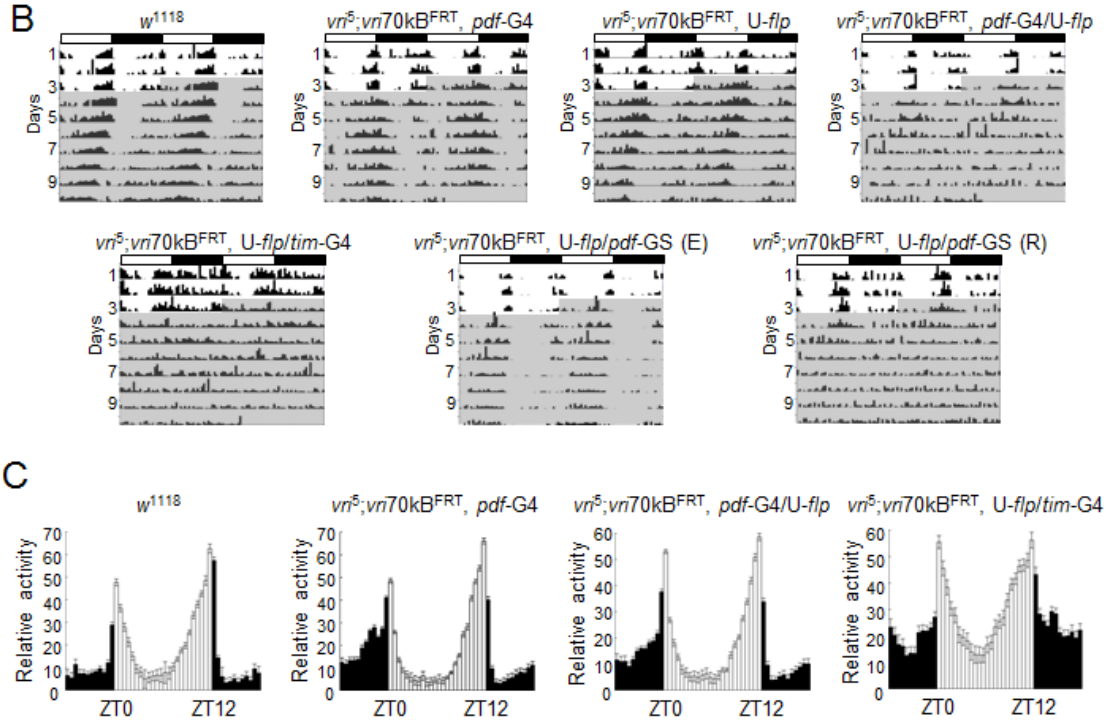

Figure 15. Continued.

vri is required for circadian activity rhythms

Since Gal4/UAS mediated FLP expression efficiently inactivated the *vri*70kb^{FRT} transgene to produce *vri* mutant tissues in adults, I used this system to test whether *vri* is necessary for locomotor activity rhythms. When *pdf*-Gal4 and *tim*-Gal4 were used to drive FLP-mediated inactivation of *vri* in lLN$_v$s and sLN$_v$s or all clock cells, respectively, activity rhythms in constant darkness (DD) were almost completely abolished, whereas control flies lacking the *pdf*-Gal4 or *tim*-Gal4 drivers or RU486 induced *pdf*-GS were highly (>80%) rhythmic with periods of ~23.4h (Table 4, Figure 15B). Diurnal activity rhythms during a 12h light:12h dark (LD) cycle, in contrast, were

similar in control and *vri* inactivated strains (Figure 15C), demonstrating that *vri* is not required for LD entrainment or anticipating light or dark transitions.

My control strain (w^{1118}), which was used to isogenize all of my *vri70kb*^{FRT} strains, showed a higher proportion of rhythmic flies (>95%) than controls lacking *pdf*-Gal4, *tim*-Gal4 or RU486 induced *pdf*-GS, but had similar ~23.5h periods (Table 4). The lower percentage of rhythmicity in these controls likely resulted from leaky expression of UAS-*flp*, which was recombined onto the same chromosome as *vri70kb*^{FRT}. Indeed, control flies produced by recombining *pdf*-Gal4 into the same chromosome as *vri70kb*^{FRT} had a percent rhythmicity (>93%) similar to that of w^{1118} (Table 4), consistent with my PCR analysis showing little if any FLP-mediated recombination in these flies (Figure 14B). Nevertheless, when the *vri70kb*^{FRT} transgene was inactivated in *vri70kb*^{FRT}, *pdf*-Gal4/UAS-*flp* flies, rhythmicity was almost completely abolished (Table 4, Figure 15B). These results show that *vri* is required for activity rhythms in DD.

Table 4. Tissue specific inactivation of *vri*70kb^{FRT} abolishes rhythmic activity.

Genotype	N	% Rhythmic	Period± s.e.m.	Strength± s.e.m.
w^{1118}	58	96.5	23.52±0.04	91.67± 5.60
vri^{5};*vri*70kB^{FRT}, U-*flp* [a]	111	82.9	23.41± 0.05	38.03± 2.42
vri^{5};*vri*70kB^{FRT}, U-*flp*/*pdf*-G4 [b]	132	3.0	23.38± 0.36	27.27± 11.45
vri^{5};*vri*70kB^{FRT}, U-*flp*/*tim*-G4 [c]	61	1.6	23.00	38.54
vri^{5};*vri*70kB^{FRT}, *pdf*-G4 [d]	16	93.8	24.0± 0.1	41.6± 7.3
vri^{5};*vri*70kB^{FRT}, *pdf*-G4/U-*flp* [e]	31	3.2	23.0	26.8
vri^{5};*vri*70kB^{FRT}, U-*flp*/*pdf*-GS (E) [f, g]	25	84.0	23.64± 0.12	43.84± 4.58
vri^{5};*vri*70kB^{FRT}, U-*flp*/*pdf*-GS (R) [f, h]	49	6.1	23.83± 0.20	24.84± 10.59
vri^{5}, U-*pdf*/*vri*^{5};*vri*70kB^{FRT},U-*flp* [i]	23	82.6(19)	23.6± 0.1	38.6± 4.0
vri^{5},U-*pdf*/*vri*^{5};*vri*70kB^{FRT},U-*flp*/*pdf*-G4 [j]	28	7.1(2)	23.0± 0.0	52.8± 15.7

[a] Complete genotype is w^{1118};*vri*^{5};*vri*70kB^{FRT}, UAS-*flp*/+.[b] Complete genotype is w^{1118};*vri*^{5};*vri*70kB^{FRT}, UAS-*flp*/*pdf*-Gal4.[c] Complete genotype is w^{1118};*vri*^{5};*vri*70kB^{FRT}, UAS-*flp*/*tim*-Gal4.[d] Complete genotype is w^{1118};*vri*^{5};*vri*70kB^{FRT}, *pdf*-Gal4/+.[e] Complete genotype is w^{1118};*vri*^{5};*vri*70kB^{FRT}, *pdf*-Gal4/UAS-*flp*. [f] Complete genotype is w^{1118};*vri*^{5};*vri*70kB^{FRT}, UAS-*flp*/*pdf*-GS. [g] Flies treated with ethanol (E) vehicle. [h] Flies treated with RU486 (R) in ethanol (see Materials and Methods). [i] Complete genotype is w^{1118};*vri*^{5}, UAS-*pdf*/*vri*^{5};*vri*70kB^{FRT},UAS-*flp*. [j] w^{1118};*vri*^{5},UAS-*pdf*/*vri*^{5};*vri*70kB^{FRT}, UAS-*flp*/*pdf*-Gal4. N, total number of flies tested.

To insure that the behavioral arrhythmicity resulting from *vri* inactivation was not due to a developmental defect, I used *pdf*-GS to inactivate *vri* only in adults. Homozygous *vri*^{5} mutant flies containing the *vri70kb*^{FRT}, UAS-*flp* and *pdf*-GS transgenes

were grown on standard fly food until the emergence of adults, which were transferred to food containing either RU486 to induce *vri* inactivation or vehicle as a control. Flies exposed to RU486 displayed arrhythmic activity, whereas controls were rhythmic with a period of ~23.5h (Table 4, Figure 15B). This result demonstrates that *vri* functions in adults to sustain rhythmic activity in DD.

The circadian oscillator continues to operate in flies lacking vri

Arrhythmic activity due to *vri* inactivation in clock cells could arise by disrupting the circadian oscillator or output pathways that regulate activity rhythms. To distinguish among these possibilities, I assessed oscillator function in *vri* inactivated flies. Upon inactivation of *vri* in all clock cells using *tim*-Gal4 driven UAS-*flp*, *Clk* mRNA levels remain high throughout the first day of DD as expected, and *tim* cycling persists at higher amplitude than in control flies (Figure 16A), presumably due to increased *Clk* expression. I was surprised to see appreciable quantities of *vri* mRNA (~50% of the control peak) after *vri70kb*^{FRT} inactivation. This residual expression is likely due to inefficient *vri70kb*^{FRT} inactivation in clock tissues other than brain pacemaker neurons in fly heads since *vri* inactivation removes sequences needed for PCR amplification. Finally, PER is rhythmically expressed in LN_vs on the third day of DD in the absence of VRI (Figure 16B). The persistence of *tim* mRNA rhythms in heads and PER rhythms in LN_vs demonstrates that *vri* is not required for circadian oscillator function, and suggests that *vri* abolishes activity rhythms by disrupting clock output.

Circadian oscillators also operate in many peripheral tissues including the Malpighian tubules (MTs) that encompass the fly renal system (Ivanchenko, et al. 2001; Plautz, et al. 1997). VRI levels cycle in MTs from control flies with a peak between CT15 and CT19, but VRI was absent when *tim*-Gal4 driven UAS-*flp* was used to catalyze *vri*70kb^{FRT} inactivation in *vri*^{5} flies (Figure 16C), demonstrating that *vri* is efficiently inactivated in this tissue. PER levels cycled in MTs from both controls and flies lacking *vri* (Figure 16C), but the PER peak occurred 4h earlier in flies lacking *vri*, suggesting that the period of these flies was shorter than control flies. Taken together, these results argue that circadian clock function is intact in brain pacemaker neurons and peripheral tissues in the absence of *vri*.

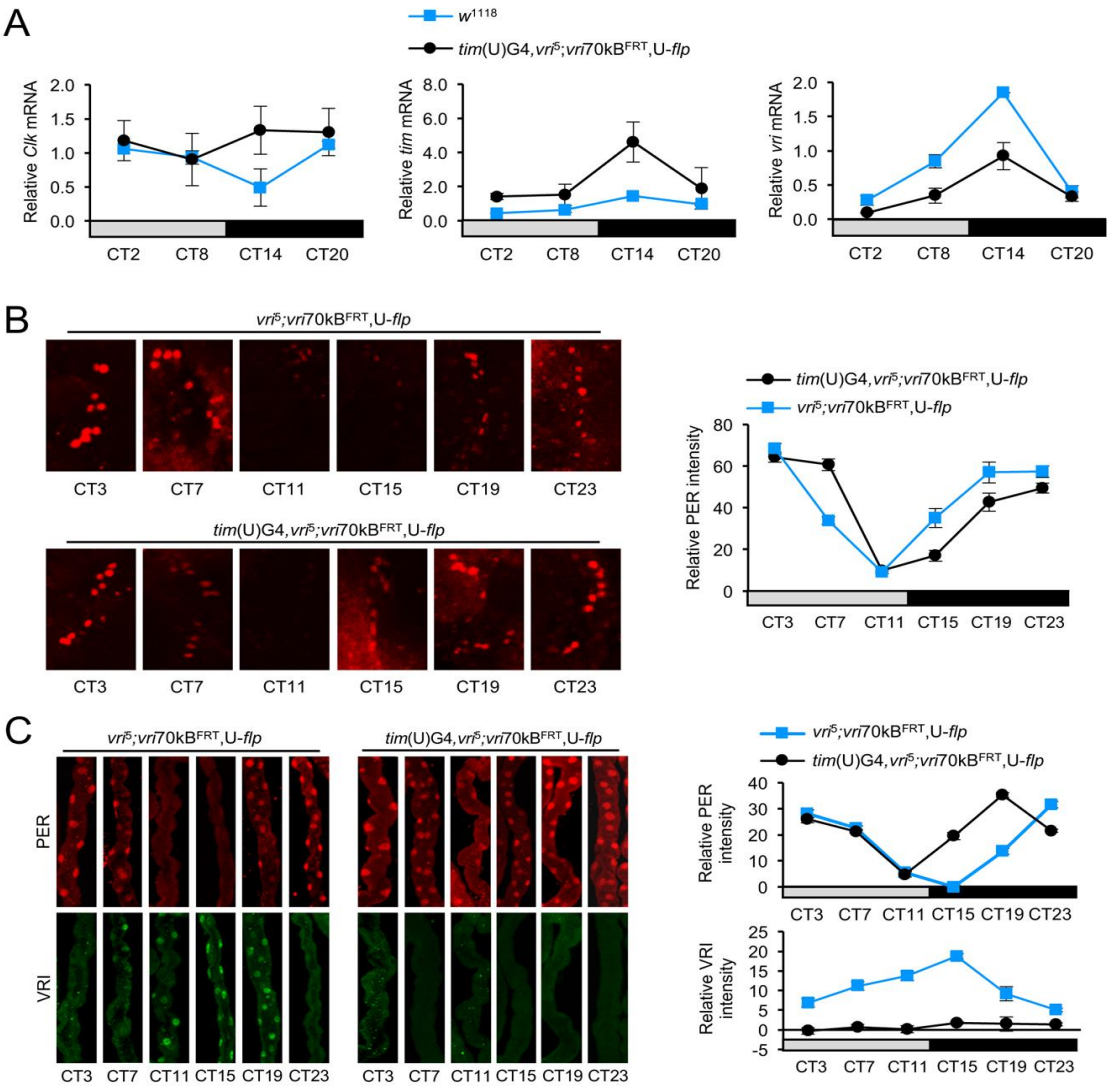

Figure 16. Circadian clock function persists in the absence of VRI.
(A) RT-qPCR quantification of *Clk*, *tim*, and *vri* mRNA levels in heads of w^{1118} and w^{1118};*tim*(UAS)Gal4,vri^{5};*vri*70kB^{FRT},UAS-*flp*/+ (*tim*(U)G4,vri^{5};*vri*70kB^{FRT},U-*flp*) flies collected at the indicated circadian times during DD1. Gray boxes, subjective lights-on; black boxes, subjective lights-off. (B) Brains from w^{1118};vri^{5};*vri*70kB^{FRT}, UAS-*flp*/+ (vri^{5};*vri*70kB^{FRT}, UAS-*flp*) and *tim*(U)G4,vri^{5};*vri*70kB^{FRT},U-*flp* flies collected at the indicated times on DD day 3 were Immunostained with PER (red) antiserum. Immunostaining was imaged and quantified in LN_v pacemaker neurons (n=6 hemispheres) as described (see Materials and Methods). (C) MTs from vri^{5};*vri*70kB^{FRT}, UAS-*flp* and *tim*(U)G4,vri^{5};*vri*70kB^{FRT},U-*flp* flies collected at the indicated times on DD day 3 were immunostained with PER (red) and VRI (green) antisera. Immunostaining was imaged and quantified from main MT segments (n = 5) as described.

Loss of vri in clock cells alters PDF expression in the sLN$_v$s

Since *vri* is not required for circadian oscillator function, I reasoned that *vri* inactivation abolishes behavioral rhythms by disrupting clock output in brain pacemaker neurons. One well characterized output of pacemaker neurons is the neuropeptide PDF, which is required for locomotor activity rhythms (Renn, et al. 1999). PDF expression is limited to four lLN$_v$s that project to the optic lobe, accessory medulla and the contralateral brain hemisphere, and four sLN$_v$s that project to the dorsal brain (Helfrich-Forster 1995). PDF rhythmically accumulates in sLN$_v$ dorsal projections (Park, et al. 2000), which are required for locomotor activity rhythms (Agrawal and Hardin 2016).

To determine if *vri* is required for PDF expression, I imaged PDF in brains from flies and larvae in which *vri* was inactivated in lLN$_v$s and sLN$_v$s. In control brains from adults, PDF is detected in optic lobe and posterior optic tract (POT) projections and cell bodies from lLN$_v$s and in the dorsal projection and cell bodies from sLN$_v$s, whereas PDF is absent specifically in the sLN$_v$ dorsal projection in flies lacking *vri* (Figure 17A). In larvae, where PDF is only expressed in sLN$_v$ precursors (Helfrich-Forster, et al. 2007), PDF is readily detected in sLN$_v$ dorsal projections in control animals, but not in the sLN$_v$ dorsal projections from *vri* inactivated larvae (Figure 17A). However, significantly ($p = 2x10^{-13}$) weaker PDF staining is detected in sLN$_v$ cell bodies than those of controls (Figure 17B). These results show that loss of *vri* drastically reduces PDF expression in small LN$_v$s.

Loss of PDF in the sLN$_v$ dorsal projection could result from low PDF expression, as seen in *cyc*^{01} flies (Park, et al. 2000), or the absence of the dorsal projection

altogether, as seen in *Lar* mutants (Agrawal and Hardin 2016). To test whether sLN_v dorsal projections are present in the absence of *vri*, CD8-GFP was used to mark the plasma membrane of lLN_vs and sLN_vs in *vri* inactivated flies. Both lLN_v and sLN_v projections were detected with CD8-GFP in the absence of VRI, but PDF was only detected in lLN_v projections (Figure 17C). Thus, although sLN_v dorsal projections are present in *vri* inactivated flies, PDF is not detected in these projections, indicating that *vri* is required for PDF expression.

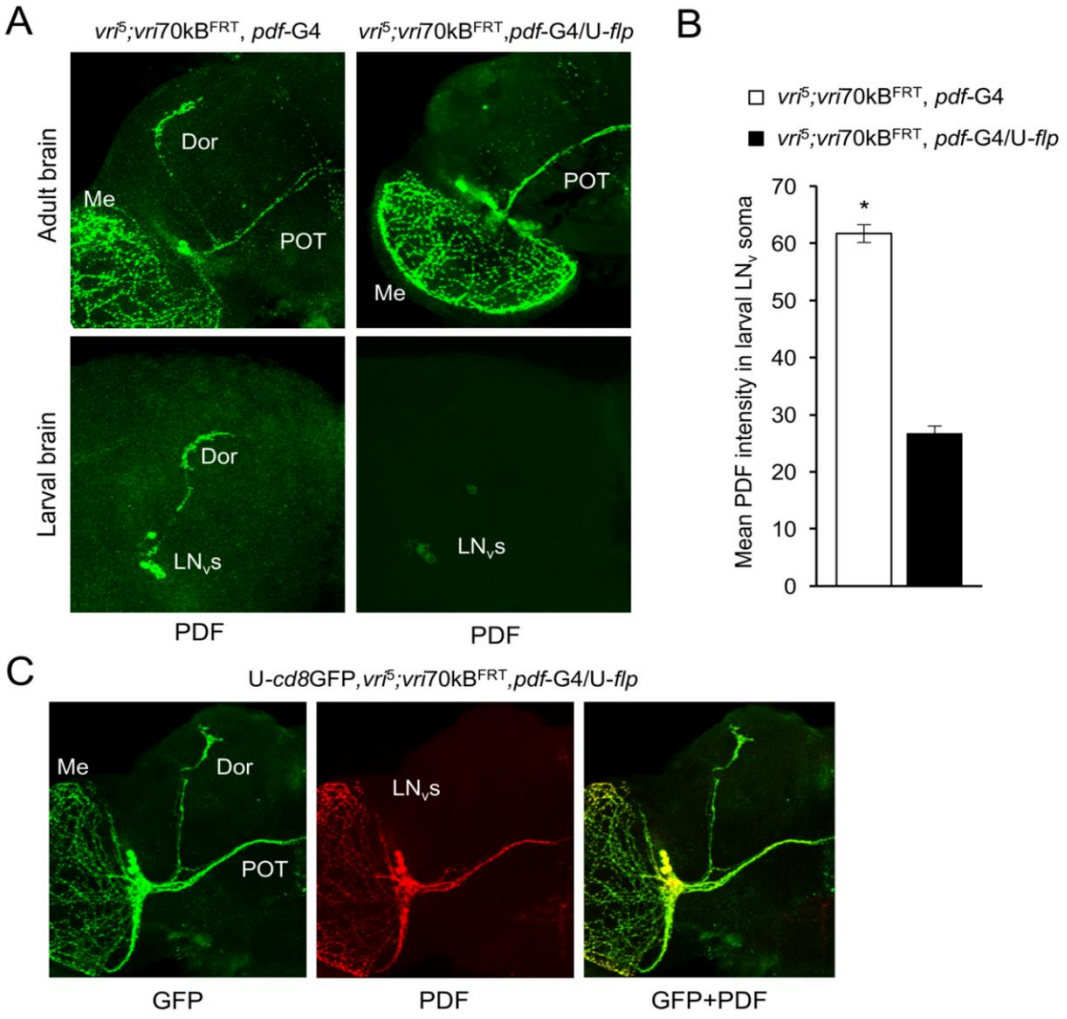

Figure 17. Loss of vri in clock cells alters PDF expression in the sLNvs.
(A) Brains from w^{1118};vri^{5};vri70kB^{FRT}, *pdf*-Gal4/+ (vri^{5};vri70kB^{FRT}, *pdf*-G4) and w^{1118};vri^{5};vri70kB^{FRT}, *pdf*-Gal4/UAS-*flp* (vri^{5};vri70kB^{FRT}, *pdf*-G4/U-*flp*) larvae and adults collected at ZT3 were Immunostained with PDF (green) antiserum and imaged as described. Me, lLN_v projections into the medulla; POT, lLN_v projections along the posterior optic tract; Dor, sLN_v projection into the dorsal brain. (B) Quantification of PDF immunostaining in LN_v cell bodies from vri^{5};vri70kB^{FRT}, *pdf*-G4 (n = 27) and vri^{5};vri70kB^{FRT}, *pdf*-G4/U-*flp* (n = 11) larval brains was carried out as described. PDF staining intensity was significantly higher (*$p < 0.05$) in LN_v cell bodies from vri^{5};vri70kB^{FRT}, *pdf*-G4 larvae than vri^{5};vri70kB^{FRT}, *pdf*-G4/U-*flp* larvae. (C) Brains from w^{1118};UAS-*cd8*GFP, vri^{5};vri70kB^{FRT}, *pdf*-Gal4/UAS-*flp* (U-cd8GFP, vri^{5};vri70kB^{FRT}, *pdf*-G4/U-*flp*) adults collected at ZT2 were immunostained with GFP (green) and PDF (red) antisera and imaged as described. Merged (GFP+PDF) images are shown as yellow. Symbols denoting lLN_v and sLN_v projections are the same as in panel A.

VRI promotes PDF accumulation via different levels of regulation

The impact of *vri* inactivation on PDF expression in LN_vs is strikingly similar to that observed in cyc^{01} flies (Park, et al. 2000), and given that *cyc* is required for *vri* expression (Blau and Young 1999), *cyc* may promote PDF expression via *vri*. To explore this possibility, I measured PDF levels in sLN_vs from cyc^{01} flies before and after inducing high levels of VRI from a heat shock promoter driven *vri* (hs-*vri*) transgene (Glossop, et al. 2003). Before heat induction, PDF levels were undetectable in the dorsal projection, whereas after VRI induction PDF levels in the dorsal projection increased dramatically (Figure 18A).

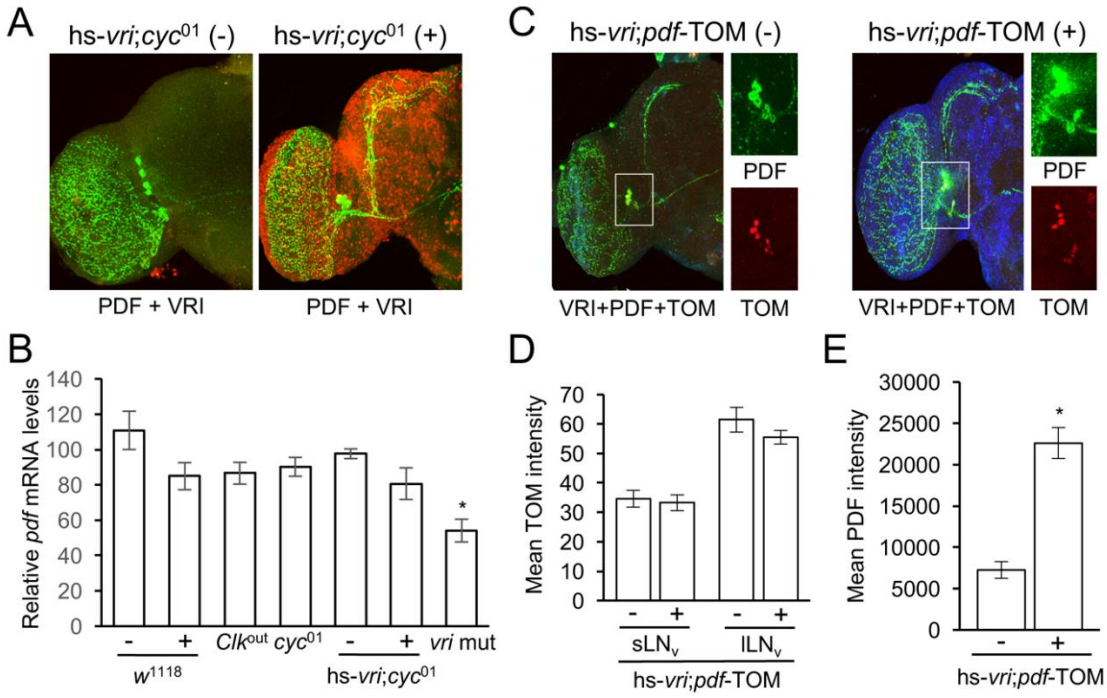

Figure 18. VRI regulates PDF expression at the post transcriptional level.
(A) Brains from w^{1118};hs-*vri*;cyc^{01} (hs-*vri*;cyc^{01}) flies that received a heatshock (+) or no heatshock (-) were immunostained with PDF (green) and VRI (red) antisera and imaged as described. Merged (PDF+VRI) images are shown as yellow. (B) The levels of *pdf* mRNA in heads from, Clk^{out}, cyc^{01}, *tim*(UAS)Gal4, vri^{5};*vri*70kB^{FRT}, UAS-*flp* (*vri* mut) and hs-*vri*;cyc^{01} and w^{1118} flies that received a heatshock (+) or no heatshock (-) were quantified via RT-qPCR (n = 3) as described. *pdf* mRNA levels were significantly ($p < 0.04$) lower than all other genotypes. (C) Brains from w^{1118};hs-*vri*;*pdf*-tdTOMATO (hs-*vri*;*pdf*-TOM) flies that received a heatshock (+) or no heatshock (-) were immunostained with PDF (green) and VRI (red) antisera and imaged for TOM fluorescence and antibody staining as described. Merged (PDF+VRI+TOM) images are shown as yellow. (D) Quantification of TOM fluorescence (mean TOM intensity) in sLN_vs and lLN_vs from hs-*vri*;*pdf*-TOM flies (n > 3 hemispheres) that were treated and imaged as described in panel C. (E) Quantification of PDF immunostaining (mean PDF intensity) in LN_v cell bodies from hs-*vri*;*pdf*-TOM flies (n > 4 hemispheres) that were treated and imaged as described in panel C. PDF immunostaining intensity was significantly ($p = 1.6x10^{-8}$) higher in heat shocked flies.

To determine if the VRI-dependent increase in PDF is due to higher levels of *pdf* mRNA, I measured *pdf* mRNA levels via RT-qPCR in heads from *vri* overexpression (hs-*vri*;cyc^{01}), *vri* inactivated (*tim*(UAS)Gal4,vri^{5};*vri*70kB^{FRT},UAS-*flp*), cyc^{01}, Clk^{out} and

control w^{1118} flies. The levels of *pdf* mRNA in *vri* overexpression flies both before and after heat induction were comparable to those in w^{1118}, cyc^{01} and Clk^{out} flies (Figure 18B), thus the high PDF levels seen in *vri* overexpression flies after heat induction are not due to an underlying increase in *pdf* mRNA. However, *pdf* mRNA levels were significantly ($p < 0.04$) reduced in *vri* inactivated flies (Figure 18B), suggesting that *vri* is required to maintain high *pdf* mRNA levels. I was surprised to see that cyc^{01} and Clk^{out} flies had quasi-normal *pdf* mRNA levels since *pdf* mRNA was previously found to be low in cyc^{02} and Clk^{Jrk} mutants (Park, et al. 2000). This difference likely results from the presence of *pdf* mRNA and protein in lLN_vs, compensatory regulation of *pdf* mRNA levels in sLN_vs and/or the loss of sLN_vs altogether in these mutants (see Chapter IV). To determine if *vri*-dependent increases in *pdf* mRNA are regulated at the level of transcription, I employed the *pdf*-dtTOMATO transcriptional reporter (Mezan, et al. 2016). As expected, *vri* induction increased PDF levels in LN_vs (Figure 18C, E), but dt-TOMATO levels were not altered (Figure 18D), indicating that *vri* does not promote *pdf* transcription. Taken together, these results indicate that *vri* promotes PDF expression at the post-transcriptional level, and that the loss of *vri* accounts for the lack of PDF in sLN_vs from cyc^{01} flies.

Arrhythmic activity is not solely due to reduced PDF expression in vri inactivated flies

If the behavioral arrhythmicity of *vri* inactivated flies is due to low PDF levels in sLN_vs, I reasoned that increasing PDF levels in sLN_v dorsal projections will restore activity rhythms. To determine if this was the case, *pdf*-Gal4 was used to drive *pdf* and

flp expression in the LN_vs of *vri*^{5} mutants carrying the *vri70kb*^{FRT} transgene. In these flies, VRI expression was eliminated in the LN_vs and PDF expression was restored in sLN_v dorsal projections (Figure 19A). However, despite the accumulation of PDF in sLN_v dorsal projections, activity rhythms were not rescued in DD (Table 4). These results show that PDF expression in sLN_v dorsal projections is not sufficient to restore activity rhythms in *vri* inactivated flies, which suggests that *vri* is required to support other processes required for rhythmic activity.

One process proposed to be important for activity rhythms is the daily remodeling of the sLN_v dorsal projection, where terminal axonal branching is maximal after dawn and minimal after dusk (Fernandez, et al. 2008). To determine whether daily changes in sLN_v arborization are compromised in *vri* inactivated flies, I used CD8-GFP to measure terminal axonal branching at the normal peak (ZT2) and trough (ZT14) times as previously described (Fernandez, et al. 2008).

Figure 19. VRI supports behavioral rhythms via processes other than PDF regulation.
(A) Left brain hemisphere from a w^{1118};*vri*^{5}, UAS-*pdf*/*vri*^{5};*pdf*-Gal4/*vri*70kB^{FRT}, UAS-*flp* (*vri*^{5}, U-*pdf*/*vri*^{5};*pdf*-G4/*vri*70kB^{FRT}, U-*flp*) fly collected at ZT2 that was immunostained with PDF (green) and VRI (red) antisera and imaged as described. Symbols denoting groups of pacemaker neurons are as described in Figure 1. Top right, magnified view of the boxed region showing sLN_v dorsal projection (Dor) terminals; Bottom right, magnified view of the boxed region showing LN_v cell bodies. (B) Brain region containing the sLN_v dorsal projection terminus from w^{1118};UAS-cd8GFP, *vri*^{5};*vri*70kB^{FRT}, *pdf*-Gal4/+ (U-cd8GFP, *vri*^{5};*vri*70kB^{FRT}, *pdf*-G4) flies collected at ZT2 and ZT14, immunostained with GFP (green) antiserum and imaged as described (see Materials and Methods). (C) Brain region containing the sLN_v dorsal projection terminus from w^{1118};UAS-cd8GFP, *vri*^{5};*vri*70kB^{FRT},*pdf*-Gal4/UAS-*flp* (U-cd8GFP, *vri*^{5};*vri*70kB^{FRT},*pdf*-G4/U-*flp*) flies collected at ZT2 and ZT14, immunostained with GFP (green) antiserum and imaged as described (see Materials and Methods). (D) Quantification of sLN_v dorsal terminal arborization from the indicated fly strains was carried out as described. A minimum of 6 sLN_v dorsal projections were analyzed at each time point for each genotype. a, sLN_v dorsal terminal arborization in U-cd8GFP, *vri*^{5};*vri*70kB^{FRT},*pdf*-G4 flies at ZT2 is significantly ($p = 0.004$) higher than at ZT14. b, sLN_v dorsal terminal arborization in U-cd8GFP, *vri*^{5};*vri*70kB^{FRT}, *pdf*-G4 flies at ZT2 is significantly ($p < 1x10^{-5}$) higher than in U-cd8GFP, *vri*^{5};*vri*70kB^{FRT}, *pdf*-G4/U-*flp* flies at ZT2 and ZT14. c, sLN_v dorsal terminal arborization in U-cd8GFP, *vri*^{5};*vri*70kB^{FRT}, *pdf*-G4/U-*flp* flies at ZT14 is significantly ($p < 0.003$) higher than in U-cd8GFP, *vri*^{5};*vri*70kB^{FRT}, *pdf*-G4/U-*flp* flies at ZT2 and ZT14. (E) Brain region containing the sLN_v dorsal projection terminus from w^{1118};UAS-*pdf, vri*^{5};*vri*70kB^{FRT}, UAS-*flp*/+ (U-*pdf, vri*^{5};*vri*70kB^{FRT}, U-*flp*) flies collected at ZT2 and ZT14, immunostained with PDF (green) antiserum and imaged as described. (F) Brain region containing the sLN_v dorsal projection terminus from w^{1118};UAS-*pdf, vri*^{5};*vri*70kB^{FRT}, UAS-*flp*/*pdf*-Gal4 (U-*pdf, vri*^{5};*vri*70kB^{FRT}, U-*flp*/*pdf*-G4) flies collected at ZT2 and ZT14, immunostained with PDF (green) antiserum and imaged as described (see Materials and Methods). (G) Quantification of sLN_v dorsal terminal arborization from the indicated fly strains was carried out as described (see Materials and Methods). A minimum of 6 sLN_v dorsal projections were analyzed at each time point for each genotype. a, sLN_v dorsal terminal arborization in U-*pdf, vri*^{5};*vri*70kB^{FRT}, UAS-*flp* flies at ZT2 is significantly ($p = 0.0004$) higher than at ZT14. b, sLN_v dorsal terminal arborization in U-*pdf, vri*^{5};*vri*70kB^{FRT}, UAS-*flp* flies at ZT2 is significantly ($p < 0.012$) higher than in U-*pdf, vri*^{5};*vri*70kB^{FRT}, U-*flp*/*pdf*-G4 flies at ZT2 and ZT14. c, sLN_v dorsal terminal arborization in U-*pdf, vri*^{5};*vri*70kB^{FRT}, U-*flp*/*pdf*-G4 flies at ZT2 is significantly ($p = 0.017$) higher than at ZT14. d, sLN_v dorsal terminal arborization in U-*pdf, vri*^{5};*vri*70kB^{FRT}, UAS-*flp* flies at ZT14 is significantly ($p = 0.0009$) higher than in U-*pdf, vri*^{5};*vri*70kB^{FRT}, U-*flp*/*pdf*-G4 flies at ZT14.

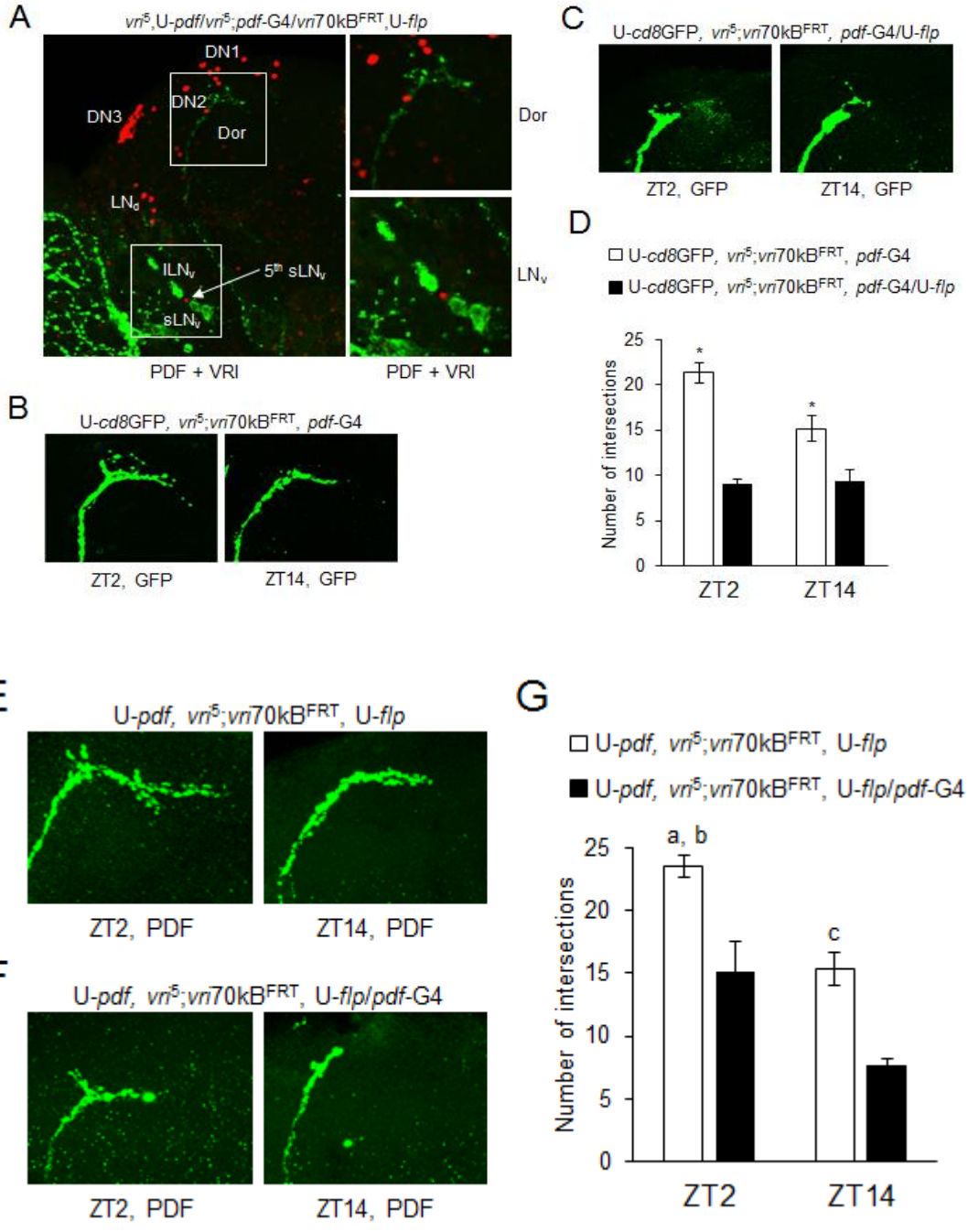
A
vri5,U-pdf/vri5;pdf-G4/vri70kBFRT,U-flp
DN1
DN2
DN3
Dor
LNd
lLNv
5th sLNv
sLNv
LNv
PDF + VRI
PDF + VRI
B
U-cd8GFP, vri5;vri70kBFRT, pdf-G4
ZT2, GFP
ZT14, GFP
C
U-cd8GFP, vri5;vri70kBFRT, pdf-G4/U-flp
ZT2, GFP
ZT14, GFP
D
U-cd8GFP, vri5;vri70kBFRT, pdf-G4
U-cd8GFP, vri5;vri70kBFRT, pdf-G4/U-flp
Number of intersections
ZT2
ZT14
E
U-pdf, vri5;vri70kBFRT, U-flp
ZT2, PDF
ZT14, PDF
F
U-pdf, vri5;vri70kBFRT, U-flp/pdf-G4
ZT2, PDF
ZT14, PDF
G
U-pdf, vri5;vri70kBFRT, U-flp
U-pdf, vri5;vri70kBFRT, U-flp/pdf-G4
Number of intersections
a, b
c
ZT2
ZT14

While terminal branching cycled in control flies (Figure 19B, D), cycling was abolished in *vri* inactivated flies, where branching remained lower than the control fly trough (Figure 19C, D). Overexpression of PDF in *vri* inactivated flies rescued rhythms in sLN_v arborization (Figure 19E, F). However, the overall levels of arborization were significantly lower at both the peak and the trough than in control flies. The absence of normal rhythms in sLN_v dorsal projection arborization may contribute to the loss in activity rhythms in *vri* inactivated flies.

Conclusions

Previous work demonstrating that *vri* is an interlocked feedback loop component were necessarily based on overexpression phenotypes because *vri* null mutants are lethal (George and Terracol 1997). Although *vri* overexpression revealed key aspects of *vri* function including repression of *Clk* via D-boxes, loss of behavioral rhythms and post-transcriptional regulation of PDF expression (Blau and Young 1999; Cyran, et al. 2003; Glossop, et al. 2003), determining whether *vri* is required for clock function and/or output awaited the analysis of viable *vri* mutant adults. To generate flies lacking *vri*, I developed a system to rescue *vri* null mutants using a *vri*70kb^{FRT} transgene that can be inactivated via FLP/FRT recombination (Figures 13, 14, 15; Tables 3, 4). Inactivating *vri*70kb^{FRT} in all clock cells or pacemaker neurons as they initiate clock function during development or only in adults abolishes rhythmic activity without disrupting circadian oscillator function (Table 4; Figures 15, 16), indicating that *vri* mediates clock output. Indeed, inactivating *vri* severely reduces PDF expression in sLN_v cell bodies and dorsal

projection (Figures 17, 18), but restoring PDF expression in the absence of *vri* in sLN_vs does not rescue activity rhythms (Table 4; Figure 19). Moreover, loss of *vri* abolishes rhythms in the arborization of sLN_v dorsal terminals (Figure 19). These results indicate that *vri* is required for multiple pathways that support activity rhythms, and perhaps more broadly as a primary relay to circadian output via regulation of rhythmic transcription that peaks at dawn.

Materials and Methods

Fly strains

The following fly strains were used in this study: w^{1118}, *tim*-Gal4 (Emery, et al. 1998), *tim(UAS)Gal4 (Blau and Young 1999), pdf*-Gal4 (Park, et al. 2000), *pdf-Gene*Switch (*pdf*-GS) *(Depetris-Chauvin, et al. 2011), pdf*-tdTOMATO (Mezan, et al. 2016), *UAS-pdf* (Renn, et al. 1999), *UAS-flp (BDSC), vri*^{k03801} (George and Terracol 1997), *vri*^{5} (*vri*^{k05901}) (George and Terracol 1997), *vri*^{2} (George and Terracol 1997), UAS-*CD8-gfp* (P(UAS-*mCD8::gfp.L*)LL6) (BDSC), *cyc*^{01} (Rutila, et al. 1998) and hs-*vri* (Glossop, et al. 2003). Flies were reared on standard cornmeal/agar medium supplemented with yeast and kept in 12 h light/12 h dark (LD) cycles at 25°C.

Transgene construction and transgenic fly generation

BAC clone CH321-28E21 (BacPac Resources) was used to generate the *vri*70kb^{FRT} transgene. Two Flippase Recognition Target (FRT) sequences were inserted into the transgene flanking the third exon of *vri* at chromosomal locations chr2L5307969

and chr2L5312358 using bacterial homologous recombination (Venken, et al. 2008). The first FRT sequence was inserted on chromosome 2L at site 5307969 using an Intron 2 recombination cassette comprised of a FRT sequence, a *Kanamycin* (*Kan*) gene flanked by loxP sites, and two homology arms generated via PCR using the 'Second intron Homology Forward' and 'Second intron Homology Reverse' primers (Table 5). After selection for recombinants and sequence verification, the *Kan* cassette was removed using CRE recombinase as described (Venken, et al. 2008). The same procedure was employed to insert an FRT at chr2L5312358 using a 3' UTR recombination cassette containing homology arms generated by amplification with the '3UTR Homology Forward' and '3UTR Homology Reverse' primers. After sequence verification, the resulting *vri*70kb^{FRT} transgene was inserted at the VK13 docking site site via *PhiC32*-mediated recombination (Venken, et al. 2006). To confirm the UAS-*flp* mediated inactivation, genomic DNA was extracted from 5-6 *vri*70kb^{FRT} flies, and PCR was performed to amplify a 392bp intact transgene fragment using the intact transgene forward and reverse primers and amplify a 649bp inactive transgene fragment using the inactive transgene forward and reverse primers (Table 5; Figure 17).

Immunostaining

Fly tissues were processed for immunostaining as previously described (Houl, et al. 2008), with minor modifications. Larval brains were dissected at the L3 stage and adult tissues were dissected 3-5 days after eclosion. Dissected tissues were fixed with 3.7% formaldehyde, washed and blocked in PAXD buffer (1X PBS, 5% BSA, 0.03%

sodium deoxycholate, 0.03% tritonX100) with 5% donkey or goat serum for 1hour, and incubated with primary and secondary antibodies diluted in PAXD buffer. The following primary antibodies were used: guinea pig anti-VRI GP3 1:25,000, rabbit anti-GFP ab290 (Abcam) 1:2000, pre-absorbed rabbit anti-PER (a gift from Michael Rosbash Laboratory, Brandeis University) 1: 15,000 and mouse anti-PDF (DSHB) 1:500. The following secondary antibodies were used at a 1:200 dilution: goat anti-rabbit Alexa 647 (Molecular Probes), goat anti-guinea pig Cy-3 (Jackson ImmunoResearch Laboratories, Inc.), goat anti-mouse Cy-3 (Jackson ImmunoResearch Laboratories, Inc.), goat anti-mouse Alex488 (Molecular Probes). For hs-*vri* immunostaining, flies were subjected to a 37°C heat shock for 30 minutes and allowed to recover for 2 hours to analyze tdTOMATO levels or 24 hours to analyze PDF levels.

Confocal microscopy

Confocal imaging was carried out as described (Liu, et al. 2015), with minor modifications. Fly tissues were imaged using an Olympus FV1000 confocal microscope 20x /0.8 NA or 100x /1.4 NA oil immersion objective lenses. Serial optical scans were obtained at 3μM intervals (with 20x objective lens) for most of the imaging experiments and 1uM thick optical scans were done to determining the degree is neuronal plasticity with 100X objective lens. Original Olympus images were saved as 12-bit oib format. When analyzing tdTOMATO, the direct fluorescence of the fluorophore was captured using HeNe 543 laser excitation as described (Mezan, et al. 2016). For sLN_v arborization rhythm analysis, images were captured with 100X /1.4 oil immersion objective with an

optical zooming of 1.2x. and further analyses were carried out as described under '*confocal image processing and analysis'* section.

Drosophila activity monitoring and behavior analysis

All fly strains used in behavior experiments except those containing vri^2 were backcrossed seven times to w^{1118} flies to minimize effects due to differences in genetic background. Locomotor activity was monitored using the *Drosophila* Activity Monitor (DAM) system (Trikinetics). One to three day old male flies were placed in monitors, and activity was recorded for 3 days in 12:12 light-dark (LD) cycles and 7 days in contact darkness (DD) at 25'C. To record activity of strains containing the *pdf*-GS driver, flies were raised in standard corn meal food until pupation. Dark-winged pupae were collected and transferred to an empty vial containing a moistened strip of Kim-wipe. After eclosion, flies were starved for >12 hours, and then fed standard food containing RU486 (500 ug/mL) for 2-3 days before activity rhythm experiments were conducted as described earlier, except the food inside behavior tubes also contained 500 ug/mL RU486. For control experiments, the vehicle (ethanol) used to solubilize RU486 was added. To investigate the activity rhythms during LD, flies were monitored in LD for 10 days, then in DD for two days to confirm the circadian phenotype of a given genotype.

Western blotting

Western blot analyses were conducted as described (Zhou, et al. 2016), with minor modifications. After protein extraction, equal amounts of RIPA S extract were run, transferred, and probed with guinea pig anti-VRI GP3, 1: 5,000 and mouse anti-beta-actin (Abcam), 1:20,000. Horseradish peroxidase-conjugated secondary antibodies (Sigma) against guinea pig and mouse were diluted 1:5,000. Immunoblots were visualized using ECL plus (GE) reagent.

RNA extraction and quantitative RT-PCR

RNA extraction and quantitative RT-PCR was performed as described (Zhou, et al. 2016), with minor modifications. Flies were entrained in 12:12 light-dark (LD) for at least 3 days, collected at the indicated time points, and frozen. Total RNA was isolated and cDNA was synthesized using Superscript II (Invitrogen). The reverse transcription (RT) product was amplified with SsoFast qPCR Supermix (Bio-Rad) in a Bio-Rad CFX96 Real-Time PCR System using pairs of gene-specific primers (Table 5). To quantify the levels of *pdf* mRNA under VRI overexpression conditions, flies containing hs-*vri* were subjected to 37°C heatshock for 30 minutes and allowed to recover for 2 hours. Flies were then collected, frozen, total RNA was extracted, and qPCR was performed as above.

Confocal Image processing and analysis

Preliminary image processing was carried out using either FV1000 confocal software or Adobe Photoshop. Quantification of staining intensities was done using ImageJ software (Schindelin, et al. 2012). For quantification purpose the region of interest was duplicated using the software, next the duplicated image was converted to 8-bit image and its threshold was set. Using the 'Analyze particle' function cell boundaries were marked on the duplicated image. Then the mean intensity (intensity/area) or raw intensity was measured on the original image using the cell boundaries marked on the duplicate image. Student two-tailed t-tests were performed (at p-value 0.05 with unequal variances, otherwise specified) on the average intensity values.

Arborization rhythm analysis

Analysis for neuronal plasticity was carried out as described (Fernandez, et al. 2008), with minor modifications. Briefly, ten concentric rings centered at the position where the first dorsal ramification opens up were drawn for each fly brain hemisphere, such that each of these rings are 10uM apart from one another. The extent of arborization was determined as a summation of all observed intersections that projections made with these rings. Scoring was performed blindly with regard to treatment. Intersections with higher order processes were difficult to determine accurately as the signal intensities fade out towards the process termini, and are thus underestimates. Student two-tailed t-tests with unequal variances were performed on the

recorded average number of intersections for each genotype to determine whether differences were statistically significant.

Activity Behavior analysis

Analyses of period, power and rhythm strength during constant darkness (DD) was carried out using ClockLab (Actimetrics) software as previously described (Agrawal and Hardin 2016). Rhythm analyses for LD activity experiments were carried out using the last seven days of data during LD. Beam break counts were recorded in 30 min bins for 7 days and average activity was calculated to generate the histograms as described (Agrawal and Hardin 2016).

Western blot quantification

Protein levels were quantified by placing a rectangle of the same size over each VRI and β-Actin protein band on films used to visualize the immunoblots, and quantifying the signal within each rectangle via densitometric analysis using the ImageJ program (Schneider, et al. 2012). The levels of VRI were calculated as a VRI: β-Actin ratio.

Analysis of quantitative RT-PCR data

For each sample, mRNA quantity was determined as described (Zhou, et al. 2016). *rp49* mRNA levels were used as a normalization control when determining the relative level of mRNA. Student two-tailed t-tests with unequal variances were performed to determine whether differences were statistically significant.

Oligo information

Table 5. Sequence information of oligo.

Oligonucleotides	
2nd intron Homology Forward	5'-GTCCGAGAATATAATGATGCAGTGGCTCTGATCATATCAATTATCTATCCGAAGTTCCTATTCTCTAGAAAGTATAGGAACTTCCTCGGCATGGACGAGCTGTACAAG-3'
2nd intron Homology Reverse	5'-GTAAGGAGAGAAGGGCATAGGATTAGTTCTCAAGCTTTGGAACTATAGATACTAGTGGATCCCCTCGAGGGAC-3'
3' UTR Homology Forward	5'-ACCTACGTCGCCTGACCCTGGGTGGACTGGCCAGCCAGGCCAGAGGATATGAAGTTCCTATTCTCTAGAAAGTATAGGAACTTCCTCGGCATGGACGAGCTGTACAAG-3'
3' UTR Homology Reverse	5'-CTGCCGCATCCGGAGGGCCGGCAGTCGCATCCACCAGTACGACACCATCGACTAGTGGATCCCCTCGAGGGAC-3'
Intact transgene Forward	5'-CCGGAGGCAAAGAGGAGA-3'
Intact transgene Reverse	5'-GATATCTATGATCACCTAGGGGAGCTC-3'
Inactive transgene Forward	5'-CCGGAGGCAAAGAGGAGA-3'
Inactive transgene Reverse	5'-CGTGCTCTGATCACTCTGCAC-3'

Table 5. Continued.

Oligonucleotides	
rp49 qPCR Forward	5’-TACAGGCCCAAGATCGTGAA-3’
rp49 qPCR Reverse	5’-GCACTCTGTTGTCGATACCC-3’
Clk qPCR Forward	5’-CGGATTCAACGTCCATGTC-3’
Clk qPCR Reverse	5’-GCTGCATGTGATGATGTGACT-3’
pdf qPCR Forward	5’-GGCTCGCTACACGTACCTTG-3’
pdf qPCR Reverse	5’-GAACCAGTCGAGGAGATCCCG-3’
tim qPCR Forward	5’-ACACTGACCGAAACACCCACTC-3’
tim qPCR Reverse	5’-GCGGCACGTTGTGATTACAC-3’
vri qPCR Forward	5’-ATGAACAACGTCCGGCTATC-3’
vri qPCR Reverse	5’-CGTCGGACTTATGGATCCTC-3’

CHAPTER IV

SUMMARY AND FUTURE DIRECTIONS

Circadian and developmental regulation of *vrille* transcription in *Drosophila*

vri mRNA functions and regulation of VRI isoform expression

In *Drosophila*, the gene *vri* produces two protein isoforms from five transcripts to control development and clock functions. *vri*-ADF mRNA produces long and short VRI, while *vri*-E produce short VRI (Figure 6). However, little is understood on how *vri* is regulating these two functions using these mRNAs/proteins. A *vri*-ADF mRNA specific mutant is hypomorphic with respect to clock function, and has residual rhythmic VRI expression in clock cells (Figure 9). The transcription of *vri*-E is rhythmic and likely to be regulated by CLK-CYC, bases on the E-boxes found on the promoter of *vri*-E (Figure 10, (Abruzzi, et al. 2011)). Therefore, it is possible *vri*-E mRNA contributes to the residual short VRI expressed in $vri^{\Delta 679}$ mutants (Figure 9). Therefore, the *Drosophila* circadian clock regulates the expression of 4 different *vri* transcripts in total, and they probably help in the oscillator mechanism.

Different tissues or even different cell types within the same tissue show distinct circadian transcriptomes, and if an overlap is present, the overlapping genes show different phases of expression in different groups of pacemaker neurons (Abruzzi, et al. 2017; Menet and Hardin 2014). Thus, these 4 *vri* transcripts that are regulated by the clock, may be expressed differentially by different tissues or cell types to carryout clock functions. Given the fact that *vri*-E and *vri*-ADF differ by the 1st exon that they use, the

promoters of these mRNAs may be differentially activated in different tissues. Whereas *vri*-A, *vri*-D and *vri*-F differ by the length of their 3' UTR, suggesting that they may have different half-lives, which may contribute to the phase differences that are observed among different groups of pacemaker neurons. Not only *vri* mRNA, but also VRI proteins show heterogeneity, and it is not understood where long and short VRI are expressed and what functions they carry out. Based on the expression of long and short VRI, I predict that both isoforms of VRI protein carry out clock functions, while development functions are mainly carried out by short VRI. Thus, further experimentation can shed light to understand the distributions and functions of these *vri* mRNAs and proteins in the timekeeping mechanism.

Translational regulation of vri-ADF mRNA

vri-ADF mRNA primarily produce short VRI proteins using an alternative translation initiation site (Figure 12). Two mechanisms are proposed to explain how ribosomes use this alternative translation initiation codon to produce short VRI from *vri*-ADF mRNAs. First, my analyses of *cis*-elements in the vicinity of the translation initiation sites that favor ribosomal recruitment, I found a downstream alternative translation initiation site, which is found in the same OFR as the first AUG, possesses a stronger Kozak sequence (Figure 12B). However, experiments done with overexpressing *vri*-ADF ORF using a cDNA clone and also overexpression of *vri*-ADF from the endogenous gene locus suggest that strength of the Kozak sequence is not the only reason for ribosomes favoring the alternative start codon. When *vri*-ADF ORF was

overexpressed using a cDNA clone, it favored overexpression of long VRI rather than short VRI, disregarding the strength of the intact Kozak sequence upstream of the alternative start codon (Figure 12A). However, when overexpression was carried out using the endogenous locus in a genomic context it favored the expression of short VRI, promoting the recruitment of ribosomes to the alternative initiation codon (Figure 12A). Since the *vri*-ADF expressing cDNA clone lacks most of the 5' UTR and intron regions of the gene, it is possible the *cis* elements that are essential for ribosomal recruitment are located in either the 5' UTR or the introns. IRES elements are a common group of sequences in *Drosophila* that are characterized to promote alternative translation initiation, and both *Rev-Erb* and *E4bp4* genes possess IRES elements on their 5' UTR facilitating alternative translation initiations in mammals (Kim, et al. 2010; Kim, et al. 2017). Therefore, the second proposed mechanism is that there are other *cis* elements like IRES elements, which work in concert with the strong Kozak sequence to bring about the initiation of short VRI translation from *vri*-ADF mRNAs, and further experiments are necessary to test these proposed hypotheses.

Transcriptional regulation of vri-E mRNA

Sequence analysis of the *vri* extended locus (4.5 kB upstream and 2 kB downstream of the gene) demonstrated that there are 12 canonical E-boxes grouped into 4 clusters; 3 clusters are near the promoter of *vri*-E mRNA and the other is located on the promoter of *vri*-ADF mRNA (Figure 11). Genome-wide CLK ChIP-chip experiments suggest that CLK binds only the cluster located on the promoter of *vri*-ADF

mRNAs and the cluster found ~3.2 kB upstream of the *vri*-E transcription start site. Although the other two clusters are closer to the *vri*-E transcription start site, there is no evidence supporting CLK binding to these E-boxes. The E-boxes on the promoter of *vri*-ADF is required for CLK-CYC binding, as well as development functions. Thus, it is important to know if these E-boxes are dispensable for clock function or for development functions. Since there are three clusters of E-boxes on the *vri*-E promoter and CLK is only bound by one cluster they may have non-redundant functions, unlike the E-boxes on the *vri*-ADF promoter. A similar strategy which was used for *vri*70kB$^{\Delta E\text{-}Box}$ mutant generation can be used to understand the functional significance of these E-boxes for *vri* transcription.

VRILLE controls PDF neuropeptide accumulation and arborization rhythms in small ventrolateral neurons to drive rhythmic behavior in *Drosophila.*

vri and Pdp1 form an interlocked feedback loop that controls output gene expression

The interlocked feedback loop is proposed to control *Clk* mRNA cycling via PDP1ε activation and VRI repression (Cyran, et al. 2003). Loss of *Pdp1ε* or *vri* indeed decreases or increases *Clk* mRNA levels, respectively, but circadian oscillator function persists in DD ((Zheng, et al. 2009); Figure 16), although coordination among clock cells and tissues in *Pdp1*^{3135} mutants is compromised during DD (Zheng, et al. 2009). Persistent clock function in the absence of *Clk* mRNA cycling is not surprising; molecular oscillator and activity rhythms continue even when the phase of *Clk* mRNA cycling is reversed (Kim, et al. 2002).

PDF regulation by vri

One important difference between *vri* and *Pdp1ε* loss of function is that LD activity rhythms are normal in the absence of *vri* (Figure 15C), but are abolished in *Pdp1*^{3135} flies (Zheng, et al. 2009). Since PDF expression is dramatically lower in both *vri* inactivated and *Pdp1*^{3135} mutants ((Zheng, et al. 2009); Figure 17A, B), some other aspect of clock output likely accounts for the difference in LD activity rhythms in the absence of *vri* and *Pdp1ε*. The extent to which PDP1ε and VRI regulate the same target genes, as implied by the interlocked feedback loop model (Cyran, et al. 2003), is not known. However, the difference between *Pdp1ε* and *vri* mutant behavior in LD suggests that PDP1ε and VRI target genes differ to some extent. Appendix C describes a preliminary study that I have carried out to identify the target genes of VRI and PDP1.

The sharp reduction in PDF levels due to *vri* inactivation is similar to that displayed by *cyc*^{01} mutants (Park, et al. 2000). In *cyc*^{01} flies *vri* expression is almost entirely eliminated (Cyran, et al. 2003), suggesting that low PDF levels in *cyc*^{01} flies may be due to the absence of *vri*. Indeed, when *vri* expression is transiently induced in *cyc*^{01} flies, PDF expression in the sLN_v dorsal projection is restored (Figure 18A). However, transient *vri* expression neither increases *pdf* transcription nor *pdf* mRNA levels (Figure 18B-D), demonstrating that *vri* acts at the post-transcriptional level to increase PDF levels. Thus, the lack of PDF in *cyc*^{01} sLN_vs is likely due to the absence of *vri* expression.

Although transient *vri* induction does not alter *pdf* transcription or overall *pdf* mRNA levels (Figure 18B-D), *vri* inactivation lowers *pdf* mRNA levels significantly (Figure 18B). How *vri* sustains normal *pdf* mRNA levels is not known. Since *vri* is a transcriptional repressor, *vri* presumably represses a gene that functions to reduce *pdf* mRNA levels. A common mechanism for reducing mRNA levels is through micro-RNAs (miRNAs), which bind mRNA 3' untranslated sequences to either promote degradation or block translation (Jackson and Standart 2007; Valencia-Sanchez, et al. 2006). Several miRNAs are either regulated by the circadian clock or produce a circadian phenotype when they or their target sites are eliminated (Mehta and Cheng 2013). Alternatively, mRNA degradation can also be promoted by RNA binding proteins, of which several are under circadian clock control and/or produce a circadian phenotype when mutant (Kojima, et al. 2011). Additional studies, such as identifying and characterizing miRNAs identified with VRI ChIP-Seq experiments, that will help *pdf* regulation will help to determine how *vri* regulates *pdf* mRNA levels in sLN_vs.

PDF levels in sLN_vs are highly regulated. In Clk^{Jrk} and cyc^{02} larvae and adults, PDF is almost completely absent in larval LN_vs and adult sLN_vs, but appears to be normally expressed in lLN_vs (Blau and Young 1999; Park, et al. 2000). The levels of *pdf* mRNA detected by *in situ* hybridization in larval and adult LN_vs from Clk^{Jrk} and cyc^{02} mutants mirror PDF levels (Blau and Young 1999; Park, et al. 2000), indicating that CLK-CYC promotes *pdf* mRNA expression in sLN_vs and their precursors, but not in lLN_vs. In contrast, I detect quasi-normal *pdf* mRNA levels in Clk^{out} and cyc^{01} fly heads by RT-qPCR (Figure 18B). This difference is in part due to the large contribution of

lLN$_v$s to *pdf* mRNA synthesis and steady-state abundance (Mezan, et al. 2016; Park, et al. 2000), and the higher sensitivity of RT-qPCR versus *in situ* hybridization for detecting *pdf* mRNA. Recent work shows that *Clk* suppresses *pdf* transcription in LN$_v$s (Mezan, et al. 2016), thus *pdf* mRNA levels in LN$_v$s from *Clk*^{out} and *cyc*^{01} flies should be high rather than low. Since *vri* acts at the post-transcriptional level to maintain high levels of *pdf* mRNA in heads and PDF protein in sLN$_v$s (Figure 18), and *vri* expression is CLK-CYC-dependent (Blau and Young 1999; Cyran, et al. 2003), increased *pdf* mRNA synthesis in sLN$_v$s from *Clk* mutants would be counterbalanced by reduced *pdf* mRNA and protein accumulation in the absence of *vri*. The offsetting effects of *Clk* and *vri* on *pdf* mRNA levels and the reinforcing effects of *Clk* and *vri* on PDF accumulation are consistent with the quasi-normal *pdf* mRNA levels and low PDF levels in sLN$_v$s from *cyc* and *Clk* null mutants. Alternatively, it is possible that *Clk* is required for larval LN$_v$ identity or survival (and the *pdf* mRNA and protein they express) during metamorphosis since there is no evidence that sLN$_v$s are present in *Clk*^{Jrk} adults (Houl, et al. 2008; Park, et al. 2000).

The impact of *vri* overexpression on *pdf* mRNA and protein levels differs depending on whether *vri* is transiently or chronically expressed. Transient *vri* overexpression in *cyc*^{01} adults increases PDF levels, but does not alter *pdf* mRNA levels (Figure 18A, B). The lack of increased *pdf* mRNA in sLN$_v$s is unexpected given that *pdf* transcription should be high in *cyc*^{01} flies due to loss of CLK-CYC dependent repression (Mezan, et al. 2016), and *vri* overexpression should further promote *pdf* mRNA accumulation. I speculate that *pdf* mRNA is maximally expressed in sLN$_v$s under normal

circumstances, thus *vri* overexpression and cyc^{01} can't appreciably increase *pdf* mRNA levels further, particularly given that *pdf* mRNA is already highly expressed in lLN_vs. Chronic *vri* overexpression sharply decreases PDF without altering *pdf* mRNA levels in larval LN_vs (Blau and Young 1999). Since high VRI levels repress *Clk* transcription, *pdf* mRNA levels remain high because *pdf* transcription and mRNA accumulation are both increased due to low CLK and high VRI levels, respectively, while PDF declines to the low levels seen in *Clk* and *cyc* null mutants (Blau and Young 1999; Park, et al. 2000). Like *Clk* and *cyc* null mutants, chronic *vri* overexpression apparently disrupts a factor required for PDF translation, maturation, transport, release or degradation, which results in low PDF levels. One factor known to control PDF abundance post-translationally is MATRIX METALLOPROTEASE 1 (MMP1), which is thought to inactivate PDF via cleavage in the extracellular matrix (Depetris-Chauvin, et al. 2014). Since *Mmp1* is a direct target of CLK (Kadener, et al. 2007), it could account for the low PDF levels when *vri* is chronically overexpressed. Thus, PDF expression in sLN_vs is regulated at the transcriptional, mRNA accumulation and protein synthesis or accumulation levels. Such intricate regulation likely insures optimal levels of PDF expression in sLN_vs, which are unique in their ability to drive activity rhythms in DD and coordinate the pacemaker neuron network (Helfrich-Forster 2014; Shafer and Yao 2014).

Regulation of sLN_v arborization rhythms by VRI

Although *vri* is required for PDF expression, simply restoring PDF in sLN_vs from *vri* inactivated flies isn't sufficient to support activity rhythms (Figure 19A), suggesting

that *vri* mediates other processes required for activity rhythms. Indeed, *vri* is also necessary for rhythms in sLN_v dorsal projection arborization (Figure 19B-D), which are thought to be regulated by CLK-CYC-dependent rhythms in the transcription factor MEF2, the GTP binding protein PURATROPHIN-1 (PURA), and MMP1 (Depetris-Chauvin, et al. 2014; Petsakou, et al. 2015; Sivachenko, et al. 2013). MEF2 is proposed to repress FAS2 to promote arborization (Sivachenko, et al. 2013), which occurs coincident with high MEF2 levels in sLN_vs late at night (Blanchard, et al. 2010), whereas PURA activates RHO1 GTPase and MMP1 degrades PDF at dusk to promote sLN_v fasciculation (Depetris-Chauvin, et al. 2014; Petsakou, et al. 2015). The arborization phenotypes in *vri* inactivated and *vri* overexpression flies suggest that VRI promotes sLN_v arborization (Figure 19C, D; Figure 18A, C). How VRI function integrates with the MEF2-FAS2, PURA-RHO1 and MMP1-PDF pathways to regulate rhythms in sLN_v dorsal projection arborization will be an important focus for future studies.

Interlocked feedback loop function and conservation

In the interlocked feedback loop, PDP1ε and VRI are proposed to activate and repress transcription, respectively, of *Clk* and other genes whose mRNAs peak at dawn (Cyran, et al. 2003; Glossop, et al. 2003). In Clk^{Jrk} and cyc^{01} mutants, which lack both *Pdp1ε* and *vri* expression, *Clk* levels remain near their normal peak at all times of day (Glossop, et al. 1999), which suggests that *Pdp1ε* is not required to activate *Clk*. Moreover, peak *Clk* mRNA levels in *Pdp1ε* mutants are the same (in LD) or slightly

lower (in DD) than the wild-type *Clk* mRNA peak (Zheng, et al. 2009), further arguing that *Clk* activation is largely independent of *Pdp1ε*. If *Clk* is activated independent of *Pdp1ε*, then *Clk* mRNA cycling is largely controlled by VRI cycling, which peaks coincident with trough levels of *Clk* mRNA early at night (Cyran, et al. 2003; Glossop, et al. 2003). This VRI-dependent regulation likely extends to hundreds of other clock controlled genes whose mRNAs peak at dawn. Since *Clk* mRNA cycling is not necessary for circadian oscillator function (Kim, et al. 2002), these results argue that the primary function of *vri* is to drive output gene mRNA cycling that peaks at dawn. In addition, *vri* regulates non-cycling transcripts such as *pdf* indirectly via post-transcriptional regulatory pathways. To determine the impact of *vri* regulation on overt rhythms, direct and indirect VRI targets must be identified in different tissues and tested for defects in physiology, metabolism and behavior. My preliminary experiments to determine VRI target genes suggest VRI is regulating many biological processes such as metabolism, immunity, neuronal development and Appendix C outlines descriptive summary of my results.

Although feedback repression by VRI in flies and REV-ERB in mammals drives rhythmic transcription of *Clk* and *Bmal1* activators, respectively, VRI is not orthologous to REV-ERB and controls clock output rather than circadian timekeeping (Cho, et al. 2012; Preitner, et al. 2002). However, the mammalian ortholog of VRI, E4BP4/NFIL3, is also rhythmically expressed and functions along with the PAR domain transcriptional activators DBP, TEF and HLF to drive rhythmic expression of target genes (Lopez-Molina, et al. 1997; Mitsui, et al. 2001; Ueda, et al. 2005; Wuarin and Schibler 1990;

Yamaguchi, et al. 2000). As in flies, E4BP4/NFIL3 and the PAR domain activators bind D-boxes to drive rhythmic transcription (Lopez-Molina, et al. 1997; Mitsui, et al. 2001; Ueda, et al. 2005; Wuarin and Schibler 1990; Yamaguchi, et al. 2000), and such binding represents a major node in rhythmic transcription in mammals along with E-box binding and RORE element binding (Ueda, et al. 2005). Knockdown of E4BP4/NFIL3 and DBP alter circadian period (Yamajuku, et al. 2011), perhaps by regulating *Per2* transcription in conjunction with CLOCK-BMAL1 (Ohno, et al. 2007a; Ohno, et al. 2007b), but the extent to which E4BP4/NFIL3 contributes to rhythmic transcription and clock output is not known. Further analysis of target genes and processes regulated by VRI may shed light on E4BP4/NFIL3 function in mammals.

Conclusion

The major objective of this project was to determine if *vri* is needed for clock and/or output functions in *Drosophila melanogaster*. Given the fact that *vri* regulates many developmental functions during embryogenesis, and *vri* mutants are embryonic lethal has obstructed answering this question for a long time. Provided that VRI is regulating the transcription of many genes which are vital for the *Drosophila* circadian clock, understanding the adult *vri* null mutant phenotype is utmost important. I approached this question initially, by eliminating the transcription of *vri*-ADF which was thought to be the transcript that regulates clock function. However, I found *vri*-E is also rhythmically expressed and contributes to clock function (Figure 9 -10). Furthermore, I found that E-boxes located upstream of the *vri* exon 1c are essential for viability of

embryos, because development specific transcription factors might be using these cis elements to control *vri*-E transcription during embryogenesis (Figure 6). Interestingly, I found *vri*-ADF encodes short VRI using an alternative translation initiation site and this short VRI majorly contributes to the total VRI in adults (Figure 12).

Then the question was approached using a FRT-FLP based inactivatable transgene. Using this method, I generated adult tissue specific *vri* null mutant, that showed a functional oscillator with arrhythmic output behavior, suggesting VRI is a main regulator of output pathways (Figure 15-16). Using immunostaining, genetic manipulations and biochemical tools I demonstrated that VRI is regulating PDF post-transcriptionally and contributes to *vri* mutant phenotype (Figure 17-18). With preliminary experiments that were carried out to determine the target genes of VRI, it has shown that many biological processes involved with development, circadian clock, transcriptional and translational regulation, metabolism, immunity and neural morphogenesis are controlled by VRI (Appendix C). Thus, further characterization of these target genes will shed light on what and how clock is controlling different biological processes.

REFERENCES

Abruzzi, K. C., et al.
2011 *Drosophila* CLOCK target gene characterization: implications for circadian tissue-specific gene expression. Genes Dev 25(22):2374-86.

Abruzzi, K. C., et al.
2017 RNA-seq analysis of *Drosophila* clock and non-clock neurons reveals neuron-specific cycling and novel candidate neuropeptides. PLoS Genet 13(2):e1006613.

Agrawal, P., and P. E. Hardin
2016 The *Drosophila* Receptor Protein Tyrosine Phosphatase LAR Is Required for Development of Circadian Pacemaker Neuron Processes That Support Rhythmic Activity in Constant Darkness But Not during Light/Dark Cycles. J Neurosci 36(13):3860-70.

Agrawal, P., et al.
2017 *Drosophila* CRY Entrains Clocks in Body Tissues to Light and Maintains Passive Membrane Properties in a Non-clock Body Tissue Independent of Light. Curr Biol 27(16):2431-2441 e3.

Aschoff, J.
1999 Masking and parametric effects of high-frequency light-dark cycles. Jpn J Physiol 49(1):11-8.

Bell-Pedersen, D., et al.
2005 Circadian rhythms from multiple oscillators: lessons from diverse organisms. Nat Rev Genet 6(7):544-56.

Benito, J., et al.
2007 Transcriptional feedback loop regulation, function, and ontogeny in *Drosophila*. Cold Spring Harb Symp Quant Biol 72:437-44.

Blanchard, F. J., et al.
2010 The transcription factor Mef2 is required for normal circadian behavior in *Drosophila*. J Neurosci 30(17):5855-65.

Blau, J., and M. W. Young
1999 Cycling vrille expression is required for a functional *Drosophila* clock. Cell 99(6):661-71.

Boothroyd, C. E., and M. W. Young

2008 The in(put)s and out(put)s of the *Drosophila* circadian clock. Ann N Y Acad Sci 1129:350-7.

Cavanaugh, D. J., et al.
2014 Identification of a circadian output circuit for rest:activity rhythms in *Drosophila*. Cell 157(3):689-701.

Chadwick, D.J., and J.A. Goode
2004 Molecular Clocks and Light Signalling: Wiley.

Chang, A. T., et al.
2015 An evolutionarily conserved DNA architecture determines target specificity of the TWIST family bHLH transcription factors. Genes Dev 29(6):603-16.

Cho, H., et al.
2012 Regulation of circadian behaviour and metabolism by REV-ERB-alpha and REV-ERB-beta. Nature 485(7396):123-7.

Cyran, S. A., et al.
2003 vrille, Pdp1, and dClock form a second feedback loop in the *Drosophila* circadian clock. Cell 112(3):329-41.

Darlington, T. K., et al.
1998 Closing the circadian loop: CLOCK-induced transcription of its own inhibitors per and tim. Science 280(5369):1599-603.

Depetris-Chauvin, A., et al.
2011 Adult-specific electrical silencing of pacemaker neurons uncouples molecular clock from circadian outputs. Curr Biol 21(21):1783-93.

Depetris-Chauvin, A., et al.
2014 Mmp1 processing of the PDF neuropeptide regulates circadian structural plasticity of pacemaker neurons. PLoS Genet 10(10):e1004700.

Dodd, A. N., et al.
2005 Plant circadian clocks increase photosynthesis, growth, survival, and competitive advantage. Science 309(5734):630-3.

Doherty, C. J., and S. A. Kay
2010 Circadian control of global gene expression patterns. Annu Rev Genet 44:419-44.

Dow, J. A.

2009 Insights into the Malpighian tubule from functional genomics. J Exp Biol 212(Pt 3):435-45.

Ehlers, C. L.
1992 Social zeitgebers, biological rhythms and depression. Clin Neuropharmacol 15 Suppl 1 Pt A:44A-45A.

Emery, P., et al.
1998 CRY, a *Drosophila* clock and light-regulated cryptochrome, is a major contributor to circadian rhythm resetting and photosensitivity. Cell 95(5):669-79.

Ewer, J., et al.
1992 Expression of the period clock gene within different cell types in the brain of *Drosophila* adults and mosaic analysis of these cells' influence on circadian behavioral rhythms. J Neurosci 12(9):3321-49.

Feng, Y., et al.
1991 Translation initiation in *Drosophila melanogaster* is reduced by mutations upstream of the AUG initiator codon. Mol Cell Biol 11(4):2149-53.

Fernandez, M. P., J. Berni, and M. F. Ceriani
2008 Circadian remodeling of neuronal circuits involved in rhythmic behavior. PLoS Biol 6(3):e69.

Frenkel, L., and M. F. Ceriani
2011 Circadian plasticity: from structure to behavior. Int Rev Neurobiol 99:107-38.

Gachon, F., et al.
2004 The loss of circadian PAR bZip transcription factors results in epilepsy. Genes Dev 18(12):1397-412.

Gachon, F., et al.
2011 Proline- and acidic amino acid-rich basic leucine zipper proteins modulate peroxisome proliferator-activated receptor alpha (PPARalpha) activity. Proc Natl Acad Sci U S A 108(12):4794-9.

George, H., and R. Terracol
1997 The vrille gene of *Drosophila* is a maternal enhancer of decapentaplegic and encodes a new member of the bZIP family of transcription factors. Genetics 146(4):1345-63.

Glossop, N. R., et al.
2003 VRILLE feeds back to control circadian transcription of Clock in the *Drosophila* circadian oscillator. Neuron 37(2):249-61.

Glossop, N. R., L. C. Lyons, and P. E. Hardin
1999 Interlocked feedback loops within the *Drosophila* circadian oscillator. Science 286(5440):766-8.

Gramates, L. S., et al.
2017 FlyBase at 25: looking to the future. Nucleic Acids Res 45(D1):D663-D671.

Guillaumond, F., et al.
2005 Differential control of Bmal1 circadian transcription by REV-ERB and ROR nuclear receptors. J Biol Rhythms 20(5):391-403.

Hardin, P. E.
2006 Essential and expendable features of the circadian timekeeping mechanism. Curr Opin Neurobiol 16(6):686-92.

—
2011 Molecular genetic analysis of circadian timekeeping in *Drosophila*. Adv Genet 74:141-73.

Hardin, P. E., and S. Panda
2013 Circadian timekeeping and output mechanisms in animals. Curr Opin Neurobiol 23(5):724-31.

Helfrich-Forster, C.
1995 The period clock gene is expressed in central nervous system neurons which also produce a neuropeptide that reveals the projections of circadian pacemaker cells within the brain of *Drosophila melanogaster*. Proc Natl Acad Sci U S A 92(2):612-6.

—
1998 Robust circadian rhythmicity of *Drosophila melanogaster* requires the presence of lateral neurons: a brain-behavioral study of disconnected mutants. J Comp Physiol A 182(4):435-53.

—
2005 Neurobiology of the fruit fly's circadian clock. Genes Brain Behav 4(2):65-76.

—
2014 From neurogenetic studies in the fly brain to a concept in circadian biology. J Neurogenet 28(3-4):329-47.

Helfrich-Forster, C., et al.

2007 Development and morphology of the clock-gene-expressing lateral neurons of *Drosophila melanogaster*. J Comp Neurol 500(1):47-70.

Hong, C. I., E. D. Conrad, and J. J. Tyson
2007 A proposal for robust temperature compensation of circadian rhythms. Proc Natl Acad Sci U S A 104(4):1195-200.

Houl, J. H., et al.
2008 CLOCK expression identifies developing circadian oscillator neurons in the brains of *Drosophila* embryos. BMC Neurosci 9:119.

Houl, Jerry Hemmevorn
2009 Spatial Expression of Core Clock genes in *Drosophila Melanogaster* Thesis Dissertation

Ivanchenko, M., R. Stanewsky, and J. M. Giebultowicz
2001 Circadian photoreception in *Drosophila*: functions of *cryptochrome* in peripheral and central clocks. J Biol Rhythms 16(3):205-15.

Iyer, S. V., et al.
1991 Chicken vitellogenin gene-binding protein, a leucine zipper transcription factor that binds to an important control element in the chicken vitellogenin II promoter, is related to rat DBP. Mol Cell Biol 11(10):4863-75.

Jackson, R. J., and N. Standart
2007 How do microRNAs regulate gene expression? Sci STKE 2007(367):re1.

Jolley, C. C., et al.
2014 A mammalian circadian clock model incorporating daytime expression elements. Biophys J 107(6):1462-73.

Kadener, S., et al.
2007 Clockwork Orange is a transcriptional repressor and a new *Drosophila* circadian pacemaker component. Genes Dev 21(13):1675-86.

Kim, D. Y., et al.
2010 hnRNP Q and PTB modulate the circadian oscillation of mouse Rev-erb alpha via IRES-mediated translation. Nucleic Acids Res 38(20):7068-78.

Kim, E. Y., et al.
2002 *Drosophila* CLOCK protein is under posttranscriptional control and influences light-induced activity. Neuron 34(1):69-81.

Kim, E. Y., et al.

2012 A role for O-GlcNAcylation in setting circadian clock speed. Genes Dev 26(5):490-502.

Kim, H. J., et al.
2017 Heterogeneous nuclear ribonucleoprotein A1 regulates rhythmic synthesis of mouse Nfil3 protein via IRES-mediated translation. Sci Rep 7:42882.

Koh, K., X. Zheng, and A. Sehgal
2006 JETLAG resets the *Drosophila* circadian clock by promoting light-induced degradation of TIMELESS. Science 312(5781):1809-12.

Kojima, S., D. L. Shingle, and C. B. Green
2011 Post-transcriptional control of circadian rhythms. J Cell Sci 124(Pt 3):311-20.

Li, M. D., et al.
2013 O-GlcNAc signaling entrains the circadian clock by inhibiting BMAL1/CLOCK ubiquitination. Cell Metab 17(2):303-10.

Li, S., and L. Zhang
2015 Circadian Control of Global Transcription. Biomed Res Int 2015:187809.

Liu, A. C., et al.
2008 Redundant function of REV-ERBalpha and beta and non-essential role for Bmal1 cycling in transcriptional regulation of intracellular circadian rhythms. PLoS Genet 4(2):e1000023.

Liu, T., et al.
2015 Circadian Activators Are Expressed Days before They Initiate Clock Function in Late Pacemaker Neurons from *Drosophila*. J Neurosci 35(22):8662-71.

Lopez-Molina, L., et al.
1997 The DBP gene is expressed according to a circadian rhythm in the suprachiasmatic nucleus and influences circadian behavior. Embo J 16(22):6762-71.

Mehta, N., and H. Y. Cheng
2013 Micro-managing the circadian clock: The role of microRNAs in biological timekeeping. J Mol Biol 425(19):3609-24.

Menet, J. S., and P. E. Hardin
2014 Circadian clocks: the tissue is the issue. Curr Biol 24(1):R25-7.

Mertens, I., et al.

2005 PDF receptor signaling in *Drosophila* contributes to both circadian and geotactic behaviors. Neuron 48(2):213-9.

Mezan, S., et al.
2016 PDF Signaling Is an Integral Part of the *Drosophila* Circadian Molecular Oscillator. Cell Rep 17(3):708-719.

Mitsui, S., et al.
2001 Antagonistic role of E4BP4 and PAR proteins in the circadian oscillatory mechanism. Genes Dev 15(8):995-1006.

Moses, K., M. C. Ellis, and G. M. Rubin
1989 The glass gene encodes a zinc-finger protein required by *Drosophila* photoreceptor cells. Nature 340(6234):531-6.

Myers, E. M., J. Yu, and A. Sehgal
2003 Circadian control of eclosion: interaction between a central and peripheral clock in *Drosophila melanogaster*. Curr Biol 13(6):526-33.

Nara I. Muraro, M. Fernanda Ceriani
2014 Behavioral Genetics of the Fly (*Drosophila Melanogaster*). *In* Circadian rhythms. J. Dubnau, ed. Pp. pp 104-115. Cambridge Handbooks in Behavioral Genetics: Cambridge University Press.

Narasimamurthy, R., and D. M. Virshup
2017 Molecular Mechanisms Regulating Temperature Compensation of the Circadian Clock. Front Neurol 8:161.

Ohno, T., Y. Onishi, and N. Ishida
2007a The negative transcription factor E4BP4 is associated with circadian clock protein PERIOD2. Biochem Biophys Res Commun 354(4):1010-5.

—
2007b A novel E4BP4 element drives circadian expression of mPeriod2. Nucleic Acids Res 35(2):648-55.

Osterwalder, T., et al.
2001 A conditional tissue-specific transgene expression system using inducible GAL4. Proc Natl Acad Sci U S A 98(22):12596-601.

Paranjpe, D. A., and V. K. Sharma
2005 Evolution of temporal order in living organisms. J Circadian Rhythms 3(1):7.

Park, J. H., et al.

2000 Differential regulation of circadian pacemaker output by separate clock genes in *Drosophila*. Proc Natl Acad Sci U S A 97(7):3608-13.

Partch, C. L., C. B. Green, and J. S. Takahashi
2014 Molecular architecture of the mammalian circadian clock. Trends Cell Biol 24(2):90-9.

Peschel, N., et al.
2009 Light-dependent interactions between the *Drosophila* circadian clock factors cryptochrome, jetlag, and timeless. Curr Biol 19(3):241-7.

Petsakou, A., T. P. Sapsis, and J. Blau
2015 Circadian Rhythms in Rho1 Activity Regulate Neuronal Plasticity and Network Hierarchy. Cell 162(4):823-35.

Pittendrigh, C. S.
1993 Temporal organization: reflections of a Darwinian clock-watcher. Annu Rev Physiol 55:16-54.

Pittendrigh, C. S., and T. Takamura
1989 Latitudinal clines in the properties of a circadian pacemaker. J Biol Rhythms 4(2):217-35.

Plautz, J. D., et al.
1997 Independent photoreceptive circadian clocks throughout *Drosophila*. Science 278(5343):1632-5.

Preitner, N., et al.
2002 The orphan nuclear receptor REV-ERBalpha controls circadian transcription within the positive limb of the mammalian circadian oscillator. Cell 110(2):251-60.

Reddy, K. L., et al.
2006 The *Drosophila* Par domain protein I gene, Pdp1, is a regulator of larval growth, mitosis and endoreplication. Dev Biol 289(1):100-14.

Reddy, K. L., et al.
2000 The *Drosophila* PAR domain protein 1 (Pdp1) gene encodes multiple differentially expressed mRNAs and proteins through the use of multiple enhancers and promoters. Dev Biol 224(2):401-14.

Renn, S. C., et al.
1999 A *pdf* neuropeptide gene mutation and ablation of PDF neurons each cause severe abnormalities of behavioral circadian rhythms in *Drosophila*. Cell 99(7):791-802.

Reppert, S. M., and D. R. Weaver
2002 Coordination of circadian timing in mammals. Nature 418(6901):935-41.

Rieger, D., et al.
2006 Functional analysis of circadian pacemaker neurons in *Drosophila melanogaster*. J Neurosci 26(9):2531-43.

Robertson, H. M., et al.
1988 A stable genomic source of P element transposase in *Drosophila melanogaster*. Genetics 118(3):461-70.

Roman, G., et al.
2001 P[Switch], a system for spatial and temporal control of gene expression in *Drosophila melanogaster*. Proc Natl Acad Sci U S A 98(22):12602-7.

Rutila, J. E., et al.
1998 CYCLE is a second bHLH-PAS clock protein essential for circadian rhythmicity and transcription of *Drosophila period* and *timeless*. Cell 93(5):805-14.

Saithong, T., K. J. Painter, and A. J. Millar
2010 The contributions of interlocking loops and extensive nonlinearity to the properties of circadian clock models. PLoS One 5(11):e13867.

Schindelin, J., et al.
2012 Fiji: an open-source platform for biological-image analysis. Nat Methods 9(7):676-82.

Schneider, C. A., W. S. Rasband, and K. W. Eliceiri

2012 NIH Image to ImageJ: 25 years of image analysis. Nat Methods 9(7):671-5.

Shafer, O. T., and Z. Yao
2014 Pigment-Dispersing Factor Signaling and Circadian Rhythms in Insect Locomotor Activity. Curr Opin Insect Sci 1:73-80.

Sivachenko, A., et al.
2013 The transcription factor Mef2 links the *Drosophila* core clock to Fas2, neuronal morphology, and circadian behavior. Neuron 79(2):281-92.

Szuplewski, S., B. Kottler, and R. Terracol
2003 The *Drosophila* bZIP transcription factor Vrille is involved in hair and cell growth. Development 130(16):3651-62.

Takahashi, J. S.

2017 Transcriptional architecture of the mammalian circadian clock. Nat Rev Genet 18(3):164-179.

Tataroglu, O., and P. Emery
2014 Studying circadian rhythms in *Drosophila melanogaster*. Methods 68(1):140-50.

—
2015 The molecular ticks of the *Drosophila* circadian clock. Curr Opin Insect Sci 7:51-57.

Taylor III, H. P.
2007 Regulation of the *Drosophila* molecular oscilator by DNA binding of clock proteins and histone modifications of *period* and *timeless*, Department of Biology and Biochemistry, University of Houston.

Tower, J., et al.
1993 Preferential transposition of *Drosophila* P elements to nearby chromosomal sites. Genetics 133(2):347-59.

Ueda, H. R., et al.
2005 System-level identification of transcriptional circuits underlying mammalian circadian clocks. Nat Genet 37(2):187-92.

Uriu, K., and H. Tei
2017 Feedback loops interlocked at competitive binding sites amplify and facilitate genetic oscillations. J Theor Biol 428:56-64.

Valencia-Sanchez, M. A., et al.
2006 Control of translation and mRNA degradation by miRNAs and siRNAs. Genes Dev 20(5):515-24.

Venken, K. J., et al.
2006 P[acman]: a BAC transgenic platform for targeted insertion of large DNA fragments in D. *melanogaster*. Science 314(5806):1747-51.

Venken, K. J., et al.
2008 Recombineering-mediated tagging of *Drosophila* genomic constructs for in vivo localization and acute protein inactivation. Nucleic Acids Res 36(18):e114.

Vinson, C. R., P. B. Sigler, and S. L. McKnight
1989 Scissors-grip model for DNA recognition by a family of leucine zipper proteins. Science 246(4932):911-6.

Wuarin, J., and U. Schibler

1990 Expression of the liver-enriched transcriptional activator protein DBP follows a stringent circadian rhythm. Cell 63(6):1257-66.

Yamaguchi, S., et al.
2000 Role of DBP in the circadian oscillatory mechanism. Mol Cell Biol 20(13):4773-81.

Yamajuku, D., et al.
2011 Cellular DBP and E4BP4 proteins are critical for determining the period length of the circadian oscillator. FEBS Lett 585(14):2217-22.

Yoshii, T., D. Rieger, and C. Helfrich-Forster
2012 Two clocks in the brain: an update of the morning and evening oscillator model in *Drosophila*. Prog Brain Res 199:59-82.

Yu, W., and P. E. Hardin
2006 Circadian oscillators of *Drosophila* and mammals. J Cell Sci 119(Pt 23):4793-5.

Yu, W., et al.
2006 PER-dependent rhythms in CLK phosphorylation and E-box binding regulate circadian transcription. Genes Dev 20(6):723-33.

Zhang, R., et al.
2014 A circadian gene expression atlas in mammals: implications for biology and medicine. Proc Natl Acad Sci U S A 111(45):16219-24.

Zheng, X., et al.
2009 An isoform-specific mutant reveals a role of PDP1 epsilon in the circadian oscillator. J Neurosci 29(35):10920-7.

Zhou, J., W. Yu, and P. E. Hardin
2016 CLOCKWORK ORANGE Enhances PERIOD Mediated Rhythms in Transcriptional Repression by Antagonizing E-box Binding by CLOCK-CYCLE. PLoS Genet 12(11):e1006430.

Zhou, Jian
2017 Characterizing the function of CLOCKWORK ORANGE in the circadian feedback loops in *Drosophila melanogaster*, Department of Biology, Texas A&M University.

APPENDIX A

CHARACTERIZATION OF *VRI* FUNCTION USING *VRI*^{DN} MUTANTS

VRI is a bZIP transcription factor that forms homodimers using the Zipper domain (Chadwick and Goode 2004; Glossop, et al. 2003). I devised a strategy to use an existing dominant negative mutant to confirm the *vri* null phenotypes independent to *vri* inactivated mutants described in Chapter III. The dominant negative transgene was generated by Dr. Nicholas Glossop, a former post-doctoral fellow in the Hardin lab, through deleting the basic domain from a *vri*-D cDNA clone, GH23983. The resulting cDNA$^{\Delta basic}$ clone was inserted into the pUAST vector was used to generate a transgenic strain having a third chromosome insert, which I will refer to as UAS-*vri*^{DN} (U-*vri*^{DN}).

Experiments to measure locomotor activity rhythms were performed with the U-*vri*^{DN} responder line showed that in the absence of any drivers, they have wild-type rhythms, and when crossed to a Gal4 driver line, the percentage of rhythmicity decreases drastically or results in arrhythmicity (Table A1). The strength of the phenotype was dependent on the strength of the driver being used. When a strong clock cell specific driver like *tim*-G4 was used to drive U-*vri*^{DN} responder, flies were arrhythmic, but only when two copies of the driver were used. With one copy of the *tim*-G4 driver flies showed a reduced percentage of rhythmicity. The reduced percentage of rhythmicity was also apparent with other Gal4 drivers like *pdf*-Gal4 (expressed in LN_vs except 5th sLN_v), *Mz520*-Gal4 (expressed in LN_vs except 5th sLN_v) and *r6*-Gal4 (expressed in only sLN_vs) ((Table A1), (Yoshii, et al. 2012)).

Table A1: *vri*^{DN} mutants show reduced percentage of rhythms or arrhythmicity.

Genotype	N	% Rhythmic	Period ± SEM	Strength ± SEM
w^{1118}	16	100.0	23.66± 0.09	87.82± 8.50
+;U-*vri*^{DN}	30	86.67	23.83± 0.11	80.27± 8.92
tim-G4;U-*vri*^{DN}	18	0	N/A	N/A
tim-G4/+;U-*vri*^{DN}	12	33.33	24.50± 0.62	23.44± 5.12
tim-G4;U-*vri*^{DN}/+	16	0	N/A	N/A
pdf-G4;U-*vri*^{DN}	16	12.5	24.50± 0.71	22.63± 4.99
*Mz*520-G4;U-*vri*^{DN}	62	56.43	23.76± 0.10	39.62± 4.77
r6-G4/+;U-*vri*^{DN}	43	44.18	24.00± 0.14	34.61± 7.08

N, total number of flies tested and SEM, Standard error mean.

Larval brain wholemount immunostaining of *tim*-G4;U-*vri*^{DN} confirmed the absence of PDF staining on the sLN_v dorsal projections, similar to *vri* inactivated mutant flies (Figure A1, Figure 17). However, when *tim*-G4;U-*vri*^{DN} adult brains were immunostained, I observed a somewhat different phenotype than in *vri* inactivated mutants (Figure A1, Figure 17). *tim*-G4;U-*vri*^{DN} adult brains have an extensive branched network of PDF positive axons all over the brain. Since I did not observe any sLN_v dorsal projections in larvae, I speculate the projections must have arisen from lLN_vs or

prothoracic ganglion neurons. The extensive PDF positive neuronal branching phenotype was observed earlier with *cyc*^{0} mutants (Park et. al., 1999).

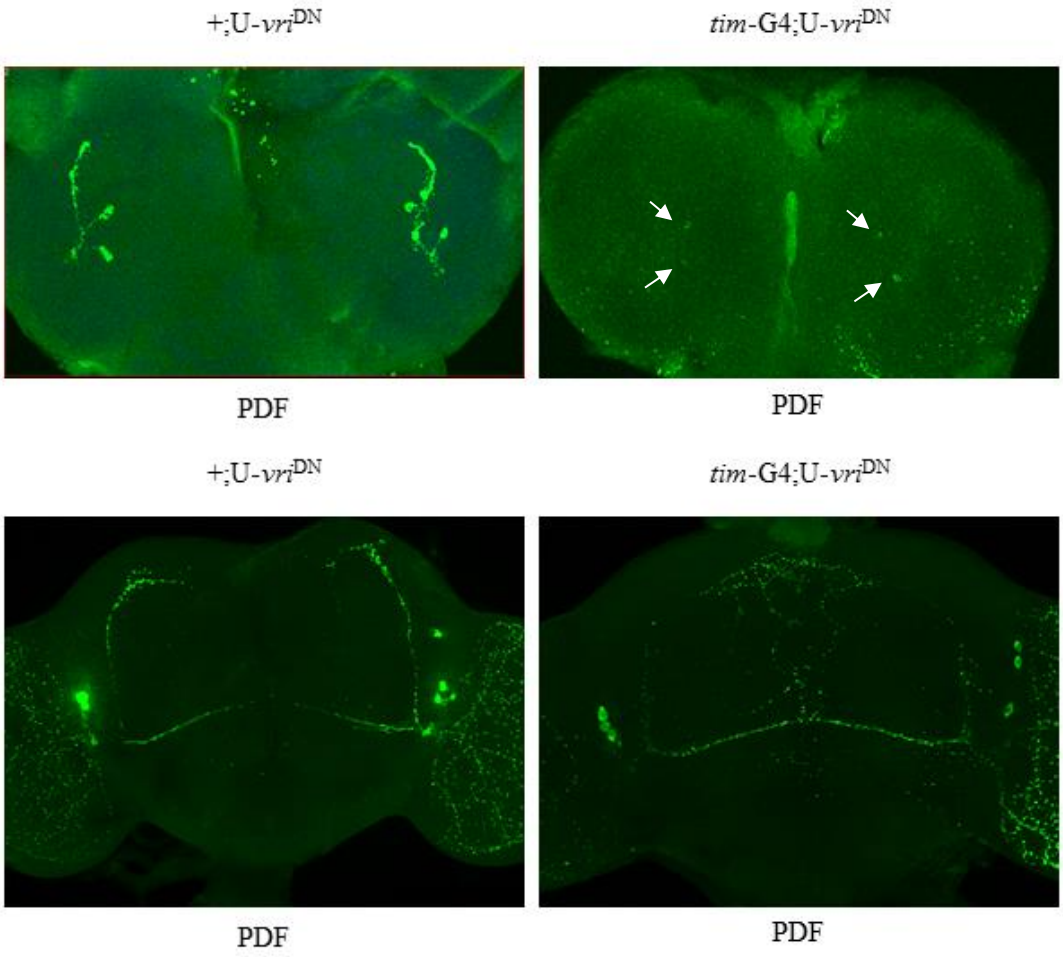

Figure A1. PDF expression patterns in *tim*-G4;U-*vri*^{DN} mutant larval and adult fly brains. Brains from *w*^{1118};+;UAS-*vri*^{DN} (+;U-*vri*^{DN}) and *w*^{1118};*tim*-Gal4;UAS-*vri*^{DN} (*tim*-G4;U-*vri*^{DN}) larvae and adults collected at ZT3 were immunostained with PDF (green) antiserum and imaged as described in Chapter III method section.

Apart from locomotor behavior, fly eclosion is under the control of circadian clock where wild-type flies show a peak of eclosion near dawn (Myers, et al. 2003; Pittendrigh and Takamura 1989). Thus, I carried out eclosion behavior experiments as described by Myers et. al. (2003), to determine if *tim*-G4;U-*vri*^{DN} flies also disrupt eclosion rhythms? Overexpression of U-*vri*^{DN} transgene in all clock cells using the *tim*-Gal4 driver resulted in arrhythmic eclosion behavior (Figure A2). Flies showed morning anticipation and a morning peak when they were kept in LD cycle, but in DD conditions these rhythms were abolished, while w^{1118} flies continue to maintain rhythms for three days in constant darkness.

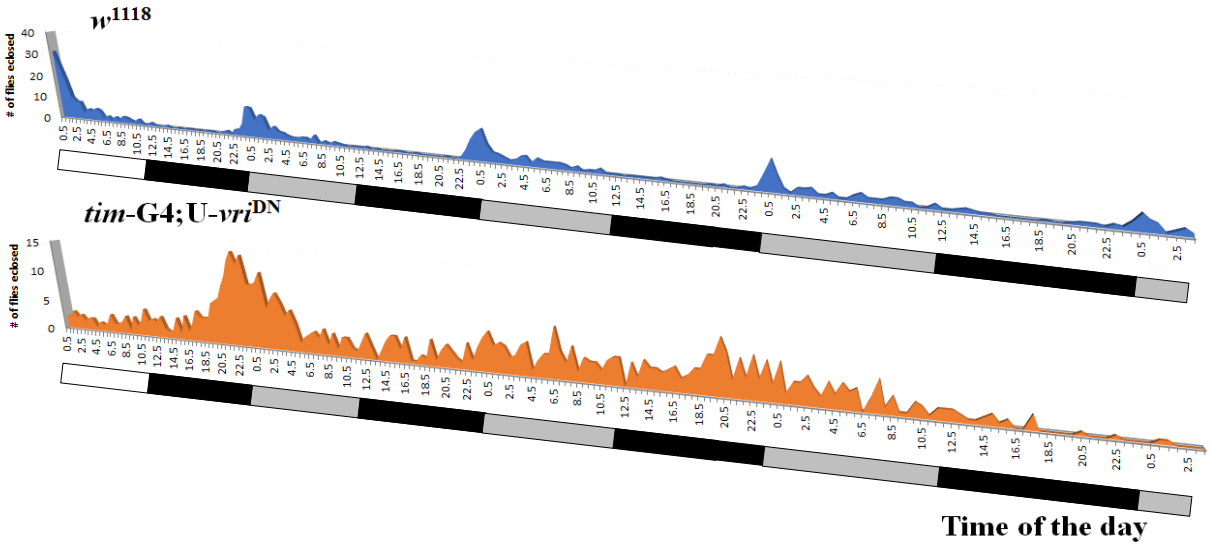

Figure A2. Eclosion rhythms of w^{1118} and *tim*-G4;U-*vri*^{DN} flies.
The area plot shaded with blue represents the number of w^{1118} flies that eclosed within 30-minutes bins over four-day period. First day was 12h:12h LD cycle and other three days were in constant darkness. Area plot shaded with brown represents the number of *tim*-G4;U-*vri*^{DN} flies that eclosed within 30-minutes bins over four days. White bar: day phase, black bars: night phase or subjective night phase and ash bars: subjective day phase.

These experiments show that two independent *vri* mutants that are viable in adults that were generated with two different mechanisms show that the loss of *vri* causes behavioral arrhythmicity and disrupted PDF expression. Also, using *tim*-G4;U-*vri*^{DN} flies I show that other rhythmic outputs like eclosion become arrhythmic in the absence of *vri*, giving us further confidence that *vri* is top tier transcription factor that controls hierarchical output genes activated by the oscillator.

APPENDIX B

FURTHER CHARACTERIZATION OF *VRI*70KB^{FRT} CONDITIONALLY INACTIVATED MUTANTS

In chapter III I demonstrated that *Clk* mRNA is constitutively expressed at its peak level in *vri* inactivated mutants. Interestingly, when CLK protein expression was analyzed in *vri* inactivated flies, I observed throughout the day the CLK was migrating at a higher molecular weight than expected (Figure B1A). The difference in migration indicates CLK may be undergoing either additional phosphorylation or another type of post translational modification in *vri* inactivated flies. To determine if the difference in migration was due to phosphorylation, I treated protein samples with λ-phosphatase. The treatment produced a faster migrating band, however, it did not migrate at the same level as a wild-type (w^{1118}) sample treated with λ-phosphatase, which represents non-phosphorylated CLK. This suggests that VRI may be controlling another type of post-translational modification on CLK. Glycosylation is another possible post-translational modification that can attribute protein migration. BMAL1, mCLOCK, mPER2 and dPER are rhythmically O-glycosylate and helps to stabilize these proteins (Kim, et al. 2012; Li, et al. 2013). Thus, the difference in CLK migration can be due to possible glycosylation modifications on CLK.

cry is another gene regulated by VRI. *vri* overexpression and *cry* promoter analyses showed that VRI is acting as a transcriptional repressor of *cry*, therefore I expected that loss of *vri* would result in high *cry* mRNA levels (Glossop, et al. 2003).

However, in *vri* inactivated mutants an unexpected result was observed. RT-qPCR experiments showed *cry* mRNA abundance is constitutively low, rather than high, in *vri* inactivated flies (Figure B1B). CRY protein expression was also constitutively lower in abundance in *vri* inactivated flies (Figure B1C).

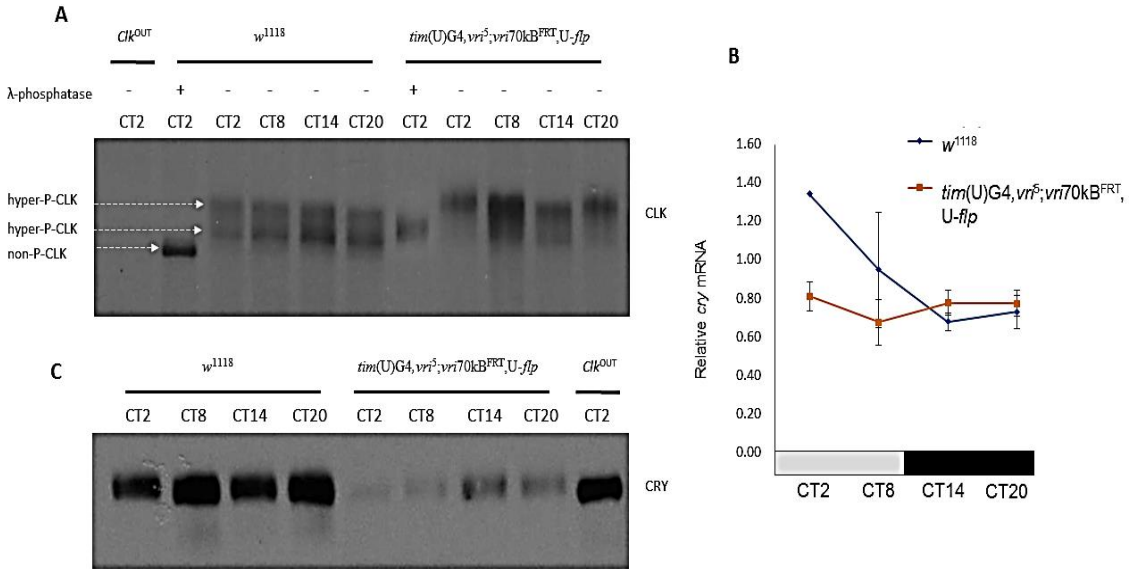

Figure B1. CLK and CRY are differentially regulated in *vri* inactivated flies. (A) Characterization of CLK protein from heads of w^{1118}, Clk^{OUT} and w^{1118};*tim*(UAS)Gal4,vri^5;*vri*70kB^{FRT},UAS-*flp*/+ (*tim*(U)G4,vri^5;*vri*70kB^{FRT},U-*flp*) flies collected at the indicated times during DD was carried out. The protein samples treated with λ-phosphatase is indicated. (B) RT-qPCR quantification of *cry* mRNA levels in heads of w^{1118} and w^{1118};*tim*(UAS)Gal4,vri^5;*vri*70kB^{FRT},UAS-*flp*/+ (*tim*(U)G4,vri^5;*vri*70kB^{FRT},U-*flp*) flies collected at the indicated circadian times during DD1. Gray boxes, subjective lights-on; black boxes, subjective lights-off (n=3). (C) Characterization of CRY protein from heads of w^{1118}, Clk^{OUT} and w^{1118};*tim*(UAS)Gal4,vri^5;*vri*70kB^{FRT},UAS-*flp*/+ (*tim*(U)G4,vri^5;*vri*70kB^{FRT},U-*flp*) flies collected at the indicated times during DD was carried out.

These unexpected results suggest, VRI may be regulating *cry* expression at the level of post-transcription. In Chapter III, I demonstrated that VRI is regulating *pdf* mRNA post transcriptionally. *cry* mRNA may be using a similar mechanism to control its transcripts and this maybe another instance where VRI regulation of a miRNA could impact a gene expression post transcriptionally.

APPENDIX C

GLOBAL CHARACTERIZATION OF VRI AND PDP1 CISTROMES

VRI and PDP1 form an interlocked feedback loop with the *Drosophila* circadian oscillator and are hypothesized to repress and activate target genes such as Clk, which contains D boxes targeted by both genes (Glossop, et al. 2003). Thus, I sought to determine the target genes of these two transcription factors to determine which circadian output genes and biological processes are controlled by VRI and PDP1, and whether they control output genes individually or together. I used two existing transgenes of VRI and PDP1 c-terminally tagged with GFP-FLAG epitopes to carryout ChIP-Seq experiments. These two transgenes rescued activity rhythms of vri^{5} and $Pdp1^{3135}$ null mutants (Table C1).

Table C1: *vri-gfp-flag* and *Pdp1-gfp-flag* transgenes rescued activity rhythms of vri^{5} and $Pdp1^{3135}$ mutants.

Genotype	N	% Rhythmic	Period ± SEM	Strength
w^{1118}	20	94.0	23.76± 0.09	82.23
+;*vri-gfp-flag*	15	93.3	24.07± 0.16	92.56
vri^{5};*vri-gfp-flag*	11	81.8	23.38± 0.13	66.78
Pdp1-gfp-flag;+	12	100.0	23.29± 0.10	92.98
+; $Pdp1^{3135}$	16	0.0	N/A	N/A
Pdp1-gfp-flag; $Pdp1^{3135}$	10	100.0	24.85± 0.11	53.19

N, total number of flies tested and SEM, Standard error mean.

To identify direct targets of VRI and PDP1, FLAG antibody conjugated magnetic beads were used to perform ChIP-Seq, as it showed high *Clk* promoter fragment enrichment in ChIP samples generated using GFP antibody conjugated magnetic beads. Also for the experiments I had to use +;*vri-gfp-flag* and *Pdp1-gfp-flag*;+ flies instead of null mutant rescue flies (*vri*^{5};*vri-gfp-flag* and *Pdp1-gfp-flag*; *Pdp1*^{3135}) since the growth rate was lower in null mutant rescue flies. ChIP-Seq experiments were carried out using head extracts at the peak and trough of expressions of VRI and PDP1 (VRI peak – ZT15 and trough – ZT3; PDP1 peak – ZT19 and trough – ZT4). Figure C1 summarizes the number of peaks, the number of genes and distribution of the peaks on the gene loci.

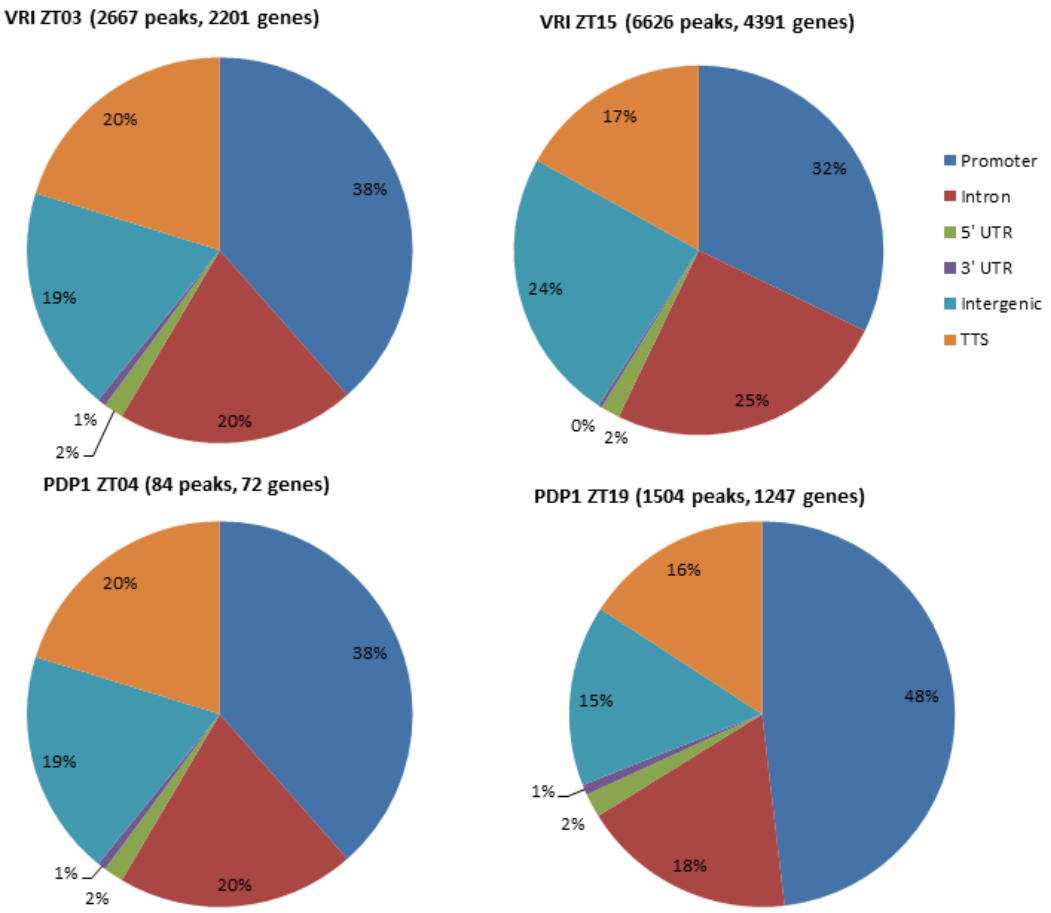

Figure C1. Summary of ChIP-seq analysis
For each sample, the number of peaks and the number of unique genes that they mapped using HOMER is indicated within parenthesis. Promoter: -1kB to +100 bp from transcription start site (TSS), Transcription termination site (TTS): -100 bp to + 1 kB from TTS, 3'UTR: 3' untranslated region, 5'UTR: 5' untranslated region and intergenic: 1 kb upstream of a TSS of one gene 1 kB downstream from the TTS of another gene.

Analysis of binding targets of VRI ZT15 and VRI ZT3 samples showed an overlap of 1669 genes, while the PDP1 ZT19 and PDP1 ZT4 samples had 62 common targets. 777 common target genes were found to be bound by VRI and PDP1 when sampling done at the peak timepoint for each protein. Out of these 777 genes, 115 are also targets of CLK (Figure C2).

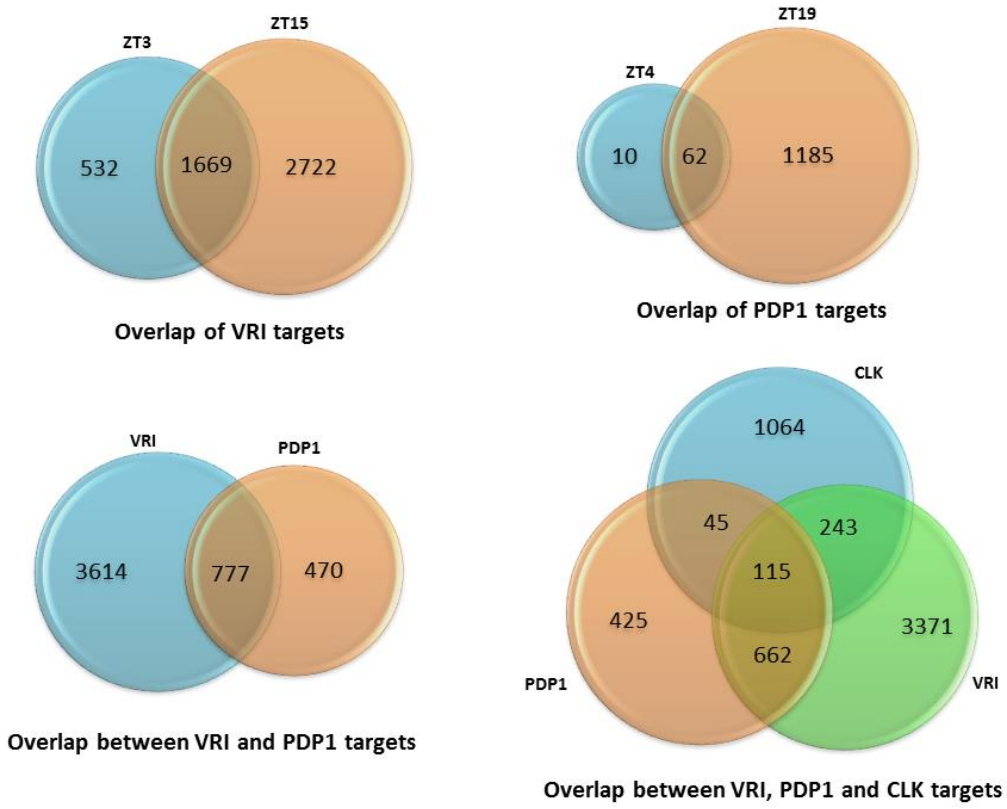

Figure C2. Analysis of the genes bound by VRI, PDP1 and CLK.

VRI and PDP1 are predicted to control the expression of ccgs that peak in the morning, while CLK is predicted to bind and activate the genes that peak in the evening. However, I found 115 genes are bound by VRI, PDP1 and CLK and it includes many evening peaking genes such as *per*, *tim*, *vri* and *Pdp1*. When binding at *per*, *tim*, *vri* and *Pdp1* were visualized I observed these peaks are found near the same region where CLK is bound (Figure C3, (Zhou 2017)). In mammals, REV-ERB also binds to genes controlled by BMAL1-CLOCK, therefore, this binding may have a functional significance that is conserved among species (Cho, et al. 2012). Thus, further

investigation such as what will happen to transcriptional rhythms of these target genes in null mutants of *Clk*, *vri* and *Ppd*, binding affinity of CLK, VRI and PDP1 on these genes are necessary to determine the significance of this binding. I also visualized VRI and PDP1 binding at *Clk* and *cry* promoters, that are already characterized as direct targets of VRI and PDP1, and observed that VRI and PDP1 rhythmically bind the *cry* promoter and 1st intron, and in the 1st intron of *Clk* (Figure C3), (Cyran, et al. 2003; Glossop, et al. 2003).

Based on the analysis of common gene that are bound by VRI and PDP1, it can be hypothesized that VRI and PDP1 have common biological functions as well as independent functions from one another. mRNAs of the common target of VRI and PDP1, can hypothesized to be expressed rhythmically with a peak in near dawn, similar to *Clk*. Thus, removal of either VRI or PDP1 should alter their mRNA expression rhythms. Without proper an understanding of the regulation of CLK, VRI and PDP1, it is hard to make any conclusion on their transcription.

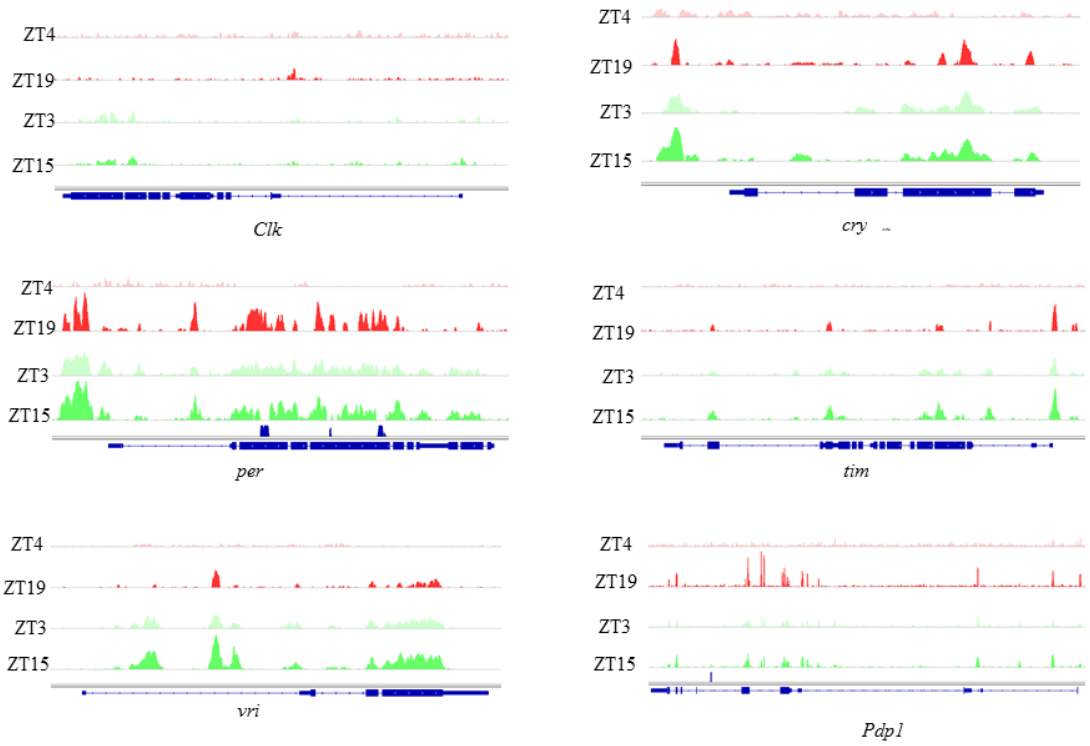

Figure C3. Visualization of VRI and PDP1 binding to core clock genes.
ChIP-seq track showing PDP1 (red) and VRI (green) binding to the core clock genes *Clk*, *cry*, *per*, *tim*, *vri* and *Pdp1* at the indicated timepoint.

To investigate the biological processes controlled by VRI, genes were bound by VRI at its peak and though were subjected to GO analysis using the DAVID GO analysis tool (Figure C4). As expected, the main processes controlled by the genes bound VRI were related to fly development and transcriptional regulation. Processes involved in regulating metabolism, sleep, locomotor behavior and immunity are shown in the ascending order of P-value, demonstrating that VRI may play a role in controlling these biological functions.

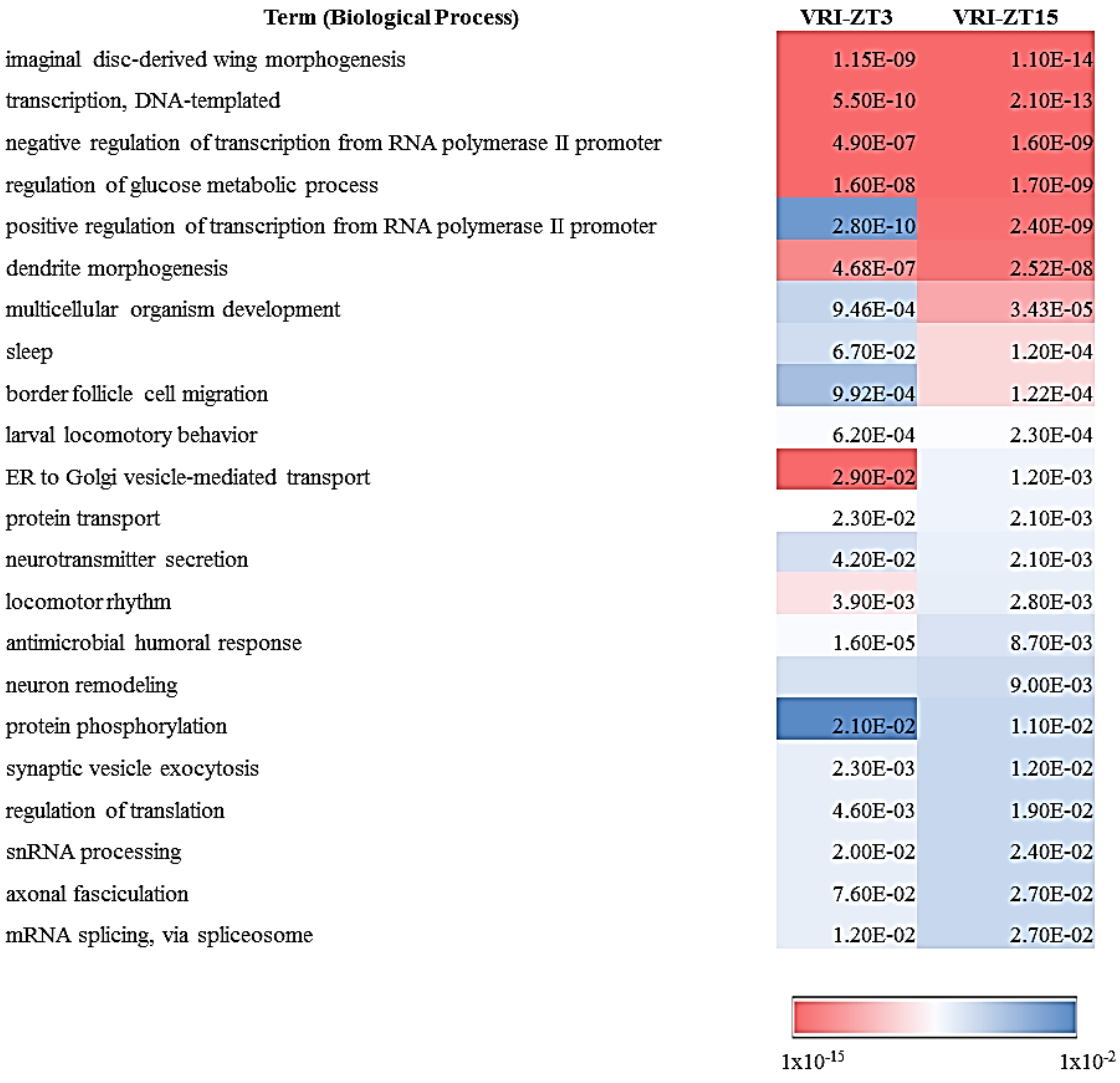

Figure C4. GO analysis of biological processes regulated by VRI
Potential biological processes controlled by VRI based on GO analysis performed with VRI's target genes. Red color indicates processes which are highly probable, white is intermediary probable and blue is less probable, to be regulated by VRI.

Interestingly, results from GO analysis also show that VRI regulates biological processes such as neuronal remodeling, synaptic vesicle exocytosis, protein transportation and axonal fasciculation which are directly relevant to the PDF expression phenotypes observed in *vri* inactivated flies. In fact, *Fas2* which is a target of VRI, was characterized earlier as a neuronal cell adhesion molecule. Overexpression of *Fas2* in LN_vs using *pdf*-Gal4 increased fasciculation due to intraaxonal adhesion, while RNAi mediated knockdown show defasciculated phenotype (Sivachenko, et al. 2013). Thus, in *vri* mutants I expect *fas2* to be overexpressed and help the fasciculated phenotype observed in *vri* inactivated mutants (Figure 19). Moreover, VRI controls translational processes as I expected based on observations made in relation to *pdf* and *cry* mRNAs. The only post translational modification identified in this analysis that VRI potentially regulates with a high significance is phosphorylation. Thus, further experimentation will be necessary to characterize the CLK post-translational regulation by VRI.

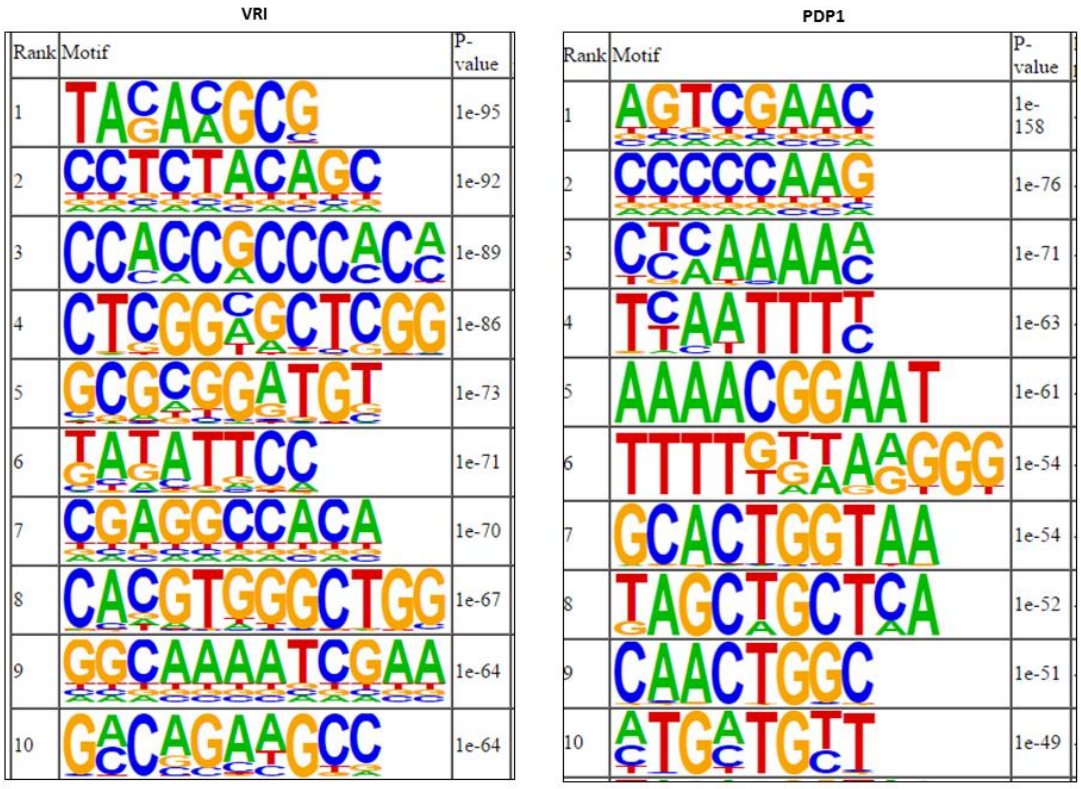

Figure C5. Binding Motif enrichment in VRI and PDP1 binding regions.

Binding motifs for VRI and PDP1 were predicted using HOMER predictor software tool. Based on the predictions, neither VRI nor PDP1 are enriched with D-box motifs, and they do not show the same binding motifs (Figure C5). This suggests that VRI and PDP1 may be controlling most of the other biological processes independently, even though they control expression of core clock genes binding to the same region (Figure C3). Thus, it is important to determine which biological processes does VRI control and which are controlled by PDP1 alone, and which are controlled by both.